

AD-A150 681

ACCURATE BASELINE DETERMINATION BY RADIO INTERFEROMETRY  
ON NAVSTAR GPS SA. (U) CHARLES STARK DRAPER LAB INC  
CAMBRIDGE MA R L GREENSPAN ET AL. 15 JUN 84

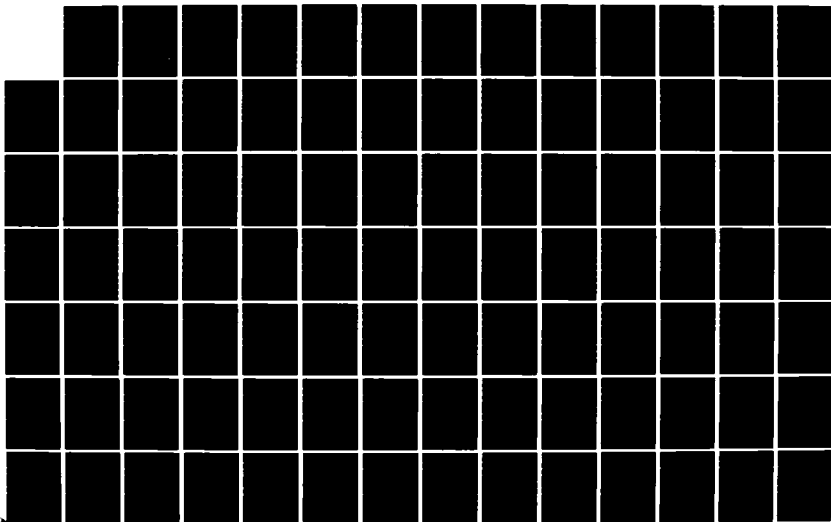
1/2

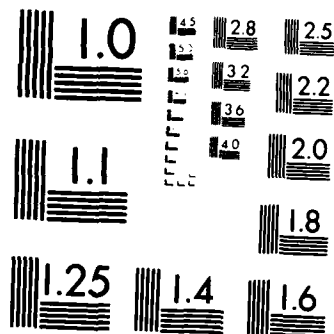
UNCLASSIFIED

CSDL-R-1719 AFGL-TR-84-0156

F/G 17/2.1

NL





MICROCOPY RESOLUTION TEST CHART  
NATIONAL BUREAU OF STANDARDS 1963 A

2

AFGL-TR-84-0156

ACCURATE BASELINE DETERMINATION BY RADIO  
INTERFEROMETRY ON NAVSTAR GPS  
SATELLITE TRANSMISSIONS

R. L. Greenspan  
A. Ng  
J. Przyjemski  
J. Veale  
C. C. Counselman III  
S. A. Gourevitch

The Charles Stark Draper Laboratory, Inc.  
555 Technology Square  
Cambridge, Massachusetts 02139

Final Report  
April 1980 - June 1982

15 June 1984

Approved for public release; distribution unlimited

This research was supported by the Air Force In-House  
Laboratory Independent Research Fund

AIR FORCE GEOPHYSICS LABORATORY  
AIR FORCE SYSTEMS COMMAND  
UNITED STATES AIR FORCE  
HANSCOM AFB, MASSACHUSETTS 01731

DTIC FILE COPY

DTIC  
ELECTE

MAR 01 1985

E


02 15

AD-A150 681


CONTRACTOR REPORTS

This technical report has been reviewed and is approved for publication.

  
THEODORE E. WIRTANEN  
Contract Manager

  
THOMAS P. ROONEY  
Chief, Geodesy & Gravity Branch

FOR THE COMMANDER

  
DONALD H. ECKHARDT  
Director  
Earth Sciences Division

This report has been reviewed by the ESD Public Affairs Office (PA) and is releasable to the National Technical Information Service (NTIS).

Qualified requestors may obtain additional copies from the Defense Technical Information Center. All others should apply to the National Technical Information Service.

If your address has changed, or if you wish to be removed from the mailing list, or if the addressee is no longer employed by your organization, please notify AFGL/DAA, Hanscom AFB, MA 01731. This will assist us in maintaining a current mailing list.

UNCLASSIFIED

SECURITY CLASSIFICATION OF THIS PAGE (When Data Entered)

REPORT DOCUMENTATION PAGE		READ INSTRUCTIONS BEFORE COMPLETING FORM
1. REPORT NUMBER AFGL-TR-84-0156	2. GOVT ACCESSION NO. <b>A150 687</b>	3. RECIPIENT'S CATALOG NUMBER
4. TITLE (and Subtitle) ACCURATE BASELINE DETERMINATION BY RADIO INTERFEROMETRY ON NAVSTAR GPS SATELLITE TRANSMISSIONS		5. TYPE OF REPORT & PERIOD COVERED Final Report April 1980 - June 1982
7. AUTHOR(s) R.L. Greenspan, A. Ng, J. Przyjemski, J. Veale, C.C. Counselman III, S.A. Gourevitch		6. PERFORMING ORG. REPORT NUMBER CSDL-R-1719
9. PERFORMING ORGANIZATION NAME AND ADDRESS C.S. Draper Laboratory, Inc. 555 Technology Square Cambridge, Massachusetts 02139		8. CONTRACT OR GRANT NUMBER(s) F19628-80-C-0040
11. CONTROLLING OFFICE NAME AND ADDRESS Air Force Geophysics Laboratory Hanscom AFB, MA 01731 Monitor: Theodore E. Wirtanen/LWG		10. PROGRAM ELEMENT, PROJECT, TASK AREA & WORK UNIT NUMBERS 61102F, 2309G1, 14ROBAA ILIR
12. REPORT DATE June 15, 1984		13. NUMBER OF PAGES 114
14. MONITORING AGENCY NAME & ADDRESS (if different from Controlling Office)		15. SECURITY CLASS. (of this report)  UNCLASSIFIED
16. DISTRIBUTION STATEMENT (of this Report)  Approved for public release; distribution unlimited.		15a. DECLASSIFICATION/DOWNGRADING SCHEDULE
17. DISTRIBUTION STATEMENT (of the abstract entered on Block 20, if different from Report)		
18. SUPPLEMENTARY NOTES R.L. Greenspan, A. Ng, J. Przyjemski, J. Veale are with The Charles Stark Draper Laboratory, Inc. Cambridge, MA 02139 C.C. Counselman III, S.A. Gourevitch are with the Massachusetts Institute of Technology Cambridge, MA 02139 <del>This research was supported by the Air Force In-House Laboratory Independent</del> Research Fund		
19. KEY WORDS (Continue on reverse side if necessary and identify by block number)  Interferometry, surveying, NAVSTAR, GPS, geodesy, distance measurements, multi- path		
20. ABSTRACT (Continue on reverse side if necessary and identify by block number)  The vector components of several baselines shorter than 100 meters have been measured by interferometric processing of NAVSTAR GPS satellite C/A-code broadcasts to an accuracy better than one centimeter, and a repeatability on the order of a few millimeters. Interferometric observables were extracted by two processing schemes. The first involved broadband cross correlation of the modulated GPS signals received by the antennas that define the unknown base- lines. The second approach uses GPS receivers at each antenna to reconstruct		

UNCLASSIFIED

SECURITY CLASSIFICATION OF THIS PAGE (When Data Entered)

UNCLASSIFIED

SECURITY CLASSIFICATION OF THIS PAGE (When Data Entered)

the satellite carrier signal from which phase differences can be measured. In both cases the interferometric baseline determinations were compared in a double-blind test with a conventional survey that was believed to be accurate to 2 mm (one-sigma) and 3 arcseconds.

Multipath was shown to be a significant effect only to the extent that reflecting structures might block the visibility of useful satellite signals. At the present time, the limit on extending the technique to precisely measure baselines exceeding 100 km is uncertainty in GPS satellite ephemerides. For baselines of intermediate length, the measurement performance is limited by uncertainties in tropospheric propagation delays.

The results of the experiments plus trends toward miniaturizing GPS equipment complete the demonstration that short baselines can be measured to sub-centimeter accuracy using highly portable equipment.

UNCLASSIFIED

SECURITY CLASSIFICATION OF THIS PAGE (When Data Entered)

ACCURATE BASELINE DETERMINATION  
BY RADIO INTERFEROMETRY ON  
NAVSTAR GPS SATELLITE TRANSMISSION



Accession For	
NTIS GRA&I	
DTIC TAB	
Unannounced	
Justification	
By	
Distribution/	
Availability Codes	
Dist	Avail and/or Special
A-1	

In this report we summarize results from two experiments which were designed to demonstrate that

- (1) Short baselines on earth can be measured in magnitude and direction within one (1) centimeter or less of error, using easily portable equipment, and that
- (2) This accuracy can be achieved by interferometric processing of the C/A-code signals currently broadcast by NAVSTAR GPS satellites.

1. EXPERIMENT I: Wideband Signal Processing

Experiment I was designed to demonstrate the extraction of interferometric observables by wideband cross-correlation of the GPS signals received at each end of a baseline. The experiment was developed when it became apparent that availability of the GPS receivers required for Experiment II would be delayed far beyond the original schedule.

Experiment I was planned to give the earliest possible credible demonstration of baseline determination using GPS signals. This was achieved by exploiting resources already in place at the Westford, Massachusetts site of the New England Radio Observatory Corporation (NEROC). These facilities included the MARK III VLBI processor which was used to produce "real-time" data representing eight lagged correlation products of the GPS receiving antenna outputs after filtering to a 2 MHz bandwidth encompassing the GPS C/A signal at 1.574 Ghz.

Other objectives of the experiment were to:

- (1) Demonstrate the effectiveness of the "MITES" antenna design (crossed-dipole mounted above a ground plane) which produces a nearly omnidirectional pattern from Zenith to within  $10^\circ$  of the horizon.
- (2) Demonstrate the effectiveness of a novel data-reduction algorithm which approximates a "maximum likelihood" estimator of the baseline vector components.
- (3) Explore the sensitivity of baseline determinations to oscillator instability and multipath to the extent that these corrupt the raw data.

The Steinbrecher Corporation fabricated the "MITES" antennas, RF subsystems, and frequency converters to condition the received signals for processing by the MARK III unit. Technical direction of Experiment I was subcontracted to MIT with Professor Charles C. Counselman III being the Principal Investigator. Program management was retained by Draper Laboratory. The final report prepared by Professor Counselman is provided in Enclosure 1. Unpublished project memoranda are provided in Enclosure 2. In these memoranda Professor Counselman concludes that, "at least when the satellite geometry is good, we can determine all three components of a baseline vector that's about 100 meters long within about 5 millimeters, one sigma, by MITES/GPS."

## 2. EXPERIMENT II: Narrowband Signal Processing

The concept behind Experiment II is to use a GPS receiver to make precise (albeit ambiguous) measurements of the instantaneous phase of each GPS carrier signal in the narrow bandwidth of the carrier tracking loop. Carrier phases from each end of a baseline being surveyed were then differenced for each satellite in view to form the interferometric observables. In a typical experiment the observables from four satellites were collected every 1.92 s during a period of about one hour. These samples were recorded on a computer disk and then processed on a minicomputer (TI 990/12) to estimate the baseline. Approximately 30 minutes of data were required to consistently resolve the phase



ambiguities that affected the baseline determination. The computer processing for a complete baseline determination required approximately one hour if every data point was used; experience showed that good results were obtained within 15-20 minutes of processing time if only every 10th sample was processed (19.2 s spacing).

The general nature of the results is that baseline measurements were repeatable at the level of 1 mm (standard deviation) in the horizontal components and 2 mm in the vertical component. The interferometric estimates agreed with a conventional steel tape and theodolite survey to within 3 millimeters on 8 of 9 components of three sample baselines and to within 6 millimeters on the ninth component.

Details of Experiment II and the analysis of its results are reported in the Symposium paper provided as Enclosure 3. The objectives of Experiment II, which were achieved, were:

- (1) To demonstrate the feasibility of sub-centimeter surveying of short baselines using easily portable, and relatively affordable observing equipment.
- (2) To assess the limits of baseline measurement accuracy and repeatability, and to identify the dominant error sources. With respect to the first objective we demonstrated:
  - (a) The independent measurement of three legs of a triangle with vector misclosure of (-2.2, -2.2, -0.3) mm in the coordinate directions (North, East, Up).
  - (b) Repeatability of one baseline measurement over four independent trials at the 1-sigma level of (0.76, 1.60, 2.40) mm in the (N, E, U) coordinates.
  - (c) The largest disagreement between any interferometrically measured baseline component and the corresponding component measured by a conventional survey was 5.7 mm. Five of the nine baseline components were measured with less than a 0.4 mm discrepancy. The nominal uncertainty of the conventional survey was given as 2 mm (one-sigma).

Efforts are currently underway under sponsorship of the Defense Department Advanced Research Project Agency to miniaturize GPS receivers

to approximately the size of a cigarette pack. It is easy to visualize that by the late 1980s short-baseline survey equipment will consist of a small portable antenna, an integrated RF/GPS receiver assembly, a crystal oscillator (with short-term stability exceeding one part in  $10^{12}$  over 100 sec), a digitizer/recorder or digitizer/modem unit, and power supplies. The electronics would be packaged in a small suitcase. Carrier phase measurements from the four satellites at a rate of 3 samples per satellite per minute over one hour of observations should be adequate to achieve sub-centimeter accuracy. An inexpensive storage medium or communication link capable of handling a total of about 1000 16-bit words for each baseline is all that is required to service data collection requirements.

With respect to the second objective, we observed that the post-fit residual error for measurement of a null (zero-length) baseline was 0.96 mm, compared to 0.55 mm, which was predicted from the tracking loop bandwidth and the estimated signal-to-source ratio. This is satisfactory agreement given the uncertainty in the signal-to-noise ratio measurement.

The post-fit residual error for baseline measurements using carrier phase observations was about 2 mm. Thus the residual was approximately twice that of the noise level of the observing system. The increase is associated to a great extent with periodic variations which affect all satellite observations in the same fashion. The period of these variations is about forty minutes (see Enclosure 3, Figure 7). The short-term scatter around the periodic variation is comparable to the noise-only residuals shown in Figure 5 of Enclosure 3). We attribute the periodic components to imperfect modeling of the differential expansion of the cables connecting each antenna to the data collection system, but this has not been conclusively established. If true, it would suggest that field survey equipment should use the smallest possible length of cable to connect the GPS antennas to the GPS receivers. At any rate, the 2 mm residual is well within our projected expectation.

Other factors that once were thought to limit the performance include oscillator drift and multipath. However, the combination of high quality quartz crystal oscillators and the use of a sequential GPS receiver which can sample the carrier phase to each satellite in view

faster than once per second combine to make oscillator drift a negligible problem. For example, if the Allen variance of the oscillator over 1 second is

$$\frac{\sigma_f}{f} = 10^{-12}$$

then the contribution of clock drift over 1 second to the differential measurement of carrier phase is  $\sqrt{2} \times 10^{-12} f$  cycles rms, which is less than 0.003 cycles (0.6 mm) at the GPS L1 frequency. At this level, clock drift would be about five times less significant than thermal noise. If one wished to economize by using a lower quality oscillator, then some of the increased frequency jitter could be offset by faster cycling among GPS satellites. For example, one commercially available GPS receiver cycles among four satellites every 20 ms.

The primary effect of multipath will probably be blockage of satellite visibility, rather than distortion of signal phase measurements. Enclosure 4 presents some calculations based on an analysis by Counselman which predict the carrier phase fluctuations attributable to a reflecting surface mounted in the vicinity of a "MITES" antenna. The specific configuration considered in that analysis was set up in an experiment to check the theoretical predictions. The results (compare Figure 10 of Enclosure 4 with Enclosure 3) were qualitatively consistent for all satellite observations and within 10% error for the satellite that suffered the greatest multipath effects. We conclude that the effects of multipath will average out of any series of GPS carrier phase measurements taken over a half hour or longer interval; moreover, any reflecting surfaces that are greater than 1000 feet from the antenna (one C/A-code "chip") will produce multipath that is reduced below thermal noise level by the GPS signal processing.\* Therefore multipath should not be a significant problem for well engineered observing systems with good siting of the receiving antennas. Exceptions might occur if one had to measure a baseline extending from a large structure, or in the vicinity of metal towers.

\*One could achieve immunity to closer sources of multipath by processing GPS P-code signals, for which the "chip" width is equivalent to a 100 foot span. The costs of a P-code receiver would be higher than for a C/A-code receiver.

It appears that the fundamental limits of baseline measurement accuracy will be thermal noise in the GPS receiver, ephemeris errors in location of GPS satellites and excess propagation delay. If the uncertainty in satellite location is  $\Delta p$  (meters), then the resulting uncertainty  $\Delta l$  in measuring a baseline whose length is  $l$  is approximately

$$\Delta l = \frac{l \Delta p}{26 \times 10^6}$$

Baseline measurement is most sensitive to "along track" errors in satellite locations and less sensitive to radial errors. For current GPS broadcast ephemerides that are no more than 1 day old, the "along track" error (one-sigma) is about 20 meters; hence,  $\Delta l/l \approx 10^{-6}$ . Clearly, improvement in ephemeris modeling will be needed to preserve centimeter level accuracy at distances in excess of about 10 km.

Propagation delays suffered by GPS signals as they traverse the ionosphere and troposphere en route from satellites to ground terminals are highly correlated at antennas separated by short distances. Thus, the effects of these delays are essentially cancelled by phase-difference processing. As baseline lengths increase, the delays tend to decorrelate. The impact of ionospheric errors may be made negligible by dual-frequency interferometry on GPS  $L_1$  and  $L_2$  frequencies.

Because uncertainties in modeling tropospheric propagation delays vary from about 10 cm rms at 90° elevation to about 50 cm rms at 20° elevation,\* and because there can occasionally be large variations in pressure, temperature, and humidity over short distances, tropospheric errors could introduce 1-cm baseline-measurement errors with baselines as short as 1 km. However, when weather conditions are quite uniform and dry at both ends of the baseline (and along the propagation paths), and when meteorological parameters are measured and incorporated in the propagation model, baseline-measurement errors presumably can be maintained to less than 1 cm for baselines much longer than 1 km. Under good weather conditions, the baseline-measurement errors due to tropospheric effects

\*Using measured values of the surface index of refraction.

can be maintained within about 10 cm for arbitrarily long baselines.\*\* For long baselines, the 1 part-per million errors due to GPS ephemeris uncertainties become dominant.

3. CONCLUSIONS:

The two experiments carried out under this program have demonstrated the use of GPS signals for the measurement of short baselines with accuracies of better than 1 cm rms. With the continued evaluation of electronic technology, the cost of interferometry equipment for such measurements is expected to drop dramatically in the near future, so that both of the described techniques will be seen to be economically attractive as compared with alternative surveying techniques.

The second technique, utilizing GPS C/A-code receivers, offers the advantage of providing absolute, as well as relative, positioning data. Moreover, with the projected application of such receivers to automobiles and other mass markets, the associated equipment costs are expected to become particularly attractive.

\*\*As indicated by typical VLBI results reported since 1978. For example, see "Analysis of Lunar Laser Ranging Data and Performance and Analysis of VLBI Observations for Geodetic Purposes," AFGL-TR-81-004, C.C. Counselman III, et al., 27 November 1980.

ENCLOSURE 1

FINAL REPORT TO THE CHARLES STARK DRAPER LABORATORY  
from the  
Massachusetts Institute of Technology  
(October 1981)

FINAL REPORT  
to the  
CHARLES STARK DRAPER LABORATORY  
from the  
MASSACHUSETTS INSTITUTE OF TECHNOLOGY

Subcontract DL-H-182631

Principal Investigator:  
Charles C. Counselman III  
Associate Professor of Planetary Science

October 31, 1981

Distribution: R. L. Greenspan, CSDL, MS 92  
C. A. Morse, MIT, E19-702  
E. Raphael, MIT, 54-620

Under this subcontract M.I.T. planned, performed, and analysed radio interferometric observations of NAVSTAR/GPS satellites.

In a 15-page memorandum dated June 11, 1980, to R. L. Greenspan from C. C. Counselman III and S. A. Gourevitch, we described the observational data that we expected to acquire, and some algorithms that we intended to use for analysis of these data.

In a second 15-page memorandum dated August 13, 1980, to R. L. Greenspan from C. C. Counselman III and S. A. Gourevitch, we further described the data-analysis algorithms.

In a 19-page memorandum dated September 30, 1980, to R. L. Greenspan from C. C. Counselman III and S. A. Gourevitch, we reported on a computer simulation of interferometric observations in which multipath effects were included.

Actual observations of the GPS satellites were performed at Haystack Observatory in December, 1980, and subsequently were analyzed to determine interferometer baseline vectors. These experiments and the initial analysis results were reported at the 1981 Spring meeting of the American Geophysical Union by C. C. Counselman III. An abstract of this presentation, entitled "Accuracy of baseline determinations by MITES assessed by comparison with tape, theodolite, and geodimeter measurements," was published in Eos (Trans. AGU), vol. 62, p. 260, on April 28, 1981.



Another presentation was made by C. C. Counselman III to the 1981 IEEE International Geoscience and Remote Sensing Symposium, and appears on pp. 219-224 of vol. 1 of the Symposium Digest.

Our data-analysis algorithm, multipath simulation results, and a few actual experimental results were also published in a journal article by C. C. Counselman III and S. A. Gourevitch, entitled "Miniature interferometer terminals for earth surveying: ambiguity and multipath with global positioning system," appearing in IEEE Transactions on Geoscience and Remote Sensing, vol. GE-19, pp. 244-252, October 1981.

The results of a comparison of our GPS radio interferometry determinations of a triangle of baselines with an independent determination by conventional survey methods were given in detail in a 9-page memorandum to R. L. Greenspan from C. C. Counselman III dated September 30, 1981.

Copies of all of the documents mentioned have already been provided to Dr. R. L. Greenspan, who was the technical monitor of this subcontract.

No inventions were made in work under this subcontract.

ENCLOSURE 2

DATA PROCESSING ALGORITHMS FOR  
EXPERIMENT I--WITH THE HAYSTACK MARK III  
BACK END and CORRELATOR

DEPARTMENT OF EARTH AND PLANETARY SCIENCES

MASSACHUSETTS INSTITUTE OF TECHNOLOGY  
CAMBRIDGE, MASSACHUSETTS 02139

54-626  
June 11, 1980

Memorandum

To: R. L. Greenspan

From: C. C. Counselman and S. A. Gourevitch

Subject: Data Processing Algorithms for Experiment I--  
With the Haystack Mark III Back End and Correlator

1. Introduction

In this memorandum we describe the data that we expect to acquire, and algorithms that we expect to use for the analysis of this data, in the "Experiment I" described in Section 4.1 of your DL Intralab Memo no. 94100-01A. In this experiment, signals received from GPS satellites by antennas in the Haystack Observatory parking lot will be processed by Haystack's Mark III VLBI correlator.

2. Block Diagram

Figure 1 shows a block diagram of some of the equipment to be used in the experiment. The GPS  $L_1$  signals received by one antenna, at nominal signal carrier frequency 1575.42 MHz, with C/A and P code modulation, and with Doppler shifts, will be converted in two stages of mixing to a "video" frequency band, nominally 0-2 MHz, and sampled once per 0.25  $\mu$ sec to yield a series of samples  $x_i$  at uniformly-space times  $t_i$ . From another antenna in a similar way we obtain a series of samples  $y_i$  at essentially the same times. Before being

sampled, the signals are clipped so that only their signs are preserved; that is, the sample values are  $\pm 1$  and can be represented by just one bit per sample.

A single video passband only 2 MHz wide can contain most of the C/A modulation power but only about 20% of the P power. In order to capture more--in fact most--of the P power, we will use several 2-MHz-wide video channels in parallel, each with a different second local oscillator frequency. These frequencies will be spaced by integer multiples of 2 MHz. To keep the present discussion simple, however, we will pretend that there is only one channel, and we will ignore the problem of how to combine the data from different channels. (This is an old problem, with a known and straightforward solution.)

Not shown in Figure 1 is the system with which the sampled, time-tagged, one-bit data are formatted, recorded on magnetic tape, and later reproduced for processing by the Mark III correlator.

### 3. Mark III Correlator

The Mark III correlator computes eight values of the crosscorrelation function between the two sampled signals, for eight discrete values of delay offset between the sample streams. It computes, once every 2 seconds of time  $t$ , the 2-second averages

$$r_l(t) = \frac{1}{N} \sum_i x_i y_{i+l} ; \quad l = -4, -3, -2, \dots, +3$$

(successive)

where  $N = 8 \times 10^6$  is the number of products  $x_i y_{i+l}$  summed; the

time span of 2 seconds ( $= 8 \times 10^6 \times 0.25 \mu\text{sec}$ ) is centered on the time  $t$ . For simplicity, we are deliberately suppressing the book-keeping details, as well as some calculus that shows that, with sufficient accuracy,  $r_\ell(t)$  computed from one-bit samples is almost equivalent to what you would get had you had an infinite number of bits. (The only significant lack of equivalence is that, with one bit, the signal-to-noise ratio is reduced by a factor of  $2/\pi$ .)

#### 4. Expected Form of $r_\ell$

Ignoring some of the "noise" effects, the expected functional form of  $r_\ell$  is

$$r_\ell = \sum_{k=1}^K A_k \cdot \Delta(\tau_k - \ell\delta) \cdot \cos[\omega_c \tau_k - \phi_{LO} - (\omega_c - \omega_{LO})\ell\delta], \quad (\text{Eqn. 1})$$

where  $k$  is the index number of a satellite (several may be visible simultaneously);  $A_k$  is the ratio of the peak (at the carrier frequency) received power spectral density of the  $k$ th satellite signal to the background noise power spectral density;  $\Delta(x)$  is a (triangle) function equal to the autocorrelation function of the C/A modulation (we ignore for now the P modulation):

$$\Delta(x) = \begin{cases} 1 - 1.023 \text{ MHz} \cdot |x| \\ \text{or} \\ 0 \end{cases}, \text{ whichever is greater;} \quad (\text{Eqn. 2})$$

$\tau_k$  is the group delay difference between the  $k$ th satellite signals at the  $x$  and  $y$  samplers;  $\delta$  is the inter-sample time interval, equal to  $0.25 \mu\text{s}$ ;  $\omega_c$  is the transmitting carrier

frequency, in radians per second, assumed the same for all transmitters;  $\phi_{LO}$  is the difference between the phases of the two different receivers' local oscillators;  $\omega_{LO}$  is the (radian) frequency of the local oscillators, assumed the same for both receivers; the difference  $\omega_c - \omega_{LO}$  is equal to  $2\pi \times 10^6$  radians second. The time-variations of the various terms in Eqn. 1 have not been shown explicitly, but need to be kept in mind. We discuss each term briefly.

The "amplitude"  $A_k$  will vary slowly due to the variation of the receiving (and to a lesser extent, the transmitting) antenna gain with elevation angle, coupled with the motion of the satellite in the sky. The variation will be by less than a factor of about 4 for elevation angles from  $10^\circ$  to  $90^\circ$ . For elevation angles above about  $20^\circ$ , our antenna has at least unity gain and the received peak C/A power spectral density should be at least  $10^{-22}$  watt/Hz. The noise power spectral density with a 5 db noise figure will be about  $1.25 \times 10^{-20}$  watt/Hz. Therefore, we can expect  $A_k \approx 8 \times 10^{-3}$  for the C/A modulation. For the P modulation, which we are temporarily ignoring,  $A_k \approx 4 \times 10^{-4}$ .

The group delay  $\tau_k$  combines the free-space propagation delay and delays within the receivers and cables. All ingredients of  $\tau_k$  are differenced between the x and y systems. The greatest contributor to  $\tau_k$  and to its time-derivative is likely to be the free-space delay. The magnitude of this delay contribution will be of the order of the baseline length measured in light-time; that is, for example, about 300 ns for a 100-meter baseline. The delay rate,  $d\tau_k/dt$ , will be of the

order of the baseline length times the apparent satellite orbital angular velocity, about  $1.4 \times 10^{-4}$  radian/second maximum. The peak delay rate for a 100-meter baseline is thus about  $4 \times 10^{-11}$  sec/sec, and the corresponding "fringe rate",  $\omega_c \dot{\tau}_k$ , about 0.4 radian/second. The corresponding minimum fringe rotation period is about 15 seconds, and the maximum amount of rotation during one 2-second integration is  $\sim 0.8$  radian  $\approx 47$  degrees, which is just tolerable: the coherence loss due to the rotation during the integration is about 3%.

The difference between the x and y receiver local-oscillator phases (and any other instrumental contributions to the phase delay in excess of the group delay  $\tau_k$ ), represented by  $\phi_{LO}$ , is expected to be a slowly varying function of time, changing by less than  $\omega_c \tau_k$  does over any relevant time interval. All of the instrumental phase drift is, by definition, lumped into the time-variation of  $\phi_{LO}$ . Thus,  $\omega_{LO}$  is a constant in Eqn. 1.

It is also permissible to regard  $\omega_c$  as a constant. The actual satellite carrier frequencies are unlikely to deviate from the nominal value of 1,575.42 MHz by more than 1 kHz. The maximum magnitudes of  $\tau_k$  and of  $l\delta$  will be  $\leq 1$   $\mu$ sec. Therefore the argument of the cosine function in Eqn. 1 cannot be in error by more than about  $10^{-3}$  cycles of phase by virtue of the error in the assumption of constant  $\omega_c$  equal to the nominal value.

Since the magnitude of  $\tau_k$  will be limited by the baseline length, for example to about 500 ns for a 500-foot baseline, the peak of the triangle function  $\Delta(\tau_k - l\delta)$  will occur in this example for  $|l| \leq 2$ . (Recall that  $\delta = 250$  ns.) The

half-width of the base of the triangle is approximately 1000 ns; therefore, even with an extreme value of  $\tau_k$ , most of the area of the triangle, corresponding to most of the "weight" of information in the  $r_l$ , will be contained within the range  $-4 \leq l \leq +3$  for which  $r_l$  is computed by the Mark III correlator. If we should wish to use a baseline much longer than 500 feet, we would have two options for extending the range of  $l\delta$ . The first option is to increase  $\delta$ . This can be done in factors of 2 (to a maximum  $\delta = 4 \mu s$ ), with a concomitant reduction of the bandwidth of a video channel. The second, more attractive, option is to make repeated passes of the tape-recorded data through the correlator. On each pass, the  $r_l$  are computed for eight values of  $l$ , but a different set of eight values can be obtained on different passes. (However, on each pass the eight values must be successive integer values.)

The form of  $r_l$  as a function of  $l$ , for a single value of  $k$ , for  $\tau_k$  equal to zero, and for two different values of  $\phi_{LO}$ , equal to 0 and  $\pi/2$ , is shown in Figure 2. With the summation over  $k$  and with a variety of values of  $\tau_k$ , obviously the picture can become very messy. With a baseline length under 500 feet, all the triangle functions overl and with the various  $\tau_k$ 's differing by "random" amounts, the relative phases of the cosines are random. Extracting order from this overlapping mess is the job of our data analysis algorithm.



### 5. Noise

The extraction must be done in the presence of significant amounts of background noise, which really is random. Again considering that only one satellite is present, to simplify the discussion, we can show that the signal-to-noise ratio at the expected peak of  $r_k$  (that is, with  $\ell\delta = \tau_k$  and with  $\omega_{LO}\ell\delta = -\phi_{LO}$ ) is

$$\text{SNR} = \frac{2}{\pi} \cdot N^{\frac{1}{2}} \cdot A_B \quad (\text{Eqn. 3})$$

where the factor  $(2/\pi)$  represents the one-bit clipping loss,  $N$  is the number of correlated pairs of samples (equal to  $8 \times 10^6$  for a single 2-MHz video channel and a 2-second integration time), and  $A_B$  is the ratio of the total signal power contained in the channel bandwidth to the noise power in this band. For the C/A modulation and a 2-MHz bandwidth,  $A_B \approx 0.5$  times the peak signal-to-noise power spectral density ratio represented by  $A_k$  in Eqn. (1). Thus, the expected single-satellite C/A SNR will be  $\sim 7$  for the bandwidth and integration time given above. (For the P signal, the combination of the 20-times-lower peak power spectral density and the 10-times-higher bandwidth reduces the SNR by a multiplicative factor of  $20^{-1} \cdot 10^1 \approx 0.16$ , if the number of video channels used is increased from 1 to 10 in order to capture the same fraction of the modulation power. It should be noted, however, that the best SNR is obtained with less than 20 MHz bandwidth for the P modulation, and less than 2 MHz for the C/A.)

The standard deviation of the error in the estimate of the "fringe phase" ( $\omega_c \tau_k - \phi_{LO}$ ), in radians, is just the

reciprocal of the SNR, in the single-satellite, noise-limited case.

The standard deviation  $\sigma_\tau$  of the error in the estimate of the group delay,  $\tau_k$ , is approximately independent of the video channel bandwidth or the number of channels combined, as long as the combined bandwidth exceeds about  $1.6f_b$ , where  $f_b = 1.023$  MHz for the C/A, and  $f_b = 10.23$  MHz for the P modulation. We find that

$$\sigma_\tau \approx \frac{\pi}{4} A_k^{-1} f_b^{-2} T^{-\frac{1}{2}}, \quad (\text{Eqn. 4})$$

where  $T$  is the integration time used. Thus, for the C/A signal alone,

$$\sigma_\tau (\text{C/A}) \approx 100 \text{ ns} \cdot T_{\text{seconds}}^{-\frac{1}{2}}, \quad (\text{Eqn. 5})$$

and for the P signal alone,

$$\sigma_\tau (\text{P}) \approx 62 \text{ ns} \cdot T_{\text{seconds}}^{-\frac{1}{2}}, \quad (\text{Eqn. 6})$$

where  $T_{\text{seconds}}$  is the integration time in seconds. According to these formulae, there is not a very great net advantage to using the wider-bandwidth P code modulation, as opposed to the C/A. The advantage of the 10 times wider bandwidth is largely canceled by the disadvantage of the lower signal-to-noise ratio. In practice, one expects, the wider-bandwidth approach would pay off because one would not be trying to "split a chip" so finely. Therefore, one would not be as susceptible to systematic errors such as those due to multipath.

## 6. Separating Satellites

From the preceding discussion it should be apparent that the worse problem in the data analysis for the planned

experiment is likely not to be background noise, but rather will be interference between satellites. The interference problem forces us to use a rather complicated algorithm in order to extract the best estimate of the baseline vector, etc., from the  $r_\ell$  data. We are considering two different, basic, approaches, which we now outline.

### 7. Traditional Approach

The traditional approach to the analysis of VLBI correlation data (as described, for example, by A. R. Whitney et al., A very-long-baseline interferometer system for geodetic applications, Radio Science, 11, 421-432, 1976) makes use of a priori information on the baseline vector, the positions and motions of the sources, etc., in order to "counter-rotate" the "fringes" and to shift the y signal in group delay relative to the x signal. If we have accurate information on the baseline and the satellite ephemerides in our experiment, then in our data analysis we can make the fringes "stand still" for any one satellite at a time. That is, the contribution of one satellite to the sum over  $k$  in Eqn. 1 can be, in effect, held nearly constant while the contributions from the other satellites "rotate". (Actually, since Eqn. 1 contains only the real-valued cosine function and not the complex exponential usually seen, one might prefer to say that our fringes don't rotate, they just travel along the  $\ell$  axis in Figure 2, as the fringe phase advances. We shall use the traditional jargon.) If the fringe rate difference between the satellite chosen to stand still and another, potentially interfering, satellite

is sufficiently high, the interfering fringes will wash out, or average to zero, well enough over the integration time.

This approach has two drawbacks in the context of our experiment. First, it requires fairly accurate information on the baseline vector; this information could be expensive to get, especially if we are going to move our antennas many times. For the a priori information to be useful in discriminating between satellites, its fractional uncertainty must be small. The effective interference attenuation factor is approximately equal to the fractional (dimensionless) uncertainty in the a priori prediction of the fringe rate difference. Probably we would need to have the magnitude of the a priori uncertainty of our baseline vector be less than a few percent of the baseline length. Also, since the fringe rate difference between two satellites would occasionally be zero or nearly zero, there would be times when the two satellites' fringes were difficult or impossible to distinguish within reasonable integration times. (Some advantage could be taken of group delay resolution, since the group delay difference between two satellites will be relatively large when the delay rate difference is small. However, this advantage will be marginal when the group delay difference, which can never exceed twice the baseline length in light-time, is less than the C/A code "chip" width, of about 1,000 ns.) Finally, the requirement of substantial a priori inputs might be considered philosophically awkward, in the sense

of "What good is your system if it needs to know the answer in advance?"

The second drawback, an extension of the first, is that, since the coherent integration time required to filter out the interference is inversely proportional to the fringe rate difference, the time required is inversely proportional to the baseline length and becomes unreasonably large for baselines shorter than about 100 feet. With 100-foot length, the maximum possible fringe rate is about 0.02 Hz, and a substantial fraction of the time there will be two satellites with fringe rates differing by as little as one-tenth the maximum, or 0.002 Hz. The beat period in this case is 500 seconds, and an integration period several times longer than this beat period will be required for effective separation of the two satellites.

We conclude that we should take an approach different from the traditional one.

### 8. C<sup>4</sup> Method

We suggest an approach based upon direct maximization of the cross-correlation of the observed cross-correlations  $r_{\ell}(t)$  with a theoretical model. We dub this approach the C<sup>4</sup> method. The idea is elementary. Using Eqn. (1), a set of theoretical values  $\hat{r}_{\ell}(t)$  may be calculated from any set of assumed, trial values of the unknown parameters: the three (constant) components of the baseline vector in an Earth-fixed coordinate system, and the (also assumed constant) instrumental group delay. These four unknowns are fundamental, and enter Eqn. (1) through  $\tau_k$ . As a first approximation,

the amplitudes  $A_k$  may be treated as constants, or at least as knowns, calculated from the elevation angles and the nominal antenna gain patterns. The quantities  $\delta$ ,  $\omega_c$ , and  $\omega_{LO}$  are constants known with more than sufficient accuracy. The phase  $\phi_{LO}$  is unknown but, because it is not a function of  $k$ , it may be suppressed by replacing the cosine function in  $\hat{r}_\ell(t)$  with the complex exponential, and then maximizing the magnitude of the complex correlation between  $r_\ell(t)$  and  $\hat{r}_\ell(t)$ . It is necessary, in order to suppress  $\phi_{LO}$  exactly, that  $\phi_{LO}$  be constant over the time interval of the "C" operation. To summarize, we shall compute

$$\hat{\tau}_k = \hat{\tau}_k(\hat{\vec{B}}, \hat{\tau}_0, t), \quad k = 1+K, \quad (\text{Eqn. 7})$$

where  $\hat{\tau}_k$  is a function of the trial value, or "guess",  $\hat{\vec{B}}$  of the baseline vector  $\vec{B}$ , the trial value  $\hat{\tau}_0$  of the instrumental group delay  $\tau_0$ , and the known time,  $t$ . Then we compute the complex correlation

$$C = C(\hat{\vec{B}}, \hat{\tau}_0) = \int \sum_{\ell} r_{\ell}(t) \hat{r}_{\ell}(t) dt \quad (\text{Eqn. 8})$$

where the time span of the integration (really a sum over discrete 2-second averages) can be quite long, perhaps the duration of the entire satellite "pass," and where

$$\hat{r}_{\ell}(t) = \sum_{k=1}^K \hat{A}_k(t) \cdot \Delta[\hat{\tau}_k(t) - \ell\delta] \cdot \exp[j\omega_c \hat{\tau}_k - j(\omega_c - \omega_{LO})\ell\delta], \quad (\text{Eqn. 9})$$

in which  $j$  is

the square root of minus one. Finally, the desired estimates of the baseline vector and  $\tau_0$  are the values of  $\hat{\vec{B}}$  and  $\hat{\tau}_0$  that maximize  $|C|^2 = C^*C$ .

With this algorithm, all of the difficulties of the traditional algorithm are hidden in the problem of finding the maximum of  $C^*C$ . A priori information is no less useful; it serves to limit the volume in 4-parameter space that needs to be searched to find the maximum. We believe that we can make the search sufficiently efficient, computationally, that this approach will be feasible. We hope to present our ideas, and some test computation results, soon.

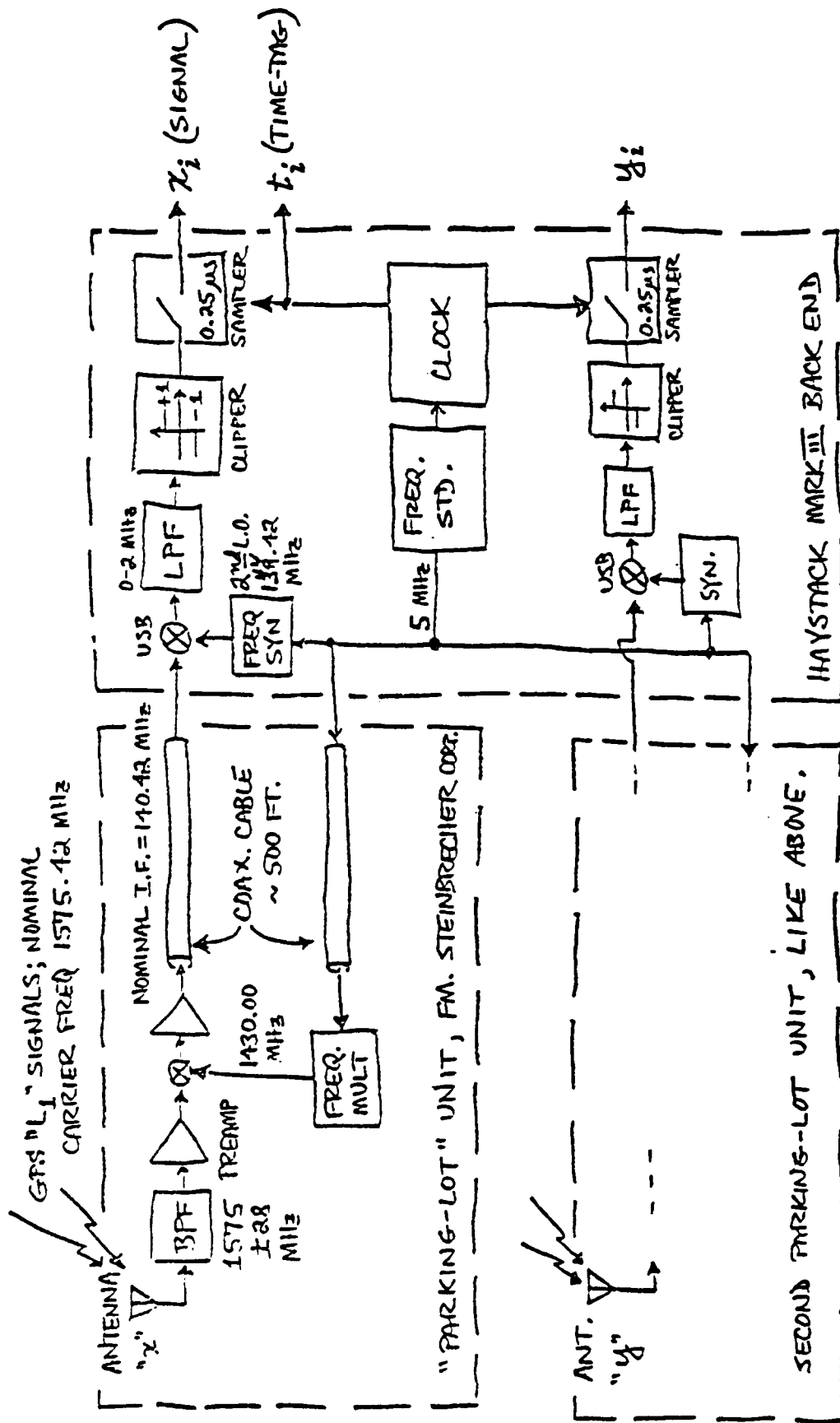


FIGURE 1. BLOCK DIAGRAM OF EQUIPMENT TO BE USED IN EXPERIMENT I. THE INTERFEROMETER BASELINE VECTOR TO BE DETERMINED EXTENDS FROM ANTENNA "x" TO ANTENNA "y".



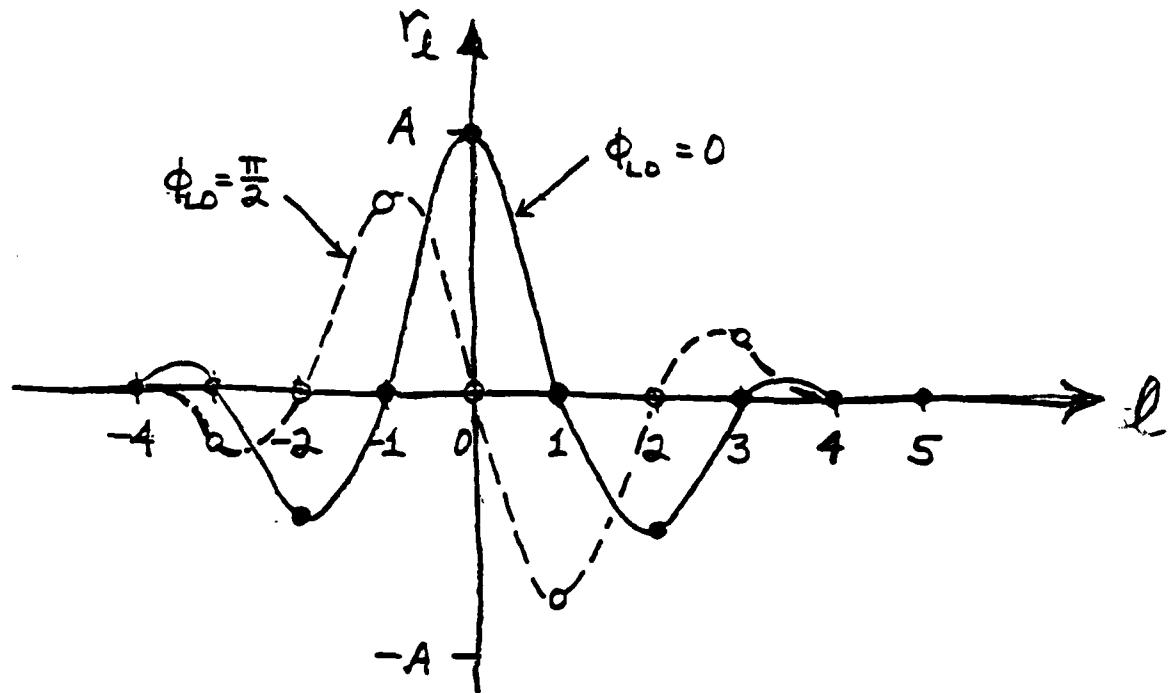


FIGURE 2. FORM OF THE CROSSCORRELATION  $r_l$  vs.  $l$  FOR  $\tau = 0$  AND FOR  $\phi_{L0} = 0$  AND  $\pi/2$ .

August 12, 1980

MEMORANDUM

TO: R. L. Greenspan

FROM: C. C. Counselman III and S. A. Gourevitch

SUBJECT: Data Processing Algorithms for Experiment I, Continued

REFERENCE: Memorandum from us to you dated 6/11/80, "Data Processing Algorithms for Experiment I ..."

I. Introduction

When we left our hero, he was estimating the unknown baseline vector,  $\underline{B}$ , by analysis of the data produced by the Mark III processor. These data consisted of a time series of sets of eight samples of the real-valued crosscorrelation function,  $r_l(t_i)$ ; here, the subscript  $l$  ( $= -4, -3, \dots, +3$ ) is an integer representing the number of discrete, 250-nanosecond "lags" by which the signal from the "x" antenna is delayed in the processor, relative to the signal from the "y" antenna; and  $t_i$  is the  $i$ -th in the series of times, uniformly spaced with  $\Delta t = t_{i-1} - t_i = 2$  seconds, at which the processor puts out data. We had derived theoretically the expected form,  $\hat{r}_l(t_i)$ , of the correlations as a function of a trial value,  $\hat{\underline{B}}$ , of the baseline vector, and a trial value,  $\hat{\tau}_0$ , of the instrumental group delay. The algorithm proposed for estimation of  $\underline{B}$  was to maximize the magnitude of the correlation,  $C$ , between the observed correlations,  $r_l$ , and the theoretical correlations,  $\hat{r}_l$ . (Note that, whereas the observed values,  $r_l$ , are real-valued, the theoretical values,

$\hat{r}_1$ , are complex; thus  $C$  is complex.) The magnitude  $|C|$  is a function of four variables:  $\hat{x}$ ,  $\hat{y}$ ,  $\hat{z}$ , and  $\hat{r}_0$ , of which the first three are the Cartesian components of  $\hat{B}$ , and the fourth,  $\hat{r}_0$ , is a "nuisance" parameter. Fortunately,  $|C|$  is a relatively weak function of  $\hat{r}_0$ ; thus, the essential computational problem is to find the maximum of a function of only (!) three variables,  $\hat{x}$ ,  $\hat{y}$ , and  $\hat{z}$ .

The purpose of the present memorandum is to document our further investigation of this algorithm for baseline estimation. For simplicity, the description will be chronological.

## II. Ambiguity Mapping

In general,  $|C|$  does not have a unique maximum. In addition to the principal, or global maximum (the highest) which, hopefully, corresponds to the desired estimate of  $B$ , there are many secondary, local maxima (with lesser values) that correspond to possible spurious estimates. We refer to all the maxima as "ambiguities," and to the process of identifying the principal maximum as "resolving the ambiguity" in the estimate of the baseline vector. We call  $|C|$  the "ambiguity function;" a map of  $|C|$  as a function of  $\hat{B}$  is called an "ambiguity map."

To be confident of finding the principal maximum, and correctly resolving the ambiguity, one must search a volume of  $\hat{B}$  space that encompasses the position of this maximum -- the desired estimate of  $B$ . This volume must also be sampled at "grid" points spaced finely enough to ensure that the desired estimate is not overlooked. Finally, one must ensure by the design of the

experiment that even in the presence of noise and other errors, random and systematic, the height of the maximum associated with the desired estimate will exceed that of the highest other maximum in the volume searched.

In our experiment, additive white noise is unlikely to be as important as systematic errors due to multipath interference and local-oscillator phase drifts. We will discuss these error sources in some detail later. For the moment, we merely observe that in practice we will probably need to search a volume of the order of a few cubic meters, set by the uncertainty of available a priori information on the baseline vector; and the grid spacing will be between about 10 and 30 centimeters. The appropriate grid spacing is set by the L1 wavelength, 19 centimeters, which determines the characteristic width of the maxima of the ambiguity function.

How easy it will be to distinguish the correct ambiguity in practice will depend not only upon the magnitudes of the errors present, but also upon the schedule of observations. The length of time spanned by the observations is particularly critical. How long is enough? To attempt to answer this question in advance of the performance of actual experiments, we have begun to simulate experiments in the computer. Figure 1 shows a map of  $|C|$  for computer-simulated VLBI observations of the existing six GPS satellites with a pair of MITES antennas separated by 30 meters along a horizontal, East-West line, located near  $72^\circ\text{W}$ . longitude,  $41^\circ\text{N}$ . latitude. The time span of the observations was

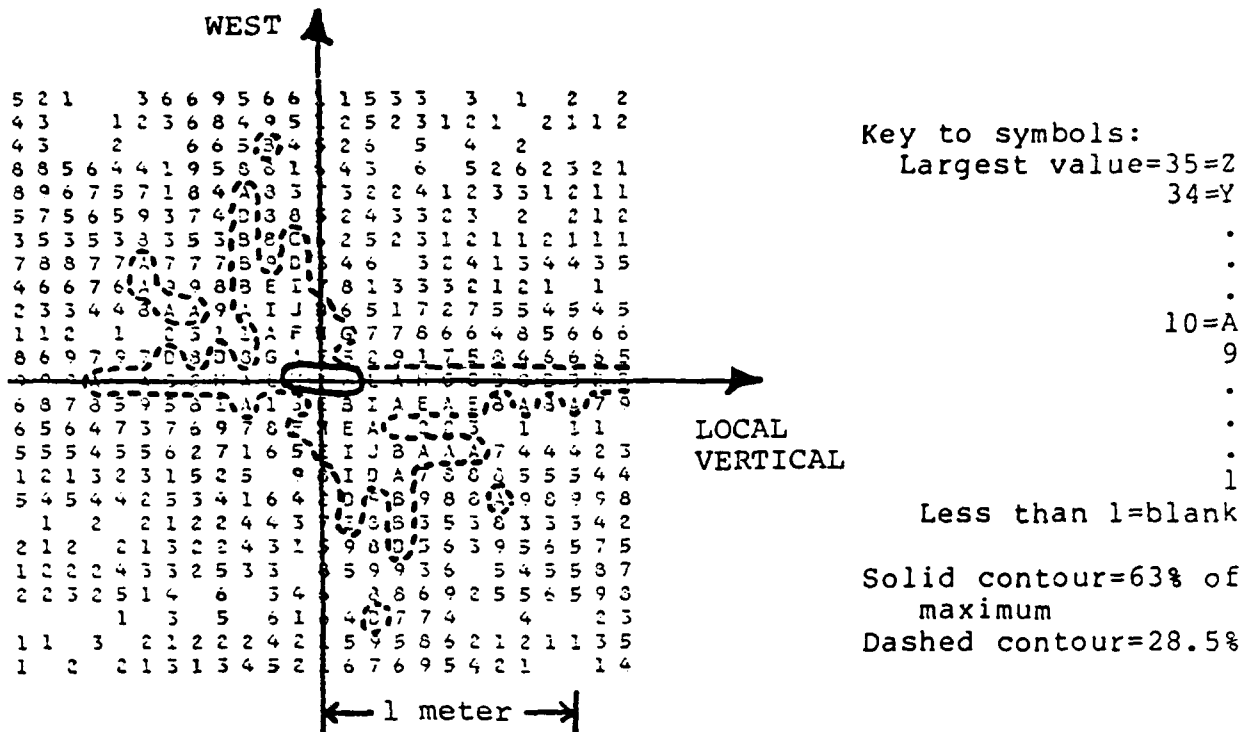


Figure 1. Ambiguity map for 1-hour experiment.

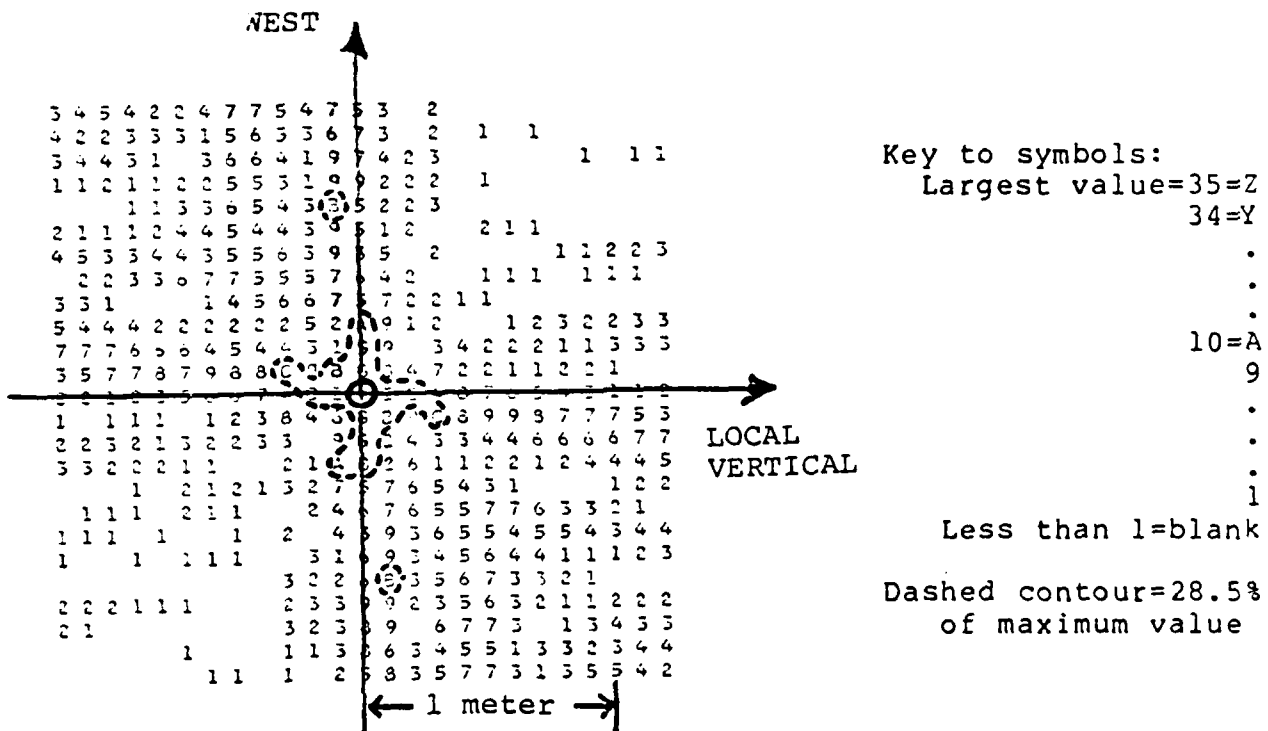


Figure 2. Ambiguity map for 2-hour experiment.

1 hour. This map is of a particular vertical plane that contains the true value of the baseline vector at the origin. No significant amount of additive noise, oscillator phase drift, multipath interference, or other error corrupted the simulated observations, which were of only the L1 (1575.42 MHz) signals. Figure 2 is like Figure 1, except the period of observation is two hours instead of one. The normalized heights of the secondary maxima are significantly reduced by the doubling of the period of observation.

### III. Broken Coherence

In the simulations that yielded the ambiguity maps shown in Figures 1 and 2, it was assumed that the local oscillator phase, although unknown, was constant. We have also simulated one- and two-hour experiments in which we assumed the oscillator phase had one constant unknown value for 800 seconds, another statistically independent constant unknown value for the next 800 seconds, another independent value for the next, and so on. Operationally, this meant that we summed the complex correlation,  $C$ , separately for each 800-second sub-interval of observations. The magnitudes of the complex sub-sums were then summed together to yield the value plotted in the ambiguity map. Thus, the coherence of the summation was broken every 800 seconds. Such a procedure would be used to process the observations from a real experiment if it were believed that the oscillators remained "coherent" -- that is, their phases remained constant within approximately 1 radian -- for about 800 seconds, but that they

could not be relied upon to remain coherent for a longer time. (Note that a phase drift rate of 1 radian per 800 seconds at 1575.42 MHz corresponds to a fractional offset in frequency of about  $1.26 \times 10^{-13}$ .) The effect of this "broken coherence" in the summation is illustrated in Figures 3 and 4 for the 1-hour and the 2-hour experiments, respectively. Mainly, the general level of background clutter seems to have been raised, and now there are many secondary peaks with heights about two-thirds of the principal-maximum height. It should also be noted that the ratio of the principal-maximum height to the peak background height is not much greater for the 2-hour experiment than for the 1-hour one.

Finally, in Figure 5 we again display the ambiguity function for the 2-hour experiment in which the coherence of the summation was broken every 800 seconds, but in this map the scale has been reduced (the grid spacing has been increased) by a factor of 3, relative to Figure 4. Our purposes in showing this reduced-scale map are two: first, to demonstrate that no important maxima were lurking just offstage in Figure 4; and second, to indicate the feasibility of using a two-step, coarse and fine, search procedure to locate the global maximum in a very large volume. A volume of, say, 200 cubic meters might be searched with a coarse grid of 30-centimeter (perhaps even larger) spacing in order to define one or more smaller regions of volume  $\sim 1$  cubic meter, in which the ambiguity function had significantly higher-than-average value. These smaller regions might then be examined with

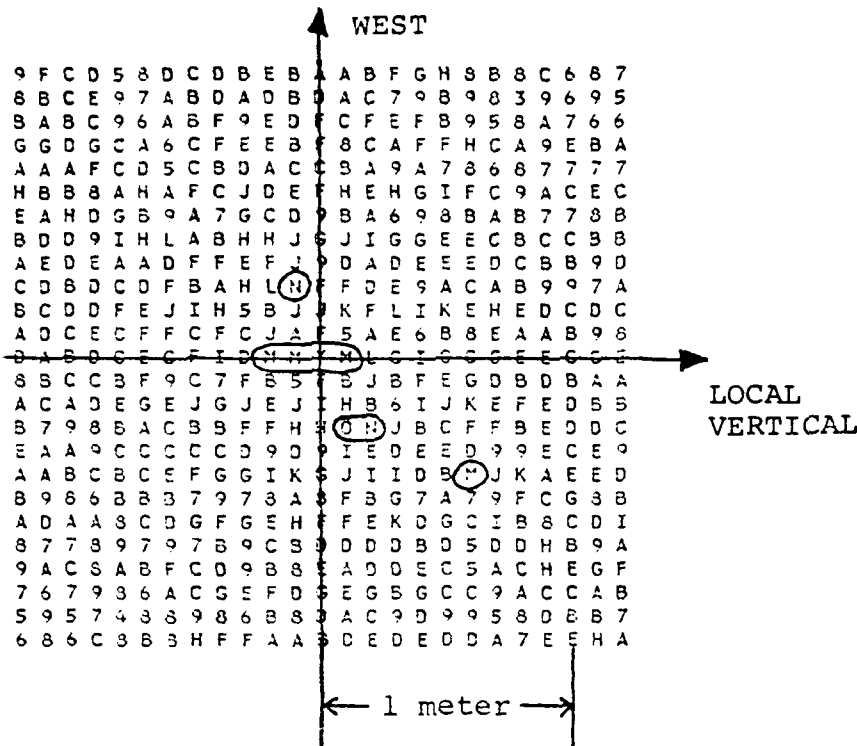


Figure 3. Ambiguity map for 1-hour experiment with broken coherence. Circled points have values above 63% of global maximum.

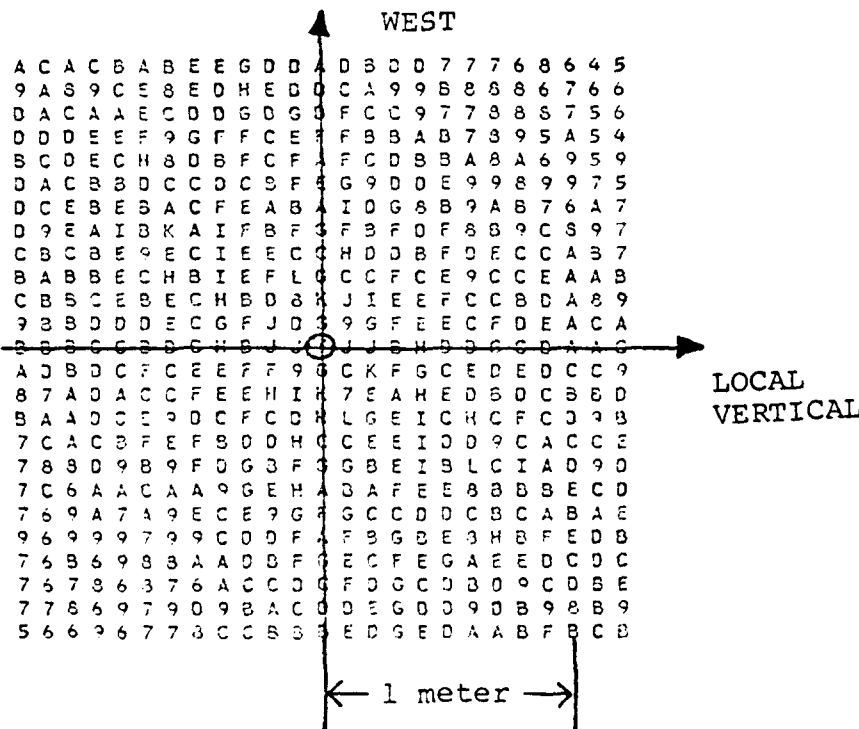


Figure 4. Ambiguity map for 2-hour experiment with broken coherence. As in Figure 2, apart from the origin there is no grid point at which the ambiguity function has more than 63% of the global maximum value.



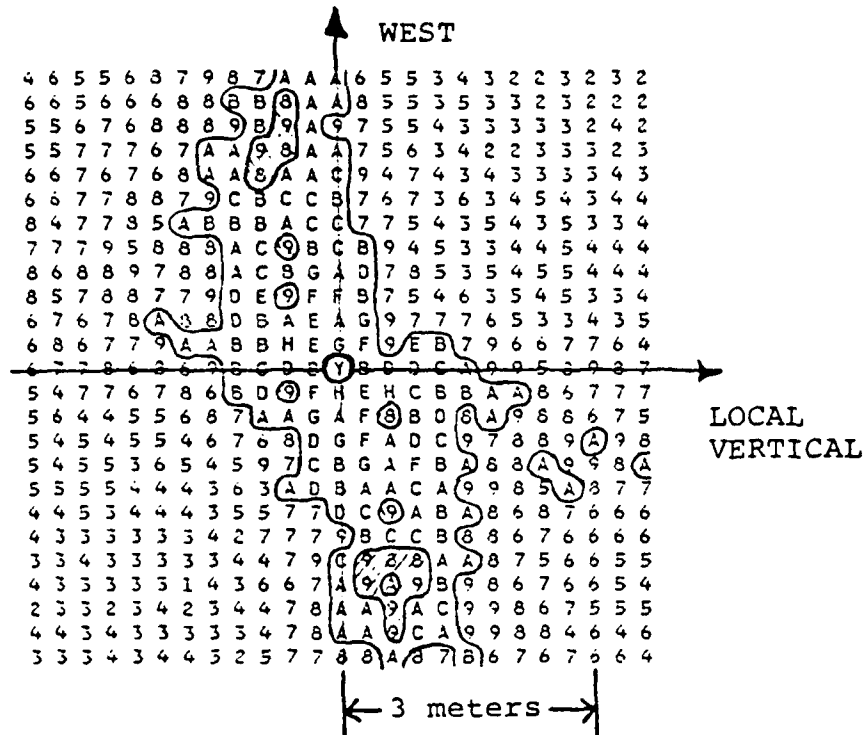


Figure 5. Like Figure 4, except the grid spacing is 30 centimeters. Only the point at the origin has value above 63% of the global maximum, which is at the origin. All grid points with values above 23.5% of the global maximum are enclosed by a solid contour in this Figure.

10-centimeter grid spacing in order to isolate the global maximum. The final "peaking up" on this maximum would be done by a standard function-maximizing routine. We have used the routine STEPIT (copyright 1965 by J. P. Chandler, Physics Department, Indiana University, Bloomington) with satisfactory results for these simulated experiments.

#### IV. Change of Observable: Complex Cross-Power

A problem with ambiguity mapping, for either a simulated or a real experiment, is that it can consume a large amount of computer time. For example, consider that one cubic meter contains  $10^3$  points of a 10-centimeter grid; to compute the correlation  $C$  for one grid point requires a summation over a long time-series of observations -- perhaps  $10^3$  points in time; and for each point in time, the product  $r_\lambda \hat{r}_\lambda$  must be summed over several values of  $\lambda$ . Each of the several million spectral density function evaluations thus indicated may, in turn, involve a fairly large number of elementary arithmetic and logical operations. There is, therefore, some incentive to improve the efficiency of the algorithm. One improvement that we have investigated and recommend adopting is to pre-process the raw correlation data, the set of eight or more  $r_\lambda$ 's, at each point in time, in order to obtain a single complex number that embodies most of the information that the full set of  $r_\lambda$ 's contained. This complex datum, which we denote by the symbol  $S$ , is the cross-power spectral density function evaluated at the GPS carrier frequency; it is computed from the  $r_\lambda$ 's by the Fourier transform relation

$$S = \sum_k r_k \cdot \exp(jl\pi/2), \quad (\text{Eqn. 1})$$

where  $j$  is the square root of minus one. Thus, we compress eight or more real-valued data into one complex datum at each point in time. This reduction of the quantity of data yields some saving in computer time. However, an even greater saving results from the fact that the theoretical value of  $S$  can be computed more easily than the  $\hat{r}_k$  can be.

Theoretically,  $S$  is related to the  $k$ -th satellite's received power  $A_k$  and interferometric phase delay  $\tau_k$ , and to the local-oscillator phase difference  $\phi_{LO}$ , by:

$$S = (1/2) \sum_k A_k \cdot \exp(j\omega_c \tau_k - j\phi_{LO}) \cdot \sum_l \Delta(\tau_k - l\delta) \\ + (1/2) \sum_k A_k \cdot \exp(-j\omega_c \tau_k + j\phi_{LO}) \cdot \sum_l (-1)^l \cdot \Delta(\tau_k - l\delta) \quad (\text{Eqn. 2})$$

[For comparison, refer to Eqn. (1) of the 6/11/80 memo; note that  $(\omega_c - \omega_{LO}) \cdot \delta \approx \pi/2$ .] Here,  $\Delta(x)$  is the triangle function defined in Equation (2) of the 6/11/80 memorandum. From Equation (2) above, it may not be obvious that the theoretical value of the new observable,  $S$ , is any easier to compute than that of the old observable,  $r_k$ . However, a good approximation to Equation (2) above is given by the simple relation

$$S \approx 2 \sum_k A_k \cdot \exp(j\omega_c \tau_k - j\phi_{LO}). \quad (\text{Eqn. 3})$$

That is,

$$\sum_l \Delta(\tau_k - l\delta) \approx 4 \quad (\text{Eqn. 4})$$

and

$$\sum_l (-1)^l \cdot \Delta(\tau_k - l\delta) \approx 0 \quad (\text{Eqn. 5})$$

for all  $k$ . These approximations are good as long as the range of values of  $k$  over which the sums extend includes all significantly nonzero values of the triangle function,  $\Delta(\tau_k - \delta)$ . The accuracies of these approximations are discussed in detail in Appendix A.

The baseline-estimation algorithm set forth in the 6/11/80 memorandum is now recast as follows.

1. First, condense the set of observed values  $r_k(t_i)$  at each point in time  $t_i$  to a single complex number  $S(t_i)$ .

2. Compute the complex correlation  $C$  between the "observed" function of time  $S(t_i)$ , and a trial, theoretical, function  $\hat{S}(t_i)$  by

$$\hat{S} = \sum_k A_k \cdot \exp(j\omega_c \hat{\tau}_k); \quad (\text{Eqn. 6})$$

$$C = \sum_i S(t_i) \hat{S}^*(t_i). \quad (\text{Eqn. 7})$$

The summation over  $i$  extends over the entire time span of the observations if the local oscillator phase is assumed to remain constant for the entire span. Otherwise,  $C$  may be sub-summed over sub-spans as described in Section III.

3. Take the magnitude of  $C$ , or the sum of the magnitudes of the complex sub-sums, and find the baseline vector that maximizes this magnitude.

This recast algorithm is faster than the one originally proposed by a factor of about 4. The improvement in speed comes partly from the elimination of any summation over  $k$  in Equation

(7), and partly from the elimination of the triangle function in Equation (6). To obtain the improved speed, we have committed a conscious error by substituting the simpler form (3) [which leads to (6)] for the more exact form (2).

What is the effect of this error on the ambiguity map, and on the estimate of the baseline vector? For the simulated experiments described in Section II, we have re-computed the ambiguity function -- the magnitude of  $C$  -- using Equation (7). In these experiments the range of values of  $\lambda$  for which the  $r_\lambda$  were obtained was  $\lambda = -4$  to  $+3$ . We find that the largest magnitude of the difference between the ambiguity function computed "exactly," according to the 6/11/80 memorandum, and that computed according to Equation (7) above, is about 3% of the principal maximum value. The position of the principal maximum is not changed by more than a few millimeters, which is the level of uncertainty due to our use of single-precision arithmetic in the computations. We conclude that the use of the faster algorithm does not significantly increase the probability of mistaking a secondary for the principal maximum, or degrade the accuracy of the baseline estimate given by the position of the principal maximum. If the slight loss of position accuracy should be deemed important, one could always refine the baseline estimate by reversion to the original algorithm, after having obtained a preliminary estimate by means of the faster algorithm. Note also (see Appendix A) that the accuracy of the faster algorithm would have been better, had the  $r_\lambda$  data been available for a wider range of  $\lambda$ .

Appendix A: Accuracies of Equations (4) and (5)

The triangle function,  $\Delta(x)$ , is defined by

$$\Delta(x) = \begin{cases} 1 - 1.023 \text{ MHz} \cdot |x| \\ \text{or} \\ 0 \end{cases}, \text{ whichever is greater.}$$

This function approximates the autocorrelation function of the C/A modulation of the GPS signal. For convenience, we also define  $\Sigma^+$  and  $\Sigma^-$  by

$$\Sigma^+ = \sum_{\ell=\ell_{\min}}^{\ell_{\max}} \Delta(\tau - \ell\delta),$$

and

$$\Sigma^- = \sum_{\ell=\ell_{\min}}^{\ell_{\max}} (-1)^\ell \cdot \Delta(\tau - \ell\delta),$$

where  $\delta = 250$  nanoseconds. In the text it is claimed that  $\Sigma^+ \approx 4$  and  $\Sigma^- \approx 0$  as long as  $\Delta(\tau - \ell\delta) = 0$  for  $\ell < \ell_{\min}$  and for  $\ell > \ell_{\max}$ . The accuracies of these two approximations may be judged by inspection of Figures A.1 and A.2. If the stated condition on the range of  $\ell$  is satisfied, then  $\Sigma^+ \approx 3.91$  and  $\Sigma^- = 0$  (exactly). As long as  $\Sigma^-$  vanishes exactly, then there is no loss of geodetic accuracy if  $\Sigma^+$  has any constant nonzero value. Thus, the difference between 3.91 and 4 is of no significance.

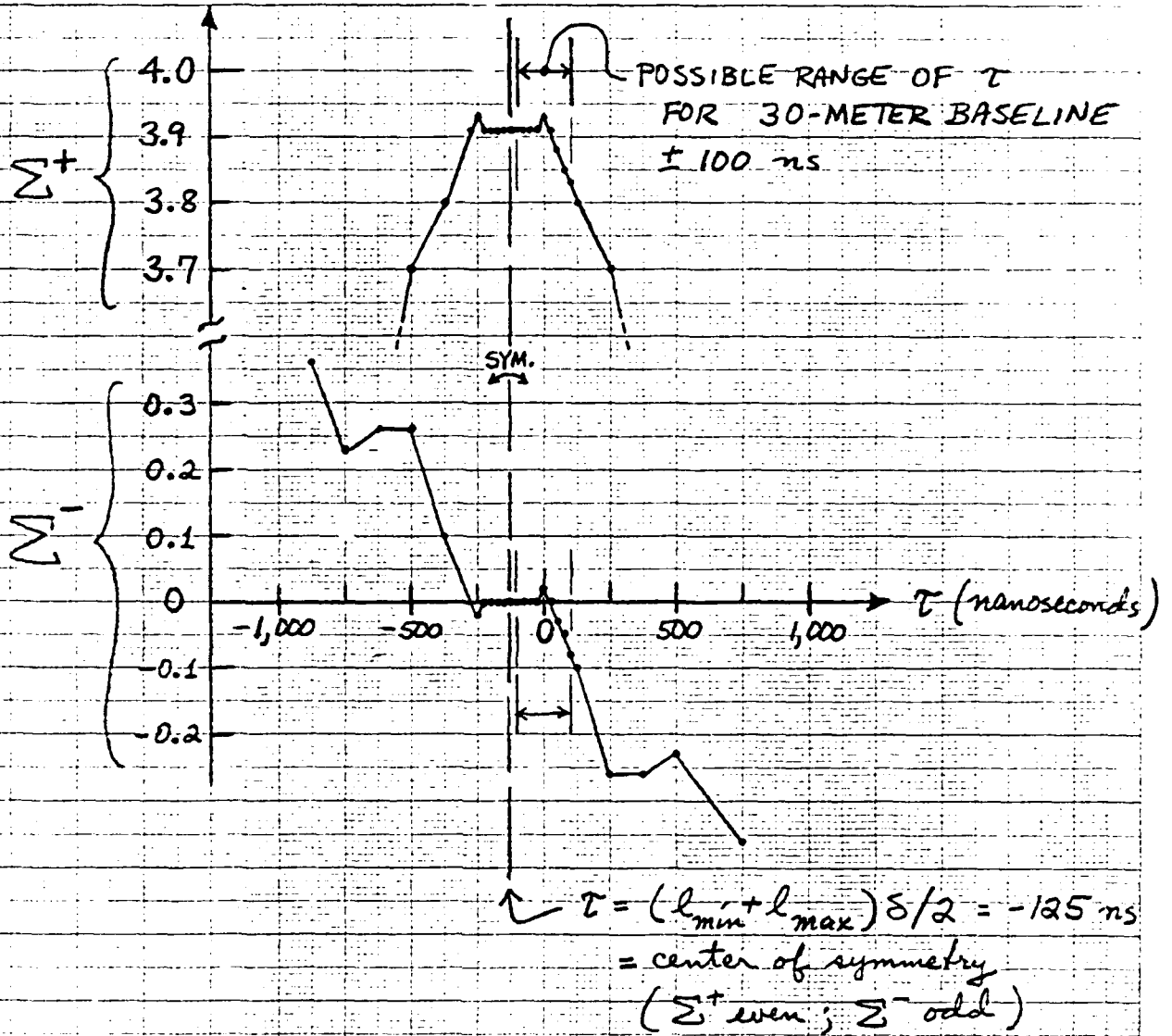


FIGURE A.1:  $l_{min} = -4$ ,  $l_{max} = +3$   
(Eight values of  $l$ )

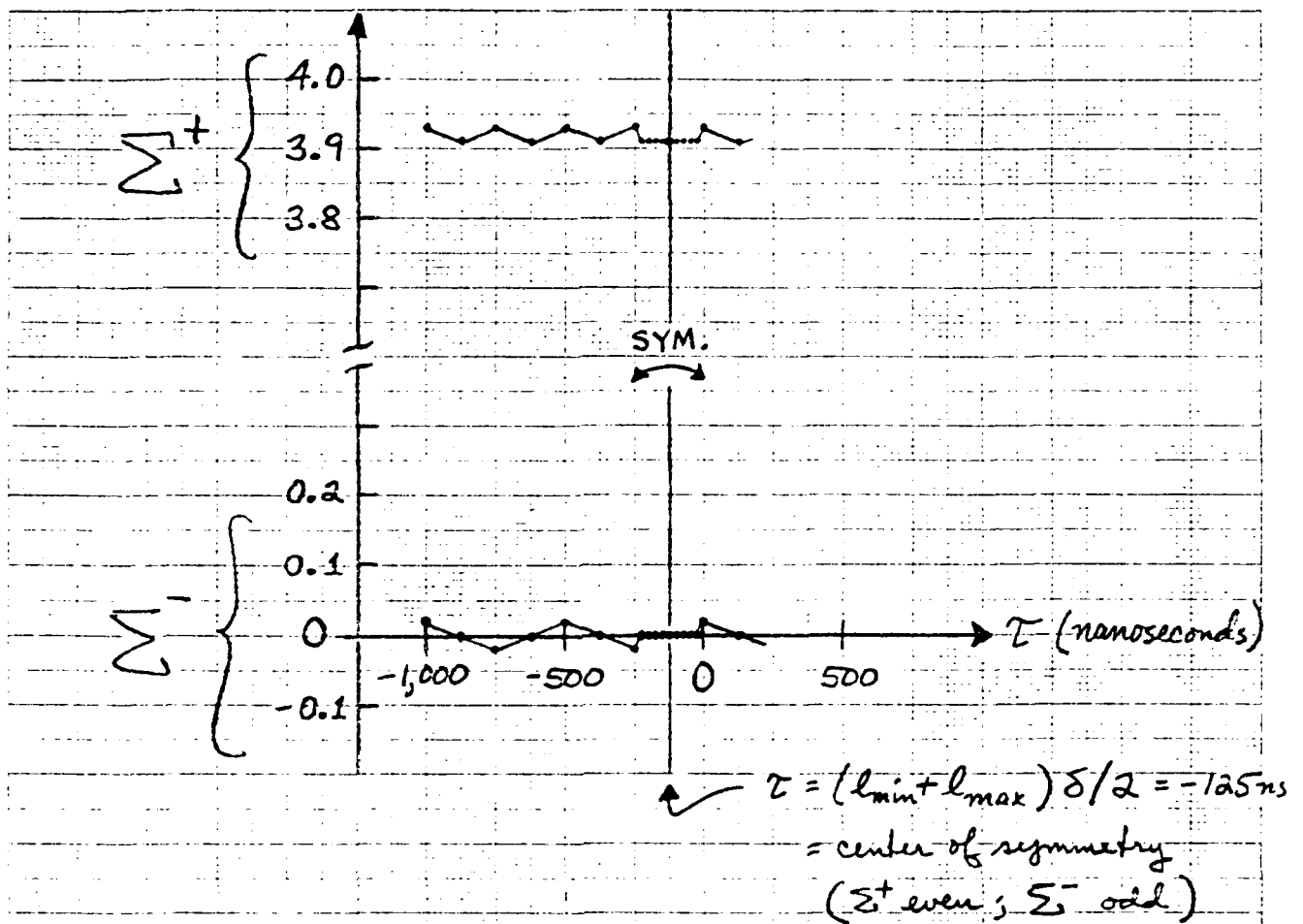


FIGURE A.2:  $l_{min} = -8$ ,  $l_{max} = +7$   
 (16 values of  $l$ )



MASSACHUSETTS INSTITUTE OF TECHNOLOGY  
CAMBRIDGE, MASSACHUSETTS 02139

54-626

September 30, 1980

MEMORANDUM

To: R. L. Greenspan

FROM: C. C. Counselman III and S. A. Gourevitch

SUBJECT: Simulation of Multipath in MITES Experiments

REFERENCE: Counselman and Shapiro, "Miniature Interferometer  
Terminals for Earth Surveying," Bulletin Geodesique, 53, pp.  
139-163 (1979).

I. Introduction

The geodetic interferometry experiments that we are planning to do with antennas of the MITES design (crossed horizontal dipoles, fed in phase quadrature, located  $3\lambda/8$  above and oriented parallel to a metallic "ground" plane) will have results affected to some degree by interference from signals reflected from nearby surfaces such as those of the earth, building walls, and fences. We are attempting to predict the effects of this interference by using the computer to simulate observations with various geometries, time spans, etc. The mathematical formulas underlying our computer code are derived in this memorandum.

## II. Vector, Matrix, and Operator Notation

We use the following notation:

Scalar quantities are denoted by either lower- or upper-case symbols, for example p or E.

A vector, which has a magnitude and a direction, is denoted by a lower- or an upper-case symbol with an arrow above it, for example  $\vec{p}$  or  $\vec{E}$ . The magnitude of any vector is represented by the same symbol without the arrow. The unit vector in the same direction is represented by the same symbol with a "hat" instead of an arrow. Thus,  $\hat{p} = p\hat{p}$ . Two other symbols for a vector,  $\langle \vec{p} \rangle$  and  $|\vec{p}\rangle$ , will be introduced below in order to facilitate the writing of outer or tensor products. In this memorandum just one coordinate system is used for the expression of vectors in component form, and it is sufficient for us to define  $\langle \vec{p} \rangle$  simply as the row, and  $|\vec{p}\rangle$  as the column, matrix of the components of the vector  $\vec{p}$ . A fuller explanation of the meanings of these symbols is given in the Appendix.

Scalars and vectors may be complex. The complex conjugate is formed by "starring". For example,  $\vec{p}^*$  is the conjugate of  $\vec{p}$ .

A right-handed Cartesian coordinate system will be used whose x and y axes are parallel to the crossed dipoles of a MITES antenna; the positive z axis extends upward. Unit vectors along the positive axis directions are  $\hat{x}$ ,  $\hat{y}$ , and  $\hat{z}$ .

The 3x1 column matrix of the x, y, and z coordinate components (each a scalar) of a vector  $\vec{v}$  is denoted by  $|\vec{v}\rangle$ . That is,

$$|\vec{v}\rangle = \begin{bmatrix} \vec{v} \cdot \hat{x} \\ \vec{v} \cdot \hat{y} \\ \vec{v} \cdot \hat{z} \end{bmatrix}.$$

The  $1 \times 3$  row matrix of the Cartesian components of  $\vec{v}$  is denoted by  $\langle \vec{v} \rangle$ .

The "inner", or scalar product  $\vec{u} \cdot \vec{v}$  of two vectors  $\vec{u}$  and  $\vec{v}$  is therefore given by the matrix product

$$\vec{u} \cdot \vec{v} = \langle \vec{u} \rangle [\vec{v}]$$

which is also written as  $\langle \vec{u} | \vec{v} \rangle$ .

The "outer", or tensor product of  $\vec{u}$  and  $\vec{v}$  is represented by  $[\vec{u}] \langle \vec{v} \rangle$ .

The parallel projection operator  $P_u$  is a square matrix defined for any nonzero vector  $\vec{u}$  by

$$P_u = [\vec{u}] \langle \vec{u} \rangle.$$

Pre-multiplication by  $P_u$  of the column matrix  $[\vec{v}]$  yields the column matrix of the components of a new vector which is parallel to  $\vec{u}$  and whose magnitude is equal to the magnitude of the projection of  $\vec{v}$  along  $\vec{u}$ . Thus,  $P_u$  "projects" a vector along  $\vec{u}$ . It is obvious from this description, and may easily be shown by direct multiplication (since  $\langle \vec{u} | \vec{u} \rangle = 1$ ), that  $P_u P_u = P_u^2 = P_u$ . That is, the parallel projection of the parallel projection is the same as the parallel projection.

The perpendicular projection operator  $Q_u$  is defined by

$$Q_u = I - P_u,$$

where  $I$  is the  $3 \times 3$  identity matrix. We call this operator a perpendicular projection operator because it subtracts away the parallel projection of the vector upon which it operates, leaving that part of the vector which is perpendicular to  $\vec{u}$ . Note that

$$Q_u Q_u = Q_u^2 = Q_u.$$

The reflection operator  $R_u$  is defined by

$$R_u = I - 2P_u.$$

For simplicity in the algebraic manipulations that follow, we assume that  $p_0 = 1$ . Note, however, that with  $p_0 = 1$ , the magnitude of the complex "length" of the vector  $\vec{p}$  is not equal to unity. The square of the magnitude, given by  $\langle \vec{p}^* | \vec{p} \rangle$ , equals 2.

#### IV. Effect of Reflecting Plane

We specify the location and the orientation of a reflecting plane by a "mirror" vector  $\vec{m}$  which is just the position vector, with respect to the origin of coordinates, of the point in the plane that is nearest the origin. Thus, the mirror vector is perpendicular to the plane and points toward it. In terms of this vector it is easy to compute the electric field vector  $\vec{E}_r$  of a reflected wave in terms of the field  $\vec{E}_i$  of an incident wave. We know that:

1. The reflected wave vector  $\vec{k}_r$  is related to the incident wave vector  $\vec{k}_i$  through the reflection operation:

$$|\vec{k}_r\rangle = R_m |\vec{k}_i\rangle$$

and

$$|\vec{k}_i\rangle = R_m |\vec{k}_r\rangle.$$

The reflected wave that arrives at a far-distant position  $\vec{r}$  traveling in the direction of  $\hat{r}$  was originally radiated in the direction of the unit vector  $\hat{k}_i$  whose components are given by  $R_m |\hat{r}\rangle$ . (Here we assume  $r \gg m$ , and ignore parallax.) Therefore in Equation III-1,

$$Q_k = I - P_k = I - |\hat{k}\rangle\langle\hat{k}| = I - R_m |\hat{r}\rangle\langle\hat{r}| R_m.$$

Since  $R_m^2 = I$ , we may write

$$Q_k = R_m Q_r R_m.$$

2. At the reflecting plane the incident and the reflected fields are related through a boundary condition. For simplicity in this memorandum we assume that reflecting planes are perfectly conducting so that the sum of the in-plane components of the electric fields (direct plus reflected) is zero. Thus, the field is reflected with a reversal of the sign of the in-plane component and no change of the normal component. At the plane, therefore, we have

$$|\vec{E}_r\rangle = -R_m |\vec{E}_i\rangle.$$

Combining this result with the result for  $Q_k$  derived in paragraph 1 above, we obtain

$$\begin{aligned} |\vec{E}_r\rangle &= -R_m \cdot (\text{scalar factors}) \cdot R_m Q_r R_m |\vec{p}\rangle \\ &= - (\text{scalar factors}) \cdot Q_r R_m |\vec{p}\rangle, \end{aligned}$$

where the "scalar factors" depend only on the path length.

3. The length of the reflected ray path exceeds that of the direct ray path by  $2\hat{k}_i \cdot \vec{m} = -2\hat{k}_r \cdot \vec{m}$ . (Again, we are ignoring parallax.) This addition to the path length may be ignored in the  $r^{-1}$  factor because  $r \gg m$ , but must be incorporated in the complex exponential phase factor because generally  $m$  is not negligible compared to the wavelength. The added path length is accounted for by substituting  $(\vec{r} - 2\vec{m})$  for  $\vec{r}$  in the argument of the complex exponential.

Now combining the results of paragraphs 1, 2, and 3, we have

$$|\vec{E}_r\rangle = -k^2 r^{-1} \exp(i\langle \vec{k} | (\vec{r} - 2\vec{m}) \rangle) Q_k R_m |\vec{p}\rangle,$$

in which  $\vec{k} = k\hat{r}$ . Thus, the expression for the reflected field at a distance  $r \gg m$  is the same as the original expression derived in Section III but with two changes:

1. The dipole moment  $|\vec{p}\rangle$  is replaced with its negative reflection,  $-R_m |\vec{p}\rangle$ .
2. The vector  $\vec{r}$  representing the position of the observer with respect to the antenna at the origin is replaced by  $(\vec{r} - 2\vec{m})$ , which is the observer's position with respect to the image of the antenna in the reflecting plane.

#### V. Effect of Horizontal "Ground" Plane

In this Section we apply the result derived in Section IV to compute the effect of the MITES antenna's "ground" plane, which is described by the mirror vector

$$|\vec{g}\rangle = \begin{bmatrix} 0 \\ 0 \\ -g \end{bmatrix}$$

where  $g = 3\lambda/8$ . At a distance  $r \gg g$  from the origin, the electric field of the wave reflected by the ground plane is

$$|\vec{E}_r\rangle = -k^2 r^{-1} \exp(i\langle \vec{k} | (\vec{r} - 2\vec{g}) \rangle) Q_k R_g |\vec{p}\rangle, \quad (\text{Eqn. V-1})$$

where  $\vec{k} = k\hat{r}$ .

But because for the MITES antenna  $\vec{p}$  is perpendicular to  $\vec{g}$ ,

$$R_g |\vec{p}\rangle = |\vec{p}\rangle.$$

Thus, in this special case (only!), the operator  $R_g$  may be deleted from Equation (V-1). With this deletion the expression

for the reflected field becomes very similar to the one for the direct field, and the two are easily combined to obtain the total field,  $\vec{E}_{\text{tot}}$ :

$$|\vec{E}_{\text{tot}}\rangle = k^2 r^{-1} \exp(i\langle \vec{k} | \vec{r} \rangle) (1 - \exp(-2i\langle \vec{k} | \vec{q} \rangle)) Q_k |\vec{p}\rangle.$$

This expression, in turn, is simplified by moving the origin of coordinates to the point in the ground plane directly below the center of the crossed dipoles -- that is, to the point with "old" coordinates  $|\vec{q}\rangle$ . In "new" coordinates, the total field radiated by a MITES antenna is

$$\begin{aligned} |\vec{E}_a\rangle &= k^2 r^{-1} \exp(i\langle \vec{k} | \vec{r} \rangle) (\exp(i\langle \vec{k} | \vec{q} \rangle) - \exp(-i\langle \vec{k} | \vec{q} \rangle)) Q_k |\vec{p}\rangle \\ &= 2ik^2 r^{-1} \exp(i\langle \vec{k} | \vec{r} \rangle) \sin(\langle \vec{k} | \vec{q} \rangle) Q_k |\vec{p}\rangle, \end{aligned} \quad (\text{Eqn. V-1})$$

where again we have neglected the change in the  $r^{-1}$  factor.

#### VI. Signal Received from a Transmitter

The complex amplitude of the signal received by an antenna at a distant position  $\vec{r}$  is proportional to the inner or "dot" product of the complex conjugate of the receiving antenna's effective electric dipole moment vector with the radiated electric field vector evaluated at  $\vec{r}$ . Denoting the receiving antenna's electric dipole moment by  $\vec{q}$ , we have

$$A = \langle \vec{q}^* | \vec{E}_a \rangle \quad (\text{Eqn. VI-1})$$

where  $A$  is proportional to the received signal amplitude. By "effective" dipole moment here we mean the dipole moment of an infinitesimal antenna having the same polarization as the actual antenna, multiplied by the "gain" of the actual antenna. The gain factor can account, for example, for the effect of incorporating a reflector or multiple array elements into one

"antenna" structure. By "signal" here we mean the current or the voltage delivered to a load. The constant of proportionality between A and the received signal amplitude contains not only the antenna gain factor but also various impedances, etc. Assuming that it is constant, we are not concerned with it and will not discuss it further.

The MITES antennas will be used to receive signals transmitted by the GPS satellites, not to radiate signals for the satellites to receive. But for expository purposes in this memorandum we have been calculating the field radiated by a MITES antenna as if it were transmitting. We continue in this vein, and now calculate the amplitude of the signal that a GPS satellite antenna would receive from a MITES antenna. By reciprocity, we know that the result for the received amplitude will be the same as we would obtain if we treated the GPS antenna as the radiator and the MITES antenna as the receiver.

A GPS satellite antenna has circular polarization with  $\vec{q}$  perpendicular to  $\vec{r}$  and  $\vec{k}$ . (GPS satellites are always oriented so that their antennas face earthward.) Thus,  $\vec{q}$  can be expressed as a simple rotation of  $\vec{p}$ :

$$|\vec{q}\rangle = D|\vec{p}\rangle, \quad (\text{Eqn. VI-2})$$

where D is a matrix rotation operator that depends on the azimuth  $\phi$  and the zenith angle  $\theta$  of the satellite relative to the MITES antenna. The matrix D can be written as the product of two matrices  $D_\phi$  and  $D_\theta$ , the first being a function of the azimuth alone, and the second a function of only the zenith angle:

$$D = D_\phi D_\theta.$$



Here,

$$D_{\theta} = \begin{pmatrix} \cos\theta & 0 & \sin\theta \\ 0 & 1 & 0 \\ -\sin\theta & 0 & \cos\theta \end{pmatrix}$$

represents a rotation, about the y axis, of the z axis toward the x axis, and

$$D_{\phi} = \begin{pmatrix} \cos\phi & -\sin\phi & 0 \\ \sin\phi & \cos\phi & 0 \\ 0 & 0 & 1 \end{pmatrix}$$

represents a rotation about the (original) z axis, of the x axis toward the y axis. Thus,

$$D = \begin{pmatrix} \cos\theta\cos\phi & -\sin\phi & \sin\theta\cos\phi \\ \cos\theta\sin\phi & \cos\phi & \sin\theta\sin\phi \\ -\sin\theta & 0 & \cos\theta \end{pmatrix}.$$

(Note that we are not accounting for a possible third rotation, about an axis parallel to the wave-propagation direction  $\hat{r}$ . In other words, we are ignoring the "third" Euler angle,  $\psi$ . Such a rotation would only change the phase of A, by the same angle as the rotation, by virtue of the circularity of the polarization of the GPS antenna. That is,  $D_{\psi} = e^{i\psi}$ .)

From the definition of D it follows that

$$\begin{aligned} |\hat{k}\rangle &= D |\hat{z}\rangle \\ \text{and} \\ Q_k &= D Q_z D^{-1}. \end{aligned} \quad (\text{Eqn. VI-3})$$

Combining Equations (V-1), (VI-1), (VI-2), and (VI-3), and omitting the constant factor  $(2ik^2r^{-1})$ , we obtain

$$\begin{aligned} A &= \langle \vec{p}^* | Q_z D^{-1} | \vec{p} \rangle \sin(\vec{k} \cdot \vec{g}) e^{ikr} \\ &= \langle \vec{p}^* | D^{-1} | \vec{p} \rangle \sin(\vec{k} \cdot \vec{g}) e^{ikr} \\ &= \langle \vec{p} | D | \vec{p}^* \rangle \sin(\vec{k} \cdot \vec{g}) e^{ikr}. \end{aligned} \quad (\text{Eqn. VI-4})$$

By direct substitution and multiplication we find

$$\langle \vec{p} | D | \vec{p}^* \rangle = e^{i\phi} (1 + \cos\theta). \quad (\text{Eqn. VI-5})$$

The received power is proportional to

$$\begin{aligned} A^*A &= (1 + \cos\theta)^2 \sin^2(\langle \vec{k} | \vec{g} \rangle) \\ &= (1 + \cos\theta)^2 \sin^2((3\pi/4)\cos\theta). \end{aligned} \quad (\text{Eqn. VI-6})$$

Thus -- except for a constant factor -- we have derived the directive power gain of the MITES antenna as a function of zenith angle, for circular polarization. The power gain, as expected, varies with zenith angle but is independent of azimuth. Equation (VI-5) shows, however, that the received signal phase varies with azimuth -- in fact, is just equal to the azimuth -- whereas it is independent of zenith angle.

The constant factor by which the right side of (VI-6) must be multiplied in order to obtain the power gain of the MITES antenna with respect to the standard (fictitious), isotropic, circularly polarized, reference antenna is determined by the condition that the integral of the gain over the visible hemisphere ( $0 \leq \theta \leq \pi/2$ ;  $0 \leq \phi < 2\pi$ ; note that the gain is zero for the other hemisphere,  $\pi/2 \leq \theta \leq \pi$ ) equals  $4\pi$ . We find that the numerical value of the factor is about 1.23. However, for engineering purposes, and especially considering that we have neglected the effects of dissipation, the finite sizes of the dipole elements and the ground plane, etc., the value of the factor is approximated well enough by unity. The function of  $\theta$  that appears on the right side of (VI-6) will be denoted by  $G(\theta)$ :

$$G(\theta) = (1 + \cos\theta)^2 \sin^2((3\pi/4)\cos\theta), \quad (\text{Eqn. VI-7})$$

and we will refer to  $G(\theta)$  simply as the "antenna gain." Values of this function are given in Table 1.

Table 1. Directive Power Gain (ref. isotropic, circ. pol.) of MITES Antenna vs. Zenith & Elevation Angles, from Equation (VI-7).

<u>Zenith Angle, <math>\theta</math> (deg)</u>	<u>Elevation Angle (deg)</u>	<u>Gain, G (dimension- less)</u>	<u><math>10 \log_{10} G</math> (dbic)</u>
0	90	2.00	+3.01
10	80	2.11	3.24
20	70	2.41	3.82
30	60	2.77	4.42
40	50	2.95	4.70
50	40	2.69	4.30
60	30	1.92	+2.83
70	20	0.94	-0.28
80	10	0.22	-6.62
90	0	0.00	$-\infty$

# VII. Interferometric Cross-Power Observable

The interferometric, complex, cross-power observable  $S$  that was defined in our August 12, 1980, memorandum (revised August 13, 1980) for a single GPS satellite, except for constant factors, is given by

$$S = B^*A$$

where  $A$ , given by Equation (VI-4), is the complex amplitude of the signal received from the MITES antenna located at the origin of coordinates, and  $B$  is the complex amplitude of the signal received from an identical MITES antenna located at the position  $\vec{b}$ . (We continue to use the "new" definition of the origin of coordinates that we introduced in Section V: the point in the ground plane directly below the center of the crossed dipoles of the MITES antenna.) To obtain an expression for the complex amplitude  $B$  we simply take the expression (VI-4) for  $A$  and substitute  $\vec{r}-\vec{b}$  for  $\vec{r}$  in the argument of the complex exponential phase factor  $e^{i\vec{k}\cdot\vec{r}} = \exp(i\langle\vec{k}|\vec{r}\rangle)$ . We ignore the parallax of the baseline -- that is, we ignore the difference between the directions of the wave vectors at the two MITES antenna locations -- and we assume that the two antennas have parallel orientations, so that their dipole moment vectors and hence their azimuth phase factors are identical. Thus, we obtain

$$S = B^*A = G(\theta) \exp(i\langle\vec{k}|\vec{b}\rangle) \quad .$$

### VIII. Multipath at One Antenna

The reflection of the field by the ground plane at each MITES antenna, which we considered in Section V, is an example of multipath propagation, but it is an uninteresting, or "benign," example so long as the ground-plane mirror vector  $\vec{g}$  and the dipole moment vector  $\vec{p}$  are the same at each antenna. Multipath is interesting, or "pathological," only when it is present at one antenna in a form that is not duplicated at the other antenna. To simulate pathological multipath we assume that at one antenna -- the one at the origin of coordinates -- in addition to the horizontal ground-plane reflector there is a vertical plane "mirror," described by a horizontal mirror vector,  $\vec{m}$ , given by

$$[\vec{m}] = \begin{bmatrix} m \cos \nu \\ m \sin \nu \\ 0 \end{bmatrix}.$$

By virtue of the reflection in this mirror the complex amplitude  $A$  of the signal received at the satellite from the original MITES antenna is augmented by  $A_m$ . To derive an expression for  $A_m$  we apply the arguments of paragraphs 1, 2, and 3 of Section IV to Equation (VI-4), and obtain

$$A_m = -\langle \vec{p}^* | D^{-1} R_m | \vec{p} \rangle \sin(\langle \vec{k} | R_m | \vec{g} \rangle) \exp(i \langle \vec{k} | (\vec{r} - 2\vec{m}) \rangle), \quad (\text{Eqn. VIII-1})$$

where, as in Equation (VI-4), we have omitted the constant factor  $(2ik^2 r^{-1})$ . Since the ground plane is horizontal and the other mirror is vertical,  $\langle \vec{g} | \vec{m} \rangle = 0$  and  $\langle \vec{k} | R_m | \vec{g} \rangle = \langle \vec{k} | \vec{g} \rangle$ . Thus, in this special case, Equation (VIII-1) reduces to

$$A_m = -\langle \vec{p}^* | D^{-1} R_m | \vec{p} \rangle \sin(\langle \vec{k} | \vec{g} \rangle) \exp(i \langle \vec{k} | (\vec{r} - 2\vec{m}) \rangle), \quad (\text{Eqn. VIII-2})$$

Now the interferometric cross-power observable is

$$S_{\text{tot}} = S + S_m$$

where

$$S = S(\vec{b}) = B \cdot A = G(\theta) \exp(i \langle \vec{k} | \vec{b} \rangle) \quad (\text{Eqn. VIII-3})$$

is due to the signal received directly (without reflection in the vertical mirror), and

$$S_m = B \cdot A_m = -\{G(\theta) - 2 M \sin^2(\langle \vec{k} | \vec{g} \rangle)\} \exp(i \langle \vec{k} | (\vec{b} - 2\vec{m}) \rangle), \quad (\text{Eqn. VIII-4})$$

in which

$$M = \langle \vec{p}^* | D | \vec{p} \rangle \langle \vec{p} | \hat{m} \rangle \langle \hat{m} | D | \vec{p}^* \rangle \quad (\text{Eqn. VIII-5})$$

In deriving Equations (VIII-4) and (VIII-5) we substituted

$I - 2P_m = I - 2|\hat{m}\rangle\langle\hat{m}|$  for the operator  $R_m$  in Equation VIII-1, and used  $\langle \vec{p}^* | D^{-1} | \hat{m} \rangle = \langle \hat{m} | D | \vec{p}^* \rangle$ . Substitution of the definitions of  $\vec{m}$ ,  $D$ , and  $\vec{p}$  into Equation VIII-5 yields

$$\begin{aligned} M &= (1 + \cos\theta) - \sin^2\theta \cos(\nu - \phi) e^{i(\nu - \phi)} \\ &= \{(1 + \cos\theta)^2/2\} \{1 - [\tan^2(\theta/2)] e^{2i(\nu - \phi)}\} \quad (\text{Eqn. VIII-6}) \end{aligned}$$

The quantity  $M$  can also be written in a form that involves only dot products:

$$M = 1 + \langle \hat{k} | \hat{z} \rangle - \langle \vec{p}^* | \hat{k} \rangle \langle \hat{k} | \hat{m} \rangle \langle \hat{m} | \vec{p} \rangle \quad .$$

Finally, substitution of (VIII-6) into (VIII-4) yields the simple result

$$S_m = S(\vec{b} - 2\vec{m}) \cdot F, \quad (\text{Eqn. VIII-7})$$

where

$$F = -[\tan^2(\theta/2)] e^{2i(\nu - \phi)} \quad (\text{Eqn. VIII-8})$$

Note that the magnitude of  $F$  is a function of only the zenith angle,  $\theta$ , whereas the phase angle depends on only the azimuth of the satellite relative to the mirror.

The magnitude dependence on zenith angle is easy to understand physically: In the zenith direction the MITES antenna has circular polarization matched to the wave that propagates to it directly from the satellite. But the sense of circular polarization of a wave is reversed by reflection at a perfectly conducting surface, so the MITES antenna has zero response to a reflected wave coming from the zenith. At the zenith,  $|F| = 0$ . Viewed from the horizon, the MITES antenna has horizontal, linear polarization so that it responds equally to waves with the two opposite senses of circular polarization. At the horizon,  $|F| = 1$ . The form of the  $\theta$ -dependence between the zenith and the horizon may also be derived directly by detailed consideration of the antenna polarization. Since, in most practical observing situations, reflections would be more likely to come from near the horizon than from near the zenith, we expect that usually the magnitude of  $F$  will be near unity.

The phase-angle dependence on the azimuth of the satellite relative to the mirror is also easily understood physically. This dependence stems from the  $e^{i\phi}$  term in Equation (VI-5): The phase of the signal received by a MITES antenna changes with the azimuth from which the wave approaches the antenna. But this azimuth is changed by  $2(\psi - \phi)$  by the reflection in the vertical mirror.

The negative sign of the right side of (VIII-8) is due to the reversal of the sign of the horizontal component of the electric field, that occurs upon reflection at the perfectly conducting surface of the vertical mirror.

### IX. Program Logic

In this Section we outline the logic of the computer program that simulates observations in the presence of multipath.

At each time for which an observation is to be made, the program executes a "DO" loop over all of the GPS satellites. Before this loop is entered, the total value of the interferometric observable is set equal to zero. Within the loop, the contributions of the individual satellites to the observable are added into this total. A satellite may contribute not at all (if it is below the horizon or occulted by the vertical mirror), via direct propagation alone, or through multipath propagation, depending upon its direction relative to the observer's horizon and the vertical-mirror plane, and upon the size, shape, and distance of the mirror.

For each satellite, the unit vector  $\hat{r}$  in the direction of the satellite is computed from the orbital elements, etc. The sign of the dot product of  $\hat{r}$  and the unit vector  $\hat{z}$  in the direction of the observer's local vertical is tested to see whether the satellite is above the observer's horizon. If it is not, then no further computation is done for this satellite. Otherwise, the dot product of  $\hat{r}$  with the unit vector  $\hat{m}$  in the direction of the mirror (see Section VIII) is tested to see whether the satellite is occulted by the vertical plane mirror. We consider this mirror to have a finite size; its shape is semi-circular, like one end of a quonset hut. The cosine of half the angle subtended at the observing antenna by the diameter of the mirror is specified by a program input parameter named QUON.



If  $\langle \hat{r} | \hat{m} \rangle$  is greater than QUON, then the satellite is occulted by the mirror and no further computation is done for this satellite. Otherwise, the value  $S(\vec{b})$  of this satellite's "direct" contribution is added to the interferometric observable (see Section VII). This contribution is due to the wave propagated directly to the antenna from the satellite. Now we test  $\langle \hat{r} | \hat{m} \rangle$  again to determine whether, from the position of the antenna, an image of the satellite appears within the diameter of the mirror. If  $\langle \hat{r} | \hat{m} \rangle$  is greater than (-QUON), then no such reflection is visible and no further computation is done for this satellite. Otherwise, the value of the interferometric observable is augmented by  $S_m = S(\vec{b} - 2\vec{m}) \cdot F$ , the contribution due to the wave reflected to the antenna by the mirror (see Section VIII). This completes the computation for one satellite at one time.

We conclude by correcting a minor mis-statement that we made deliberately, in order to simplify the preceding description: What our simulation program computes at each observing time is, in reality, not the complex cross-power  $S$ , but the set of eight real-valued cross-correlations  $r_l$ ,  $l = -4, -3, \dots, +3$ , defined in our June 11, 1980, memorandum. For direct-path propagation, we compute  $r_l$  for the baseline  $\vec{b}$  according to Equation (1) of that memorandum. For the reflected-path propagation, we compute  $r_l$  for the baseline  $\vec{b} - 2\vec{m}$ , and multiply the result by  $F$ , by analogy with Equation (VIII-7) in the present memorandum. It is easy to see that this analogous procedure is the correct one, because  $S$  and  $r_l$  are linearly related. (See our memorandum dated August 12, 1980.)

# Appendix on Vector Notation

To facilitate the writing of outer or tensor products we introduce two special symbols,  $\langle \hat{u} |$  and  $|\hat{v}\rangle$ , that represent vectors in two different, but complementary spaces. The spaces are related such that a vector product is formed by multiplying together one vector from each space. Thus the inner or "dot" product  $\hat{u} \cdot \hat{v} = \hat{v} \cdot \hat{u} = \langle \hat{u} | \hat{v} \rangle = \langle \hat{v} | \hat{u} \rangle$ , and the outer or tensor product of  $\hat{v}$  and  $\hat{u}$  is written  $|\hat{v}\rangle \langle \hat{u}|$ . The symbols  $\langle \hat{u} |$  and  $|\hat{v}\rangle$  behave as row and column matrices, respectively, and indeed, once a coordinate system is adopted, the vector components may be written in matrix form as in Section II of this memorandum. If we write  $|\hat{i}\rangle = |\hat{x}\rangle$ ,  $|\hat{j}\rangle$ , and  $|\hat{z}\rangle$  for  $i = 1, 2$ , and  $3$ , respectively, then the identity operator  $I$  can be written

$$I = \sum_{i=1}^3 |\hat{i}\rangle \langle \hat{i}|;$$

$$|\hat{v}\rangle = \sum_i |\hat{i}\rangle \langle \hat{i} | \hat{v} \rangle = \sum_i |\hat{i}\rangle v_i ;$$

$$\langle \hat{u} | = \sum_i \langle \hat{u} | \hat{i} \rangle \langle \hat{i} | = \sum_i \langle \hat{i} | u_i ;$$

thus,

$$\langle \hat{u} | \hat{v} \rangle = \langle \hat{u} | I | \hat{v} \rangle = \sum_i \langle \hat{u} | \hat{i} \rangle \langle \hat{i} | \hat{v} \rangle = \sum_i u_i v_i = \hat{u} \cdot \hat{v}.$$

The components of an operator  $M$  are  $M_{ij} = \langle \hat{i} | M | \hat{j} \rangle$ , so that the components of the expression  $|\hat{v}\rangle = M |\hat{u}\rangle$  are found from

$$v_i = \langle \hat{i} | \hat{v} \rangle = \sum_j \langle \hat{i} | M | \hat{j} \rangle \langle \hat{j} | \hat{u} \rangle = \sum_j M_{ij} u_j ,$$

whereas  $\langle \hat{v} | = \langle \hat{u} | \tilde{M}$  has components

$$v_i = \langle \hat{v} | \hat{i} \rangle = \sum_j \langle \hat{u} | \hat{j} \rangle \langle \hat{j} | \tilde{M} | \hat{i} \rangle = \sum_j u_j \tilde{M}_{ji} .$$

Evidently,  $\tilde{M}$  is the transpose of  $M$ .

DEPARTMENT OF EARTH AND PLANETARY SCIENCES

MASSACHUSETTS INSTITUTE OF TECHNOLOGY  
CAMBRIDGE, MASSACHUSETTS 02139

54-626

September 30, 1981

Memorandum

To: R. L. Greenspan  
From: C. C. Counselman III  
Subject: Comparison of GPS Radio Interferometry Determination of  
a Triangle of Baselines with Independent Determination  
by Conventional Survey

Introduction

On December 17, 1980, we set a portable "Miniature Interferometer Terminal for Earth Surveying" (MITES) antenna atop each of three temporary survey marks that we had established near the Haystack Observatory in Westford, Massachusetts. These antennas yielded radio interferometric observations of the NAVSTAR Global Positioning System (GPS) satellites. We analyzed the data from an observation period of about 78 minutes, by the method described by C. C. Counselman and S. A. Gourevitch in the October 1981 issue of IEEE Transactions on Geoscience and Remote Sensing, to determine the baseline vectors between the marks. We repeated the experiment on December 29, 1980, with a different antenna on each mark. On the latter date, we also performed an experiment to determine how severely the baseline determination would be affected by the parking of a car next to one antenna during the observing period. My Dasher station wagon was parked broadside to one antenna, with its side about 60 cm to the south-east. Observations made under this condition were analyzed to

obtain a second set of baseline determinations for this day. The results of all three experiments were handed to you in my office on February 23, 1981.

During January, 1981, the surveying firm of Harry R. Feldman, Inc., of Boston, Mass., used conventional surveying instruments to determine the same baseline vectors, except for an overall azimuth rotation which remained unknown. After I had given you our radio interferometry results, you showed me for the first time the Feldman survey results. We compared the MITES with the Feldman results for the lengths of the baselines, but not for the individual horizontal components because of the lack of a survey determination of azimuth. We began to compare the vertical components but found a puzzling, gross, discrepancy that demanded further investigation.

In May, 1981, I found the apparent explanation of the vertical discrepancy: one simple numerical transcription error by Feldman. In July 1981, we obtained the result of an accurate ( $\pm 3.3$  arcsec) astronomical determination of the azimuth of one of the baseline vectors from Bob Magee and Mark Nasson of CSDL (their memo no. DSSG/M81-19). I have now combined their azimuth determination with Feldman's original between-baselines azimuth-difference determinations to obtain azimuths for all baselines. Thus, I have been able to compute all three rectangular components, North (N), East (E), and Up (U), of each baseline vector according to the combination of Feldman's and Magee's results.

In the present memorandum the results of these computations are presented and compared with our originally reported interferometry results which were in the same NEU coordinates. You will recall that in order to transform the interferometry results from the 1950.0 mean equatorial coordinates, in which our geometrical calculations had been performed, to the topocentric NEU system, I assumed that the U axis pointed toward geocentric latitude  $42^{\circ} 37' 22''$ , longitude  $71^{\circ} 09' 19''$ , and that the E axis was parallel to the equatorial plane of date.

#### Results

In Table I are given the N, E, I components and the length of the baseline vector that extends from our laser-pad, manhole-rim, X-cut, temporary survey mark (Feldman's point number 4) to our front parking lot, screw-head, temporary survey mark (adjacent to, but not the same as, Feldman's front parking lot "pin", their point number 2). In addition to the MITES and the survey results in this table we include the Geodimeter measurement that Feldman, Inc., made but did not include in its final report to you.

In Table 2 are the results for the vector from our screw-head temporary survey mark in the oil-tank area, near but not the same as Feldman's pin (their point no. 1), to our manhole-rim X-cut (Feldman no. 4).

In Table 3 are the results for the vector from our front-lot screw head to our oil-tank screw head.

In Table 4 are the N, E, U components of the three short offset vectors to our temporary marks from the nearby, permanent marks: one from the NGS disk in the center of the laser-pad manhole (Feldman pt. no. 3) to the rim X-cut (F. pt. no. 4); one from the steel pin set by Feldman in the front lot (F. pt. no. 2) to our nearby screw head; and one from the steel pin set by Feldman in the oil tank area (F. pt. no. 1) to our nearby screw head. The N and E component values given in Table 4 were computed by me from the Feldman and Magee distance and azimuth measurements. The U component of the offset vector was not measured by the surveyors except at the manhole; I measured the two others myself with a bubble level and a hand-held scale.

In Table 5, the vector misclosure around the triangle of baselines is shown for each of the three MITES experiments. (The conventional survey results reported by Feldman had been adjusted so that they closed exactly. No such adjustment was made for the MITES results.)

#### Discussion

The tables indicate that both the MITES and the conventional survey results are accurate at about the estimated level of uncertainty, about 5 mm in each coordinate except for the second MITES experiment on Dec. 29, when the car was parked next to one antenna. The uncertainty for this experiment is higher mainly because of the poorer satellite geometry, not because of the car. Note that the baseline of Table 2 had a car at neither end, yet the repeatability of its vertical-component determination on

December 29 is about as poor as for the two baselines which had the front-lot antenna in common. The triangle closure error (Table 5) is extraordinary large for the Dec. 29 "car" experiment because in this experiment, for unknown reasons, each of the three baselines exhibited a centimeter-sized upward shift. Still, it seems fair to say that, at least when the satellite geometry is good, we can determine all three components of a baseline vector that's about 100 meters long within about 5 millimeters, one sigma, by MILES/GPS.

Table 1. North (N), East (E), and Up (U) components and length (L) of the baseline vector extending from the laser-pad to the front parking lot temporary survey marks, from various determinations. Uncertainties are subjectively estimated, and are intended to represent about  $\pm 1$  standard deviation.

Determination (Method/Date)	Baseline Component			
	N (mm)	E (mm)	U (mm)	L (mm)
MITES/Dec. 17	7,110 $\pm$ 5	-91,784 $\pm$ 5	-1,289 $\pm$ 5	92,068 $\pm$ 5
MITES/Dec. 29	7,105 $\pm$ 5	-91,782 $\pm$ 5	-1,287 $\pm$ 5	92,065 $\pm$ 5
MITES/Mean*	7,107 $\pm$ 4	-91,783 $\pm$ 4	-1,288 $\pm$ 4	92,067 $\pm$ 4
MITES/Dec.29/car**	7,107 $\pm$ 7	-91,784 $\pm$ 7	-1,278 $\pm$ 10	92,067 $\pm$ 10
Survey	7,101 $\pm$ 5	-91,780 $\pm$ 5	-1,291 $\pm$ 5	92,063 $\pm$ 5
Geodimeter	---	---	---	92,074 $\pm$ 10
Difference: MITES/ Mean-Survey	6 $\pm$ 6	-3 $\pm$ 6	3 $\pm$ 6	4 $\pm$ 6
Difference: MITES/ Mean-Geodimeter	---	---	---	-7 $\pm$ 11

\* Simple arithmetic average of the Dec. 17 and the first Dec. 29 result shown, although computed with more precision before rounding to the nearest millimeter. The MITES/Dec.29/car result was not included in this average.

\*\* Obtained from observations late on Dec. 29, while a car was parked with its side 60 cm from the center of the antenna in the front parking lot. The satellite viewing geometry was significantly poorer during these observations than for the earlier ones; thus, the baseline uncertainty is magnified, especially for the U component.



Table 2. North (N), East (E), and Up (U) components and length (L) of the baseline vector extending from the oil-tank to the laser-pad temporary survey marks, from various determinations. Uncertainties are subjectively estimated, and are intended to represent about  $\pm 1$  standard deviation. The uncertainties for the survey are greater for this baseline than for the others because only for this baseline was the line of sight obstructed so that a dog-leg had to be surveyed.

<u>Determination</u>	<u>Baseline Component</u>			
	<u>N</u>	<u>E</u>	<u>U</u>	<u>L</u>
<u>(Method/Date)</u>	(mm)	(mm)	(mm)	(mm)
MITES/Dec. 17	-71,362 $\pm$ 5	101,187 $\pm$ 5	-56 $\pm$ 5	123,820 $\pm$ 5
MITES/Dec. 29	-71,357 $\pm$ 5	101,180 $\pm$ 5	-52 $\pm$ 5	123,811 $\pm$ 5
MITES/Mean <sup>*</sup>	-71,359 $\pm$ 4	101,184 $\pm$ 4	-54 $\pm$ 4	123,816 $\pm$ 4
MITES/Dec.29/car <sup>**</sup>	-71,365 $\pm$ 7	101,181 $\pm$ 7	-44 $\pm$ 10	123,816 $\pm$ 10
Survey	-71,347 $\pm$ 7	101,180 $\pm$ 7	-47 $\pm$ 7	123,805 $\pm$ 7
Difference: MITES/ Mean-Survey	-12 $\pm$ 8	4 $\pm$ 8	-7 $\pm$ 8	11 $\pm$ 8

\* Simple arithmetic average of the Dec. 17 and the first Dec. 29 result shown, although computed with more precision before rounding to the nearest millimeter. The MITES/Dec.29/car result was not included in this average.

\*\* Obtained from observations late on Dec. 29, while a car was parked with its side 60 cm from the center of the antenna in the front parking lot. Note that neither of the antennas at the ends of the baseline vector whose components are given in this table were affected. The satellite viewing geometry was significantly poorer during these observations than for the earlier ones; thus, the baseline uncertainty is magnified, especially for the U component.

Table 3. North (N), East (E), and Up (U) components and length (L) of the baseline vector extending from the front parking lot to the oil-tank temporary survey marks, from various determinations. Uncertainties are subjectively estimated, and are intended to represent about  $\pm 1$  standard deviation.

<u>Determination</u>	<u>Baseline Component</u>			
	<u>N</u>	<u>E</u>	<u>U</u>	<u>L</u>
<u>(Method/Date)</u>	(mm)	(mm)	(mm)	(mm)
MITES/Dec. 17	64,242 $\pm$ 5	-9,400 $\pm$ 5	1,346 $\pm$ 5	64,940 $\pm$ 5
MITES/Dec. 29	64,249 $\pm$ 5	-9,401 $\pm$ 5	1,342 $\pm$ 5	64,947 $\pm$ 5
MITES/Mean <sup>*</sup>	64,246 $\pm$ 4	-9,400 $\pm$ 4	1,344 $\pm$ 4	64,944 $\pm$ 4
MITES/Dec.29/car <sup>**</sup>	64,251 $\pm$ 7	-9,406 $\pm$ 7	1,365 $\pm$ 10	64,950 $\pm$ 7
Survey	64,248 $\pm$ 4	-9,399 $\pm$ 4	1,338 $\pm$ 4	64,944 $\pm$ 4
Difference: MITES/ Mean-Survey	-2 $\pm$ 6	-1 $\pm$ 6	6 $\pm$ 6	0 $\pm$ 6

\* Simple arithmetic average of the Dec. 17 and the first Dec. 29 result shown, although computed with more precision before rounding to the nearest millimeter. The MITES/Dec.29/car result was not included in this average.

\*\* Obtained from observations late on Dec. 29, while a car was parked with its side 60 cm from the center of the antenna in the front parking lot. The satellite viewing geometry was significantly poorer during these observations than for the earlier ones; thus, the baseline uncertainty is magnified, especially for the U component.

Table 4. North (N), East (E), and Up (U) components of the short offset vectors from the permanent to temporary survey marks. Estimated uncertainty is  $\pm 1$  mm in each component of each vector.

<u>Site</u>	<u>Vector</u>		<u>N</u>	<u>E</u>	<u>U</u>
	<u>From</u>	<u>To</u>	(mm)	(mm)	(mm)
Laser pad manhole	NGS disk	Rim X-cut	262	-5	208
Front lot	Steel pin	Screw head	-269	27	-16
Oil tank	Steel pin	Screw head	48	227	-1

Table 5. Vector misclosure around the triangle of baselines for each of the MITES experiments. The entries in this table were obtained by summation of the corresponding entries in Tables 1, 2, and 3; the square root of the sum of the squares was taken for the uncertainties.

<u>Experiment</u>	<u>N</u>	<u>E</u>	<u>U</u>
	(mm)	(mm)	(mm)
Dec. 17	$-10 \pm 9$	$4 \pm 9$	$1 \pm 9$
Dec. 19	$-3 \pm 9$	$-3 \pm 9$	$3 \pm 9$
Dec. 19/car*	$-7 \pm 12$	$-10 \pm 12$	$43 \pm 17$

\* Obtained from observations late on Dec. 29, while a car was parked with its side 60 cm from the center of the antenna in the front parking lot. The satellite viewing geometry was significantly poorer during these observations than for the earlier ones; thus, the baseline uncertainty is magnified, especially for the U component.

ACCURACIES OF BASELINE DETERMINATIONS BY MITES  
 ASSESSED BY COMPARISONS WITH TAPE, THEODOLITE,  
 AND GEODIMETER MEASUREMENTS

C. C. Counselman III, S. A. Gourevitch, R. W.  
 King, T. A. Herring, I. I. Shapiro (Dept. Earth  
 & Planetary Sci., M.I.T., Cambridge, MA 02139)  
 R.L. Greenspan (C.S. Draper Lab., Camb., MA 02139)  
 A.E.E. Rogers, A.R. Whitney, R.J. Cappallo (NEROC  
 Haystack Observatory, Westford, MA 01886)

On Dec. 17, 1980, portable MITES antennas [ref. Bull. Geod. 53, 139-163 (1979)] were set atop three survey marks near the Haystack Observatory building. These antennas yielded radio interferometric observations of the NAVSTAR/GPS satellites which were analyzed to determine the vector baselines between the survey marks. Observations were repeated 12 days later with different antennas on the marks. For the determination of each baseline on each day all of the observations from the entire time that five satellites were above 20° elevation--1.3 hours--were used. No data were deleted or downweighted and the same parameters were estimated using the same algorithm in every case. On each day, the triangle of separately estimated baselines closed within 1 cm in each vector component; and for each baseline, the two determinations agreed within 1 cm. In January, 1981, the firm of H. Feldman, Inc., surveyed the triangle conventionally by means of steel tape, 1" theodolite, laser Geodimeter, and precise level. The MITES experimenters and the conventional surveyors did not communicate, but both delivered their results in writing to a referee (R.L.G.) for comparison. The results for the lengths of the sides of the triangle were, in millimeters:

	Side 1	2	3
Tape	64,944 ±5	92,063 ±5	123,805 ±5
MITES	64,944 ±7	92,067 ±5	123,816 ±7
Geodimeter	n.a.	92,074 ±10	n.a.

We conclude that, at least for short baselines, the resolution of interferometer fringe ambiguities is not difficult; also, at the centimeter level of accuracy, multipath interference is not a significant problem with MITES.

ENCLOSURE 3

ACCURACY OF RELATIVE POSITIONING BY  
INTERFEROMETRY WITH RECONSTRUCTED  
CARRIER GPS: EXPERIMENTAL RESULTS

ACCURACY OF RELATIVE POSITIONING BY  
INTERFEROMETRY WITH RECONSTRUCTED  
CARRIER GPS: EXPERIMENTAL RESULTS\*

Richard L. Greenspan  
Arthur Y. Ng  
Joseph M. Przyjemski  
James D. Veale

The Charles Stark Draper Laboratory, Inc.  
Radio Navigation Division  
555 Technology Square  
Cambridge, MA 02139

ABSTRACT

Several short baselines were measured by means of interferometric (phase-difference) processing of the reconstructed carrier signals received from four GPS satellites. After 1 hour of observation, the baseline estimates agreed with surveyed values within 5 millimeters in each coordinate. Ambiguities in the carrier phase data were typically resolved within the first 15 minutes of observation. The baseline lengths typically converged to 1 centimeter of their final value within 15 to 30 minutes of observation. The sensitivity of the baseline estimates to multipath was demonstrated and theoretical predictions of multipath effects were confirmed. This experimental program demonstrated the feasibility of surveying short baselines to subcentimeter accuracy using highly portable electronic equipment. Unpredictable components of propagation delay will be the limiting error source for longer baselines.

---

\* This work was sponsored by the U.S. Air Force Geophysics Laboratory under Contract F19628-80-C0040.

## INTRODUCTION

The Charles Stark Draper Laboratory, Inc. (CSDL) has conducted a series of experiments to demonstrate that short baselines on earth can be measured in magnitude and direction to within 1 centimeter or less of error through the use of easily portable electronic equipment. These measurements were obtained by interferometric processing of GPS signals received at two antennas that were sited at the ends of the baselines to be measured.\* The GPS signals were amplified and cabled to a GPS receiver wherein the narrow-band carrier signal was reconstructed by conventional codetracking procedures. The instantaneous carrier phase for each satellite in view was sampled periodically to form the set of observables from which vector baselines were estimated. The following sections describe the experimental setup, summarize the data collection and the subsequent results of baseline estimation, and give a preliminary interpretation of our findings with respect to the development of GPS instrumentation for geodetic applications.

## EXPERIMENTAL DESIGN

Figure 1 is a schematic representation of the hardware configuration of the experiment. The antennas (Miniature Interferometer Terminals for Earth Surveying (MITES)) and preamplifiers were developed for CSDL by The Steinbrecher Corporation in collaboration with Professor Charles C. Counselman III of MIT. The MITES antennas are tuned to receive the GPS  $L_1$  frequency 1.57542 GHz. The antenna is functionally comprised of two orthogonal, horizontal, halfwave resonant dipole elements fed in phase quadrature to achieve circular polarization in the zenith direction (Reference 1). The dipoles are mounted on a cylindrical brass shaft at a height of  $3/8$  wavelength above a metallic horizontal ground plane, 1 square yard in extent (Figure 2). The antenna provides a nearly uniform gain from the zenith to about a 20-degree elevation above the horizontal. Therefore, signals from all satellites at or above a 20-degree elevation are simultaneously received during a data collection session as long as they are not occulted by obstacles. Signals from individual satellites are resolved in the GPS receiver by means of their specific code structure.

In these experiments, the antennas are precisely located over survey markers by means of a pointed brass rod inserted through a vertical hole bored into the cylindrical center shaft.

The antenna output is coupled to the preamplifier unit by a 4-foot length of RG-233 cable. A four-section cavity bandpass filter with 25-megahertz, 3-db bandwidth is provided to reject out-of-band interference with only 1 db midband insertion loss. A limiter provides burn-out protection from strong interfering signals. The system noise figure is set at about 4 db by a low-noise GaAs FET preamplifier. The net system gain is approximately

---

\* For the purposes of this paper, short baselines are those for which propagation disturbances are highly correlated at either end and are therefore cancelled by interferometric processing.

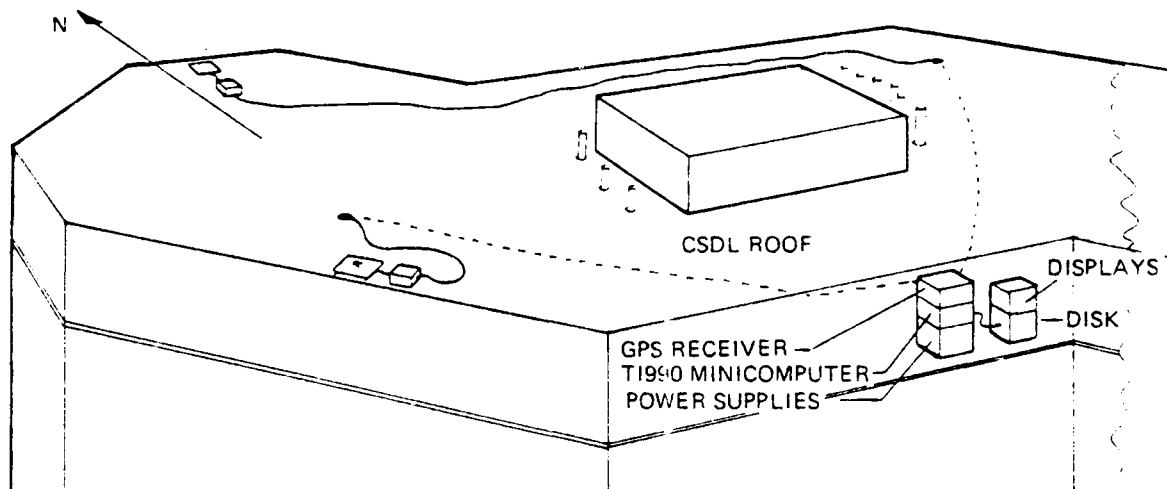


FIGURE 1. EXPERIMENTAL SETUP.

26 db. The preamplifier output is connected to the input port of the GPS receiver by approximately 35 meters of RG-214 double-shielded coaxial cable.

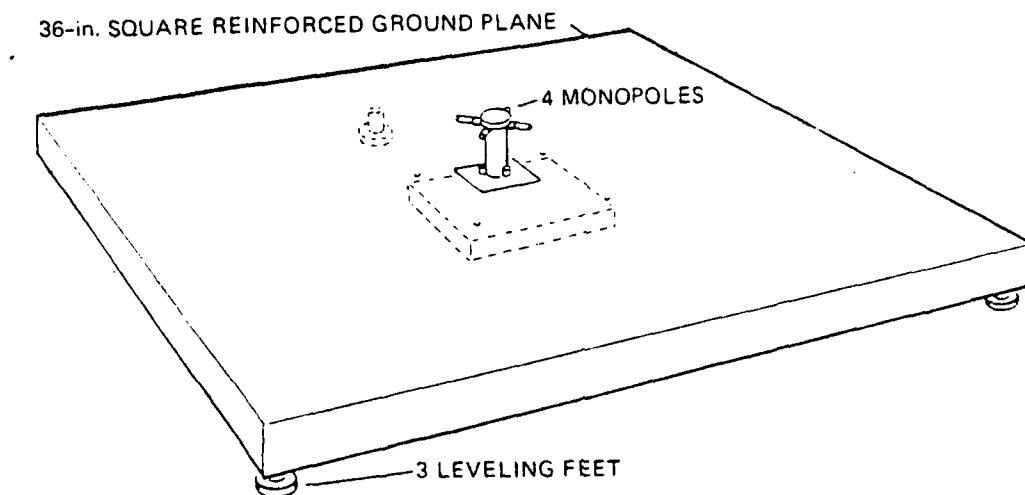
The GPS receiver is the breadboard prototype of a device that was under development at CSDL. The hardware consists of a single RF channel with frequency conversions selected to receive the  $L_1$  frequency. For this experiment, the receiver software is configured to sequentially track four satellite signals from each baseline antenna after they have been acquired. The receiver implements a variation of the Costas-loop having an arctangent error response to track the data-modulated C/A signals received from a single satellite over one 24-millisecond interval. At the end of each interval, it switches under software control to process the next satellite in the next interval. Code tracking is also executed to make GPS timing information available. Data recovery to obtain satellite ephemerides is performed as part of the initial signal acquisition function.

All eight receiver channels are used for data collection. The procedure is to cable antenna outputs from both ends of a test baseline to the receiver and to process up to four satellites from each end. Thus, the current configuration implements a connected element interferometer. However, we encountered one source of phase drift between antenna outputs that gives the observables the characteristics of independent element interferometry.

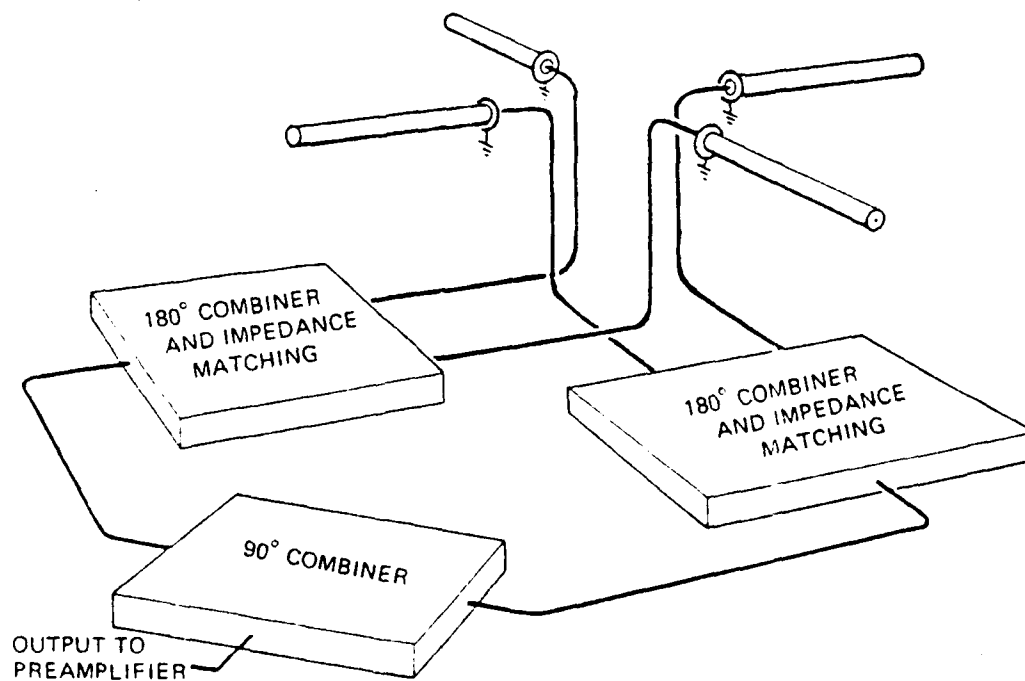
Sequencing among eight channels takes approximately 192 milliseconds. Thus, five samples of the carrier phase of each satellite in view are available every second. These carrier phase samples are ambiguous by multiples of one-half wavelength because of the arctangent implementation. However the sampling rate is fast enough that carrier cycles are not lost. Therefore, a constant time offset (equivalent to an integral multiple of half wavelengths) can be estimated for each satellite signal as part of the data reduction.

In these experiments the antenna/preamplifier units were located on the rooftop at CSDL and cabled to the GPS receiver in a laboratory one floor





a) MECHANICAL DESIGN



b) ELECTRICAL DESIGN

FIGURE 2. MITES ANTENNAS.

below the roof (Reference 2). Figure 3 illustrates the orientation of eight markers that were placed on the rooftop to define potential baselines. These markers were surveyed by tape and by theodolite to determine the baseline lengths, the elevation of the markers with respect to marker A1 and the angles of the baselines with respect to north. The angular measurements are

estimated to have a standard deviation of 3 arcseconds; the point to point distance errors are estimated to have a standard deviation of 2 millimeters. Tables 1 and 2 summarize the survey data.

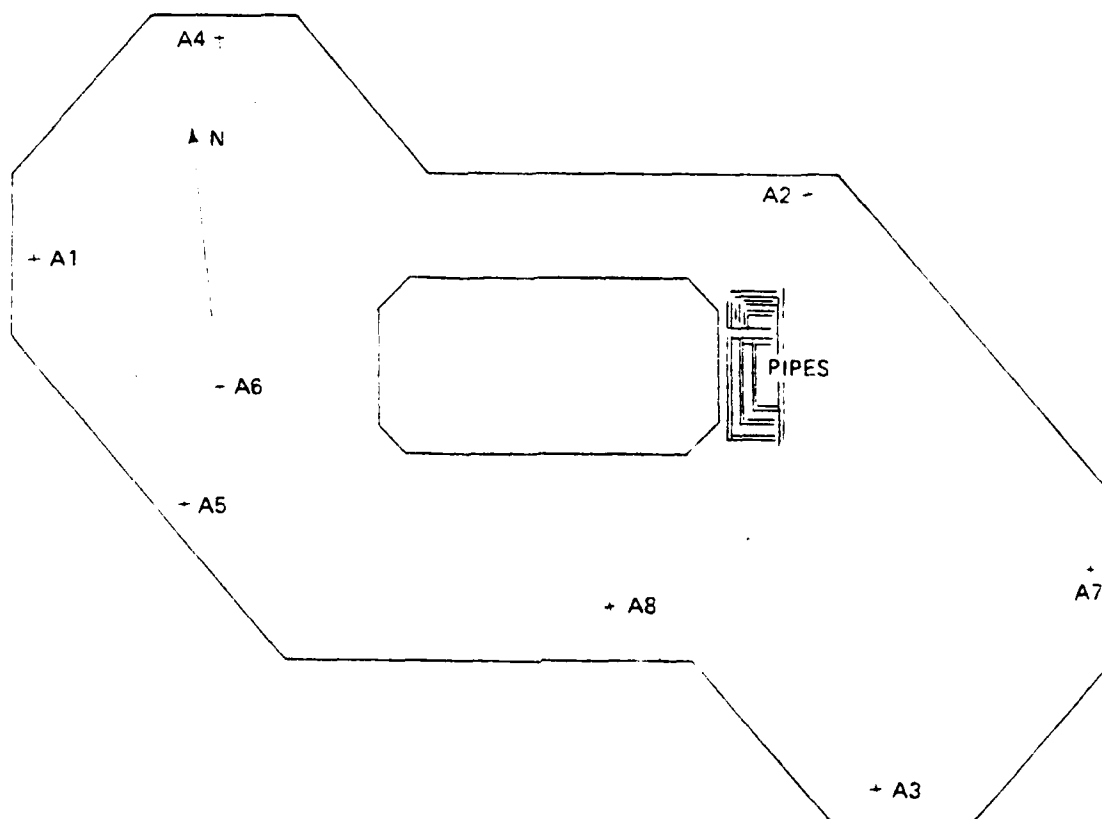


FIGURE 3. SITING OF SURVEYED BASELINES ON CSDL ROOF.

During any data collection session, two antennas are centered over the surveyed points; they are leveled and oriented within a few degrees of north using a bubble level and compass. The orientation is important because the antenna patterns will introduce an electrical phase angle equal to their difference in azimuth orientations. Because the two antennas are essentially identical with a circular symmetry, their phase centers can be taken at the height of the ground plane directly above the survey markers. The antennas have screw-type leveling legs; therefore one must measure the height of each antenna above the marker in order to properly compare the interferometry results with the conventional survey. This was done by measuring the height of the central shaft above the marker plate for each experiment. This measurement is accurate to about 1 millimeter.

All experiments were conducted when three or more GPS satellites were visible above a 20-degree elevation as seen from Cambridge, Massachusetts.

This limited the potential viewing time to about 78 minutes each day of which about 16 minutes were required for signal acquisition, ephemeris collection, and determination of GPS system time. Therefore, data collection typically spanned about 1 hour. As a result, only one baseline was measured per day. Figure 4 (Courtesy of C. Counselman) illustrates the azimuth and elevation histories of the visible satellites during a data collection session. Since the GPS satellites are in a nearly 12-hour orbit, the same pattern repeats from day to day at progressively earlier times (4 minutes per day).

TABLE 1. HORIZONTAL COMPONENTS OF REFERENCE BASELINES.

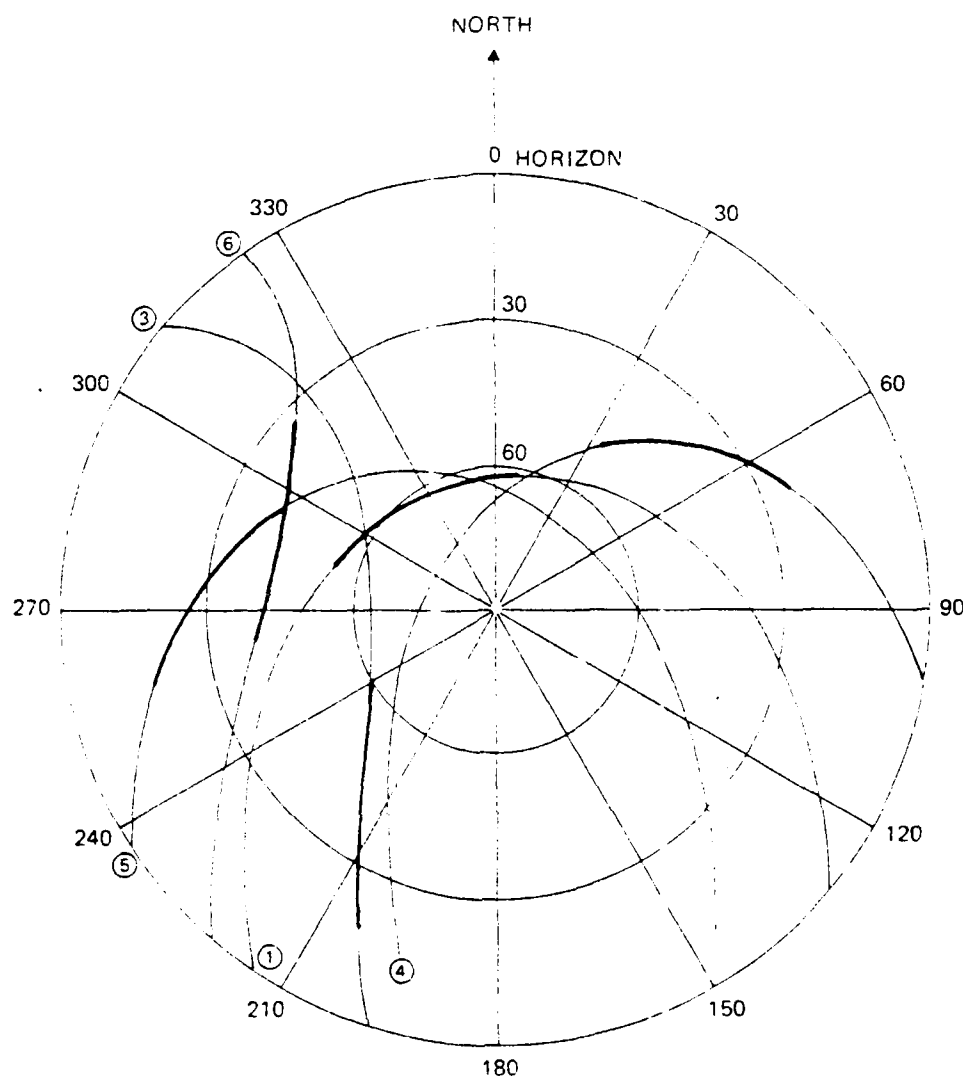
	DISTANCE (meters)	ANGLE FROM NORTH (degrees)
A1A4	19.6470	44.7808
A4A2	40.9507	110.9572
A1A2	52.0859	90.7712
A2A7	31.6031	148.5794
A3A7	20.9295	48.4691
A8A3	22.0182	131.4213
A5A8	29.8460	109.2713
A5A3	50.9205	118.6541
A1A5	18.9920	154.3862
A5A6	8.2000	22.7211
A1A6	14.8620	130.0446
A5A4	31.5772	10.2689
A6A4	23.6363	5.9788

TABLE 2. ELEVATION OF REFERENCE MARKERS.

	ELEVATION (cm)
A1	0.00
A2	-11.45
A3	-10.65
A4	-8.80
A5	-8.95
A6	-8.70
A7	-0.60
A8	-0.35

#### EXPERIMENTAL OBSERVATION

Data collection began on August 13, 1981 with observations of baseline A1A2. The first surveys used carrier phase differences (integrated Doppler)



- CIRCLED NUMBERS ARE GPS NAVSTAR SATELLITE DESIGNATORS
- SATELLITE TRACKS ARE DARKENED TO INDICATE SIMULTANEOUS VISIBILITY ABOVE 20° ELEVATION

FIGURE 4. VISIBILITY OF GPS SATELLITES.

as the observable. The resulting baselines disagreed from the survey by several centimeters. Although this was encouraging, we began an intensive review of the data collection procedures and the data reduction software in order to determine the cause of unanticipated trends in the post-fit residuals. These trends were the evidence that led to the discovery of a significant timing error in the processing software. By the end of September 1981, the processing software was debugged and extended to include the option for phase

difference processing, as well as integrated Doppler difference processing. Data collection for baseline measurements was concentrated in October 1981, with further observation sessions during December to assist in diagnosing the measurement error sources. Table 3 summarizes the data base collected during this period. Weather conditions during baseline measurements ranged from clear, calm, and dry with temperatures around 22 C to wet and windy with temperatures around 10 C.

TABLE 3. BASELINE MEASUREMENT DATA BASE.

Dates	Baselines	Comments
October 1,3	Null	Used to estimate noise level attributable to receiver electronics
October 7,8,9,13	A5A4	Used to estimate measurement repeatability and closure of triangular survey
October 14,15	A1A5	
October 16	A1A4	
October 21,23,26	A5A4	Diagnostic tests for observed phase drifts
October 27	A5A4	Reflecting mirror placed to produce multipath
December 15,16,17	Null	Diagnostic for contribution of electronics to post-fit residuals

#### DATA REDUCTION

The GPS receiver generates sets of eight phase measurements taken sequentially over a 192-millisecond interval which corresponds to the sampling period of the receiver's phase tracking filters. For a baseline AB, the observations are sequenced as Satellite n at A, Satellite n at B, Satellite n + 1 at A, and so forth. The receiver software also outputs estimates of the carrier phase rates and accelerations so that all observables can be referred to a common epoch. Experience has shown that the phase rate terms are adequate for this interpolation; there is no apparent improvement of the post-fit residuals when the acceleration term is included.

The bandwidth of the carrier phase-tracking filter is approximately 1/2 hertz. Therefore, the minimum period between useful sets of observables is approximately 2 seconds. Although all of this data are available, we have typically chosen to process data at 19.2-second intervals as a good compromise between baseline measurement accuracy and processing burden. We will discuss the dependence of measurement accuracy on the number of observations in the following section.

The basic set of observables is the difference in carrier phase for the reception of each satellite at each end of the baseline. These differences are formed after the sequential observations are interpolated to a common epoch. These observables were processed in three steps. In the first

step, a linear least squares algorithm with equal weighting of residuals was applied to generate a trial solution for the ambiguous baseline components. The following set of equations was fit to the data to estimate eight parameters, including three baseline components, frequency offset, and one phase offset for each satellite.

$$\phi_{ij} = \vec{b} \cdot \vec{s}_{ij} + \alpha_j + i(\delta\theta) \quad j = 1, 2, 3, 4$$

where

$\phi_{ij}$  = the interferometric phase difference for the  $i^{\text{th}}$  observation of satellite  $j$

$\vec{b}$  = the unknown baseline vector

$\vec{s}_{ij}$  = a unit vector in the direction of satellite  $j$  at time  $i$

$\alpha_j$  = an unknown phase offset for observations of the  $j^{\text{th}}$  satellite

$\delta\theta$  = the phase shift produced by an unknown frequency offset between the receiving systems

The resulting values of  $\alpha_j$  were converted to integer multiples of  $\lambda/2$ , and a limited search around these integers was executed to determine the set of integers that minimizes an error criterion. Call these integers  $N_j$ . The final step of the processing is to refit the baseline by a five-parameter least squares procedure giving the solution to the equations

$$\phi_{ij} - N_j \lambda/2 = \vec{b} \cdot \vec{s}_{ij} + i(\delta\theta) + \beta \quad j = 1, 2, 3, 4$$

where  $\beta$  is included to fit cable length differences that are a fraction of  $\lambda/2$ .

Table 4 summarizes the results of the baseline estimation. The baseline components are presented in local-level (north-east-up) coordinates. There was no data editing in these runs, although subsequent analysis suggests that a short interval of data taken immediately after initial satellite acquisition should be suppressed to avoid contamination by the transient response of the carrier tracking filters. Each baseline listed in Table 4 was measured on a different day; one antenna was moved, repositioned and leveled from day to day. The largest disagreement between the conventional survey and the phase processed data is 5.7 millimeters (east component of A5A4), and five of the nine differences are less than 0.4 millimeters. The rms post-fit residual for phase estimation is about 2 millimeters. The horizontal disagreements for Doppler processing range between 1 to 4 centimeters, with larger errors in the vertical component, reaching 12 centimeters in one case. Vector misclosure around the triangle of baselines is -2.2, -2.2, -0.3 (mm) in the coordinate directions (N, E, U), respectively.

TABLE 4. BASELINE SURVEYS.

Baseline	Survey Mode	North (meters)	East (meters)	Up <sup>(3)</sup> (meters)	RMS Residual <sup>(4)</sup> (millimeters)
A1A4	Conventional	13.9453	13.8390	-0.0880	---
A1A4 (10/16/81)	Interferometric				
	Phase <sup>(1)</sup>	13.9481	13.8388	-0.0883	1.99
	Doppler <sup>(2)</sup>	13.9581	13.8259	-0.1256	1.39
A1A5	Conventional	-17.1253	8.2101	-0.0895	---
A1A5 (10/15/81)	Interferometric				
	Phase <sup>(1)</sup>	-17.1256	8.2131	-0.0878	2.07
	Doppler <sup>(2)</sup>	-17.1477	8.2471	-0.0111	1.47
A5A4	Conventional	31.0714	5.6292	0.0015	---
A5A4 (10/13/81)	Interferometric				
	Phase <sup>(1)</sup>	31.0715	5.6235	-0.0008	2.02
	Doppler <sup>(2)</sup>	31.0981	5.5923	-0.1217	1.50

## NOTES:

- (1) Single-differenced phase processing.
- (2) Single-differenced integrated Doppler processing.
- (3) Conventional values of the "Up" component are from Table 2; the interferometric measurements are adjusted for the heights of the antennas above the survey marks.
- (4) 187 data sets spaced at 19.22-second intervals over 1 hour. Phase observations are fit to five parameters and Doppler observations fit to three parameters.

Table 5 summarizes the results of repeated measurements of baseline A5A4. The baseline components typically differ by less than 2 millimeters, except for one measurement of the vertical component which differs by about 6 millimeters. The standard deviations are 0.76, 1.60, 2.40 (mm) in the coordinate directions (N, E, U), respectively.

DISCUSSION

The results presented in Table 4 are repeatable. This experiment gives primary evidence for the following conclusions:

- (1) Interferometric processing of carrier phase differences observed in reception of GPS signals can be used to measure short baselines to an accuracy of better than 1 centimeter in length and in each coordinate.

TABLE 5. REPEATABILITY OF BASELINE ESTIMATES  
(Baseline A5A4)

Date	North (m)	East (m)	Up (m)
October 7	-31.0731	-5.6226	0.0253
8	-31.0735	-5.6234	0.0306
9	-31.0730	-5.6227	0.0312
13	-31.0715	-5.6235	0.0313

- (2) For longer baselines, the primary error source will be statistically independent propagation delays along the path from the satellite to each baseline antenna. These propagation residuals are now believed to contribute about 1 to 2 centimeters error to long baseline measurements (References 3 and 4). For baselines of 1000 kilometers or more, satellite ephemeris errors could become significant.
- (3) The quoted accuracy from GPS observations can be achieved using highly portable equipment including a rugged, low-gain antenna (e.g., MITES), a single-channel rapidly sequencing GPS receiver and data acquisition system under control of a small minicomputer, and a high quality crystal oscillator having a short-term stability on the order of 1 part in  $10^{11}$  over 100 seconds.

We executed several variations on the basic data collection and reduction procedures in order to sharpen these conclusions. The first variation involves measurements of a "null" baseline. This is a procedure wherein the signals from one antenna are split into two paths and input to the GPS receiver as if they came from two different antennas. It is used to estimate the noise level of the baseline measurement procedure.

Figure 5 illustrates an overlay of the phase residuals for all satellites observed during the null-baseline test of October 1, 1981. In this test, the signal splitting occurred at the input to the GPS receiver. Thus the antenna, preamplifier, and all cabling is common to both ends of the "baseline". Data were collected for 35 minutes; for this data set, the least squares fit for the baseline components yields 1.8, -0.3, -0.8 millimeters with an rms post-fit residual of 0.96 millimeters. The results converge to this level within 15 minutes of observation. The residuals appear to be randomly distributed with no discernable trends. We conclude that the sequencing among receiver channels is fast enough that receiver electronics, including phase instability of the receiver frequency standard (FTS-Model 1000), is a negligible error source.

The rms post-fit residual converges to the standard deviation of the observation noise when that noise is white. The rms residual can be predicted from SNR considerations as follows. The carrier-to-noise ratio input to



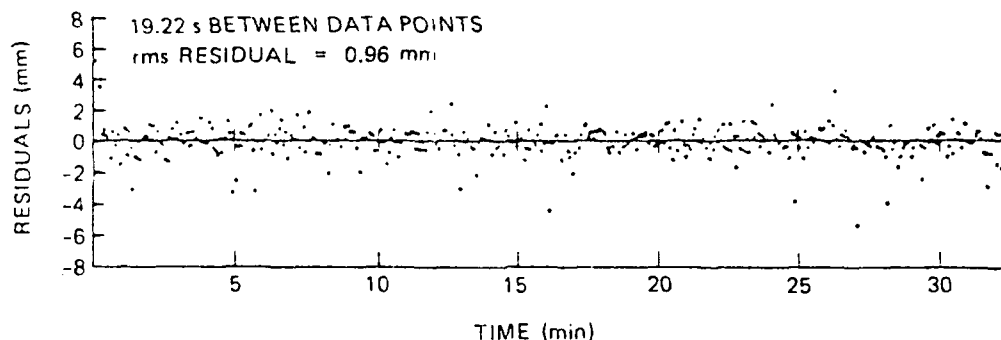


FIGURE 5. POST-FIT PHASE RESIDUALS FOR "ZERO-BASELINE"  
OBSERVATION OF OCTOBER 1, 1981.

the sequential tracking filters was estimated at  $35 + 2$  dB-Hz and the tracking loop noise bandwidth was approximately  $1/2$  Hz. For  $C/n_o = 35$  dB-Hz, the rms error in measuring phase distances is given by

$$\sigma\lambda = \sqrt{2} \cdot \frac{\lambda}{2\pi} \sqrt{\frac{B_n(\text{Hz})}{C/n_o(\text{dB-Hz})}} = 0.55 \text{ mm}$$

which is within a factor of two of the observed phase error.

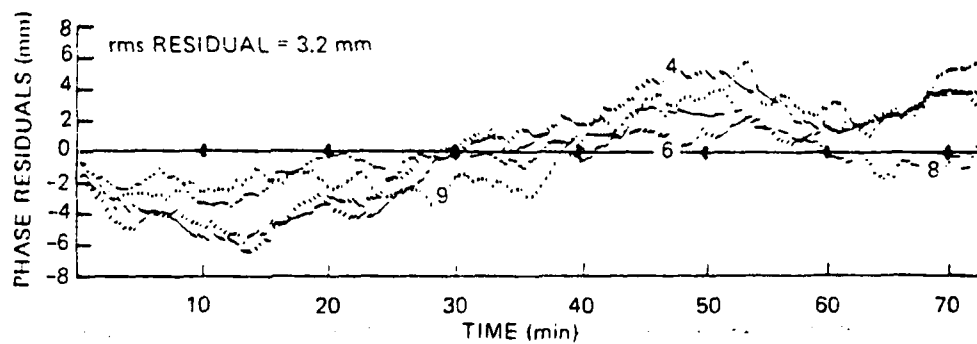
The zero-baseline data was also reprocessed in the "double-difference" mode

$$\text{Observable} = (\phi_{1j} - \phi_{1k}) - (\phi_{2j} - \phi_{2k})$$

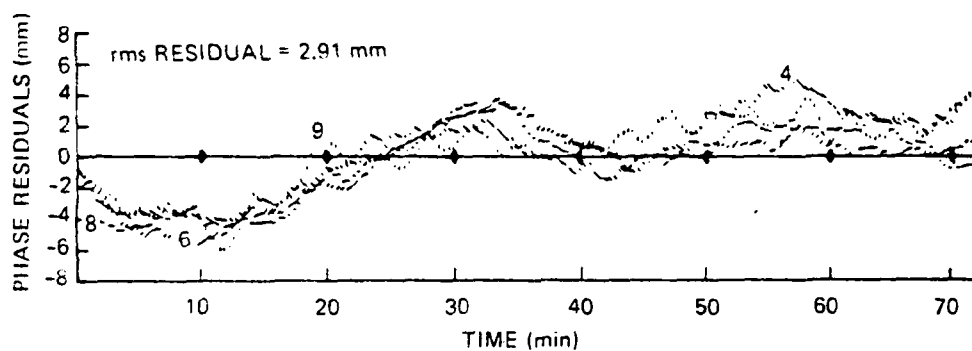
where  $\phi_{ij}$  is the carrier phase of satellite  $j$  as viewed at the  $i^{\text{th}}$  antenna. The rms residual increases by almost  $\sqrt{2}$  to 1.33, which is consistent with the assumption that these residuals are uncorrelated.

Figure 6 illustrates the phase residuals for the first processing of the observations of October 13, 15, 16 cited in Table 4. There is clear evidence of a phase slope in the data. The scatter around this slope appears to have a peak-to-peak range about 3 millimeters. The significant feature of Figure 6 is that the trend is common to all satellites. That rules out satellite-dependent antenna or multipath effects and suggests that there is a small time-varying phase drift between the two antenna channels. The observation of this slow drift term was the motivation to include a phase drift (frequency offset) parameter in the baseline estimation algorithm. The results of Table 4 were produced with the phase slope estimated. Figure 7 illustrates the post-fit residuals using this improved estimator.

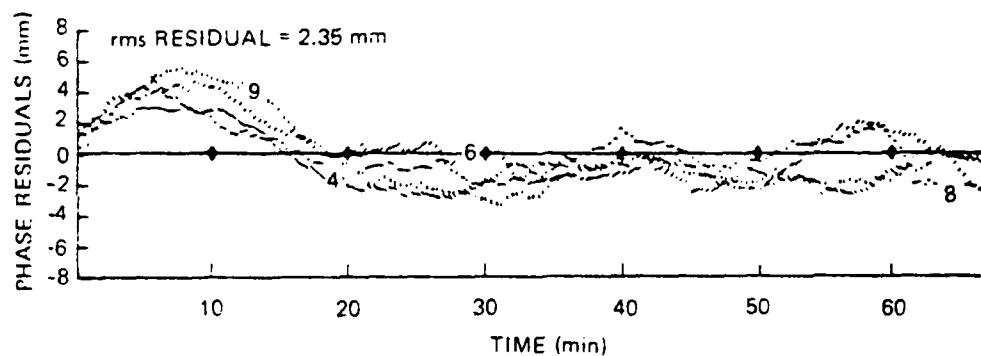
Further tests were conducted in December to diagnose the source of the drift. The results of the first null-baseline test exclude the receiver as the source of the drift. The remaining candidates were the preamplifier units or, perhaps, the cavity filters or cables.



(a) BASELINE 54, OCTOBER 13, 1981

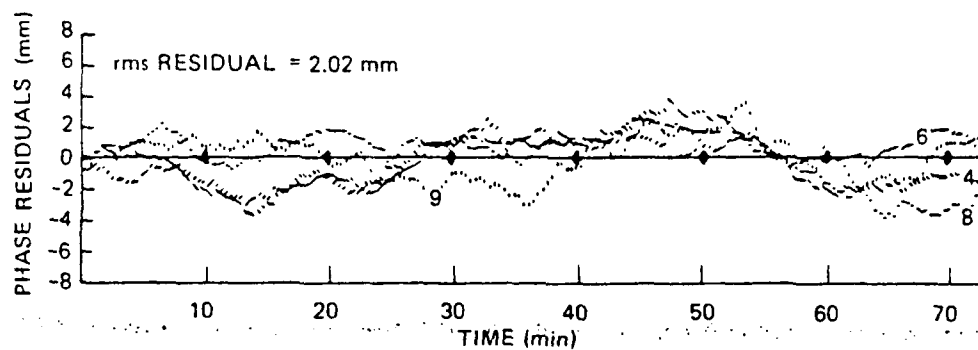


(b) BASELINE 15, OCTOBER 15, 1981

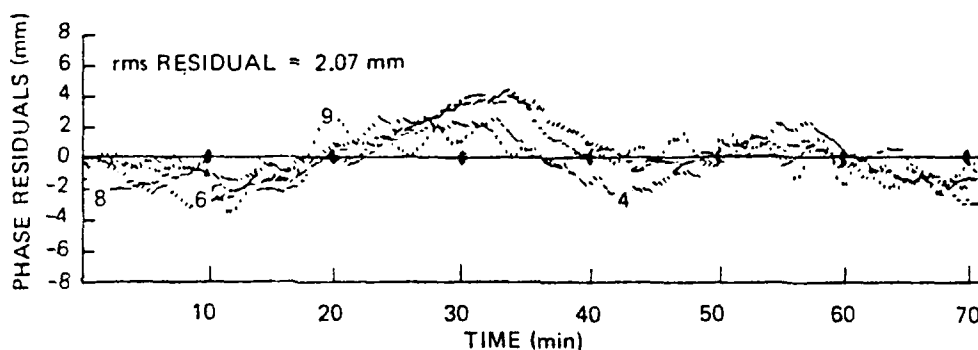


(c) BASELINE 14, OCTOBER 16, 1981

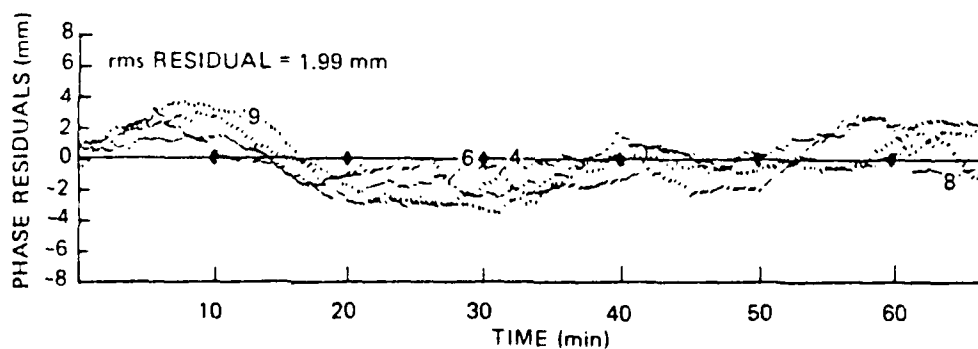
FIGURE 6. SMOOTHEd POST-FIT PHASE RESIDUALS FOR MEASURED BASELINES.



(a) BASELINE 54, OCTOBER 13, 1981



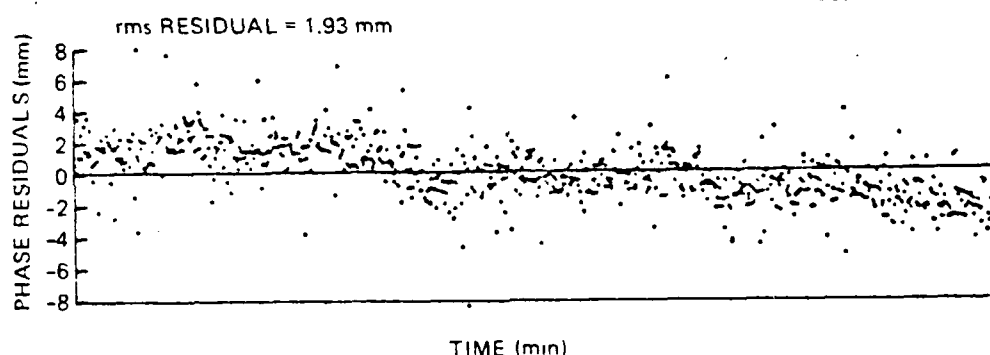
(b) BASELINE 15, OCTOBER 15, 1981



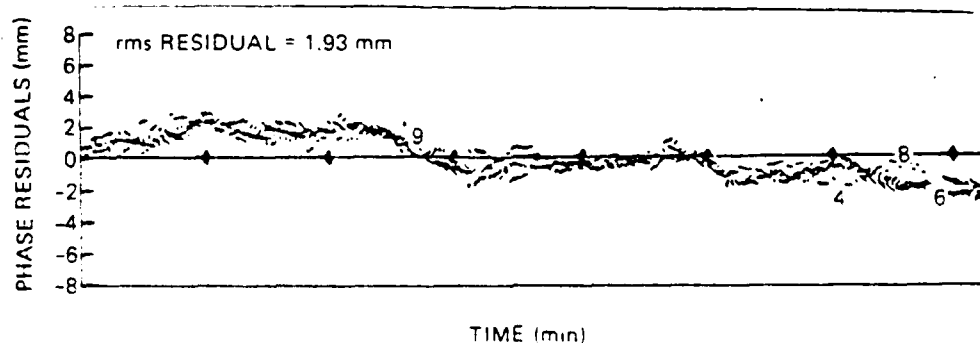
(c) BASELINE 14, OCTOBER 16, 1981

FIGURE 7. SMOOTHED POST-FIT PHASE RESIDUALS FOR MEASURED BASELINES: PHASE DIFFERENCED SLOPE ESTIMATED.

In the zero-baseline test of December 15, the antenna was cabled to one preamplifier whose output was split and cabled to the receiver. This is equivalent to the first zero-length baseline experiment, except that there is an opportunity for the cables to be a source of phase error. Figure 8 illustrates the phase residuals on a sample by sample basis and with smoothing over 5 adjacent samples (96 seconds). There appears to be a slope of about 4 millimeters per hour. Since the preamplifiers are common to both paths, this slope suggests that there was a change in the length of the cables. The thermal coefficient for electrical length of a polyethylene insulated cable (RG-214) ranges from 100 to 250 ppm/°C (Reference 4). For a temperature rise of 2°C/hour (during mid-day December), we could expect that phase slopes on the order of 5 millimeters per hour or more could be attributed to the 20-meter difference in the lengths of cables that were exposed to the changing thermal environment. The experiment was repeated with the antenna output split and amplified separately before being cabled to the receiver. A phase slope of 2 or 4 millimeters per hour was observed on successive days when different pairs of amplifiers were used. The use of independent amplifiers did not increase the phase slope. This confirms our suspicion that differential expansion of the cables produced the observed effect.



(a) POST-FIT PHASE RESIDUALS FOR "ZERO LENGTH" BASELINE, DECEMBER 17, 1981



(b) SMOOTHED POST-FIT RESIDUALS FOR ZERO LENGTH BASELINE, DECEMBER 17, 1981

FIGURE 8. EVIDENCE FOR PHASE SLOPE PRODUCED BY DIFFERENTIAL CABLE STRETCH.

Another question we considered was the rate at which the baseline estimates converge, and in particular, how much time is required to resolve the ambiguities in carrier phase differences. The result of more than ten baseline determinations is that, in most cases, the ambiguities were correctly resolved for the trial baselines from 10 to 15 minutes of observation, as long as there were several data points per minute. The exceptions occurred when the phase slope (that we attribute to cable stretch) was large. In these cases, as much as 35 minutes was required to properly resolve ambiguities. In most other cases, the baseline length was estimated with less than 1 centimeter error within 10 to 15 minutes. After that, the errors steadily decreased to the level of a few millimeters. We conclude that:

- (1) The rms residual converges rapidly after ten or more data points are processed.
- (2) The accuracy of the baseline estimate improves with the span of the observations and the number of data points. If the number of data points is fixed, then errors decrease if the observation period is increased.

The final question we address is the influence of multipath on the baseline estimation. Baseline A5A4 was remeasured on October 26 and then on October 27 a 4-foot high, 2-foot wide, 1/8 inch aluminum plate facing northwest was mounted vertically behind the antenna at A5, as illustrated by Figure 9. The procedure outlined in Reference 5 was used to predict the incidence of multipath during a 1-hour observation session. The theory predicts that signals from satellites labeled 5, 6, and 8 would not be reflected in the mirror; signals from satellite 4 would reflect for a short interval but these reflections would not produce significant phase deviations; signals from satellite 9 would be reflected during most of the observation period and this multipath would cause a peak-to-peak phase offset of about 19 millimeters. Figure 10 illustrates the observed phase residuals. The upper plot shows the residuals for October 26 (no plate) and residuals for October 27. In both cases, the residuals have been smoothed over five successive samples (19.22 seconds per sample) to suppress short-term noise fluctuations. Comparison of these residuals shows that the theory is qualitatively accurate and remarkably close to being quantitatively accurate. The N, E, U components of baseline A5A4 estimated from the data of October 26 are -31.0423, -5.6371, 0.0003 (meters), respectively. The baseline length is 31.5500 meters. These results deviate from prior measurements of A5A4 because the antenna was not accurately sited over the A5 marker on these two days. The observations of October 27 yield baseline components of -31.0048, -5.6691, and 0.1620 (meters). The baseline length is estimated as 31.5792 meters. This inauspicious placement of the reflecting plane demonstrates the possibility that multipath reflecting into a poorly sited antenna could produce baseline measurement error of a few centimeters.

#### CONCLUSIONS

We have demonstrated that reconstructed carrier processing of GPS signals can be used to achieve subcentimeter accuracy in the measurement of

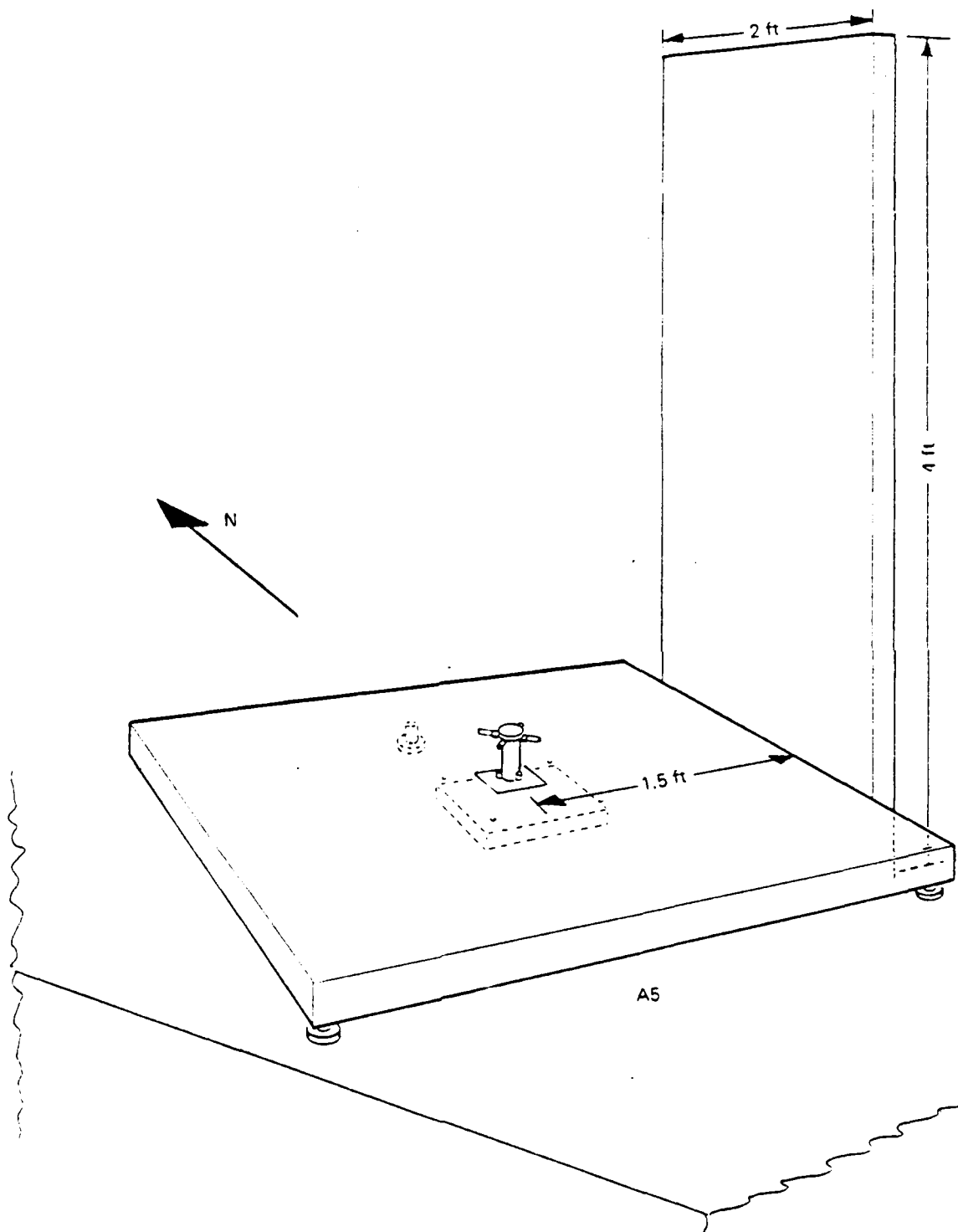
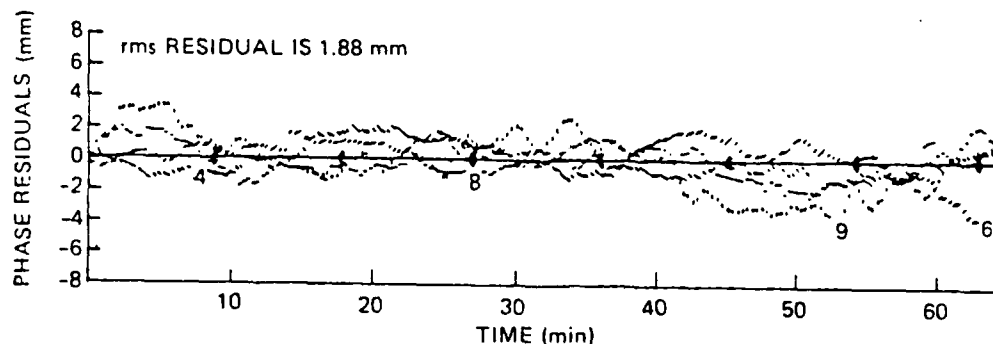
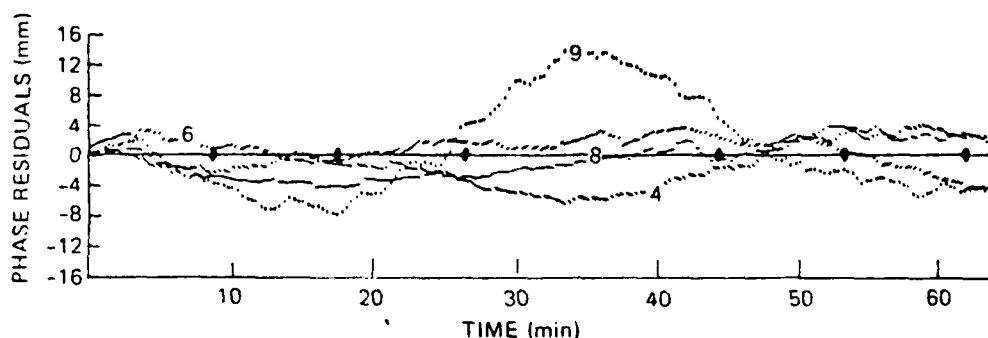


FIGURE 9. SITING OF MULTIPATH REFLECTOR.



(a) PHASE RESIDUALS FOR BASELINE  $\vec{54}$ , OCTOBER 26, 1981



(b) PHASE RESIDUAL FOR BASELINE  $\vec{54}$  WITH REFLECTING PLATE, OCTOBER 27, 1981

SATELLITE IDENTIFIER 4 \\\\\\\

6 \\\\\\\

8 - - - -

9 \\\\\\\

FIGURE 10. INFLUENCE OF MULTIPATH ON POST-FIT PHASE RESIDUALS.

short baselines. With the advent of compact GPS receivers, the field instrumentation including antennas, clocks, receivers, and data collection will be highly portable. The required GPS technology involves carrier tracking and rapid sequencing of C/A code-tracking loops. Second-generation portable GPS equipment embodying these functions is currently under development by the Defense Department.

We believe that the primary error source for longer baselines will be uncorrectable propagation delays and satellite ephemeris errors. Multipath, cable stretch, clock drift, time synchronization, and thermal noise will not

be significant error sources in a well-designed and well-sited system; nor will the suppression of these effects incur any significant penalty in cost or convenience to potential users.

#### REFERENCES

1. Counselman, C.C. and I.I. Shapiro, "Miniature Interferometer Terminals for Earth Surveying", 2nd International Geodetic Symposium on Satellite Doppler Positioning, Volume 2, University of Texas, January 1979, pp. 1237-1286.
2. Greenspan, R.L., et al., "Backpack VLBI Terminal with Subcentimeter Capability", NASA Conference Publication 2115, Radio Interferometry Techniques for Geodesy, June 19-21, 1979.
3. Bossler, J.D., C.C. Goad, and P.L. Bender, "Using the Global Positioning System (GPS) for Geodetic Positioning", Bull. Geodesique, 54, 1980, pp. 553-563.
4. Catalog TL-6, Times Wire and Cable Co., Wallingford, Conn.
5. Counselman, C.C. and S.A. Gourevitch, "Miniature Interferometer Terminals for Earth Surveying: Ambiguity and Multipath with Global Positioning System", IEEE Trans. on Geoscience and Remote Sensing, Vol. GE-19, No. 4, October 1981, pp. 244-252.



ENCLOSURE 4

EFFECTS OF MULTIPATH ON  
PHASE DIFFERENCE INTERFEROMETRY



# INTRALAB MEMORANDUM

Memo No: 15L-82-017

TO: R.L. Greenspan

FROM: A. Ng

DATE: 26 February 1982

SUBJECT: Effects of Multipath on Phase Difference Interferometry

COPIES TO: J. Veale, J. Przyjemski, P. Van Broekhoven

---

## Introduction

Multipath is a potential source of errors in measuring baselines by means of carrier phase interferometry. Reflections of the radio signal off of nearby objects can combine with the direct path signal to distort the measured carrier phase. This multipath distortion is not, in general, common to the two ends of the baseline because the topography differs, and is not common to two satellites tracked simultaneously at one end because the satellites are at different points in the sky. Formation of the interferometric phase observable with a single difference (phase at one end subtracted from phase at the other end for simultaneous measurements) cancels errors that are common to measurements made at the two ends of the baseline. Use of a second difference (phase due to one satellite subtracted from phase due to another satellite) cancels errors that are common to measurements made at either end which are the same for more than one satellite -- examples of such errors include station clock errors and cable stretch due to thermal loading. Multipath, however, falls into neither of these two classes of "removable" errors. It is therefore of interest to learn how large the multipath distortion may be and in what situations may multipath be a significant error source.

We derive an analytic expression for the contribution of multipath to the received phase for the specific case of a vertical plane reflector. The intent is to give ourselves a qualitative, and to some extent,

AD-A150 681

ACCURATE BASELINE DETERMINATION BY RADIO INTERFEROMETRY 272

ON NAVSTAR GPS SA. (U) CHARLES STARK DRAPER LAB INC

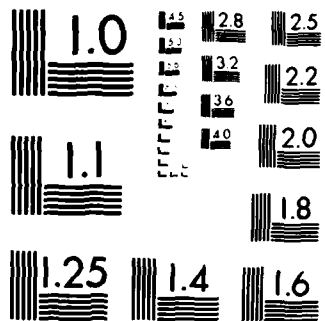
CAMBRIDGE MA R L GREENSPAN ET AL. 15 JUN 84

UNCLASSIFIED

CSDL-R-1719 AFGL-TR-84-0156

F/G 17/2.1 NL





MICROCOPY RESOLUTION TEST CHART  
NATIONAL BUREAU OF STANDARDS 1963-A

quantitative feel for the size of the multipath distortion. This result is a special case of a general expression which we give in operator notation. The general expression covers antennas like the MITES [1] antenna, that is, a quadrature fed pair of dipoles mounted at right angles to each other in the horizontal plane a distance  $g$  (for MITES,  $g = 3\lambda/8$ ) above a horizontal ground plane.

An experiment has been conducted on the CSDL roof which demonstrates the observability of multipath due to a rectangular reflector mounted in the vertical plane a short distance from one antenna of a baseline. The residuals after the fit resemble the theoretical phase error fairly closely. The experiment is described and qualitative results are presented.

#### Theoretical Development

The following analysis uses the operator notation and analysis techniques employed by Counselman and Gourevitch [2]. The situation is depicted in Figure 1. Consider a baseline consisting of antennas A and B, each with its own receiver. Only antenna A has reflecting objects around it; antenna B is assumed to be on level ground, which is by assumption an extension of the antenna ground plane. A satellite at zenith angle  $\theta$  and east azimuth  $\phi$  (referenced to north) is observed by both receivers, which track the phase of the received carrier. The observable is the difference in received phase sampled simultaneously, or nearly so. It has been shown [3] that in the absence of errors, the phase-connected, ambiguous observable is equal to  $\frac{2\pi}{\lambda}(r_0 - r_1) + n\pi$  where  $r_i$  denotes range to the satellite from receiver  $i$ , and the term  $n\pi$  accounts for half wavelength ambiguities which must be removed.

The reflection produces a relatively delayed signal that interferes coherently with the desired direct-path signal. The reflected signal arrives attenuated in strength and shifted in phase with respect to the direct signal from the satellite because of the extra propagation delay, azimuth dependence of the antenna pattern phase characteristic, and the reversal of sense of circular polarization due to reflection. The effect on the measured signal can be seen qualitatively in the phasor diagram in Figure 2. In the diagram  $\epsilon_s$  represents the portion of the

signal received from the satellite and  $c_r$  represents the portion of the signal received from the reflector. As the satellite-antenna-reflector geometry changes with time, the endpoint of  $c_r$  traces out a locus that is not necessarily circular. Indeed, given the numerous factors contributing to received multipath phase, the length and orientation of  $c_r$  with respect to  $c_s$  might well look arbitrary. We wish to know more details concerning the relationship between  $c_r$  and  $c_s$ , reasonable limits on the phase error  $\epsilon_r$ , and rate of variation of  $\epsilon_r$  as the satellite moves. One of the principal goals of this section is to characterize received multipath phase error by deriving an expression for the special case of a vertical reflector.

In the notation of [2], the direct satellite signal received by the quadrature fed crossed dipole antenna is given by the following expression, neglecting an amplitude factor that has been set to unity throughout this discussion:

$$A = \langle \vec{p}^* | D | \vec{p} \rangle \sin(\langle \vec{k} | \vec{g} \rangle) \exp(j \langle \vec{k} | \vec{r} \rangle), \quad (1)$$

where  $|\vec{p}\rangle$  is the complex column vector representing the orientation of the quadrature-fed horizontally mounted crossed dipoles of the MITES antenna:

$$|\vec{p}\rangle = \begin{bmatrix} 1 \\ j \\ 0 \end{bmatrix}, \quad j = \sqrt{-1};$$

$\langle \vec{p}^* |$  is the complex conjugate transpose of  $|\vec{p}\rangle$ ;  $D$  is an identity operator that performs a rotation in azimuth and zenith angle to locate the transmitter in space:

$$D = \begin{bmatrix} \cos\theta \cos\phi & -\sin\phi & \sin\theta \cos\phi \\ \cos\theta \sin\phi & \cos\phi & \sin\theta \sin\phi \\ -\sin\theta & 0 & \cos\theta \end{bmatrix};$$

$\langle \vec{k} |$  is the propagation (row) vector of the signal from its source and has magnitude  $2\pi/\lambda$ ;  $|\vec{g}\rangle$  is the ground plane vector and  $|\vec{r}\rangle$  is the range vector from the antenna to the satellite. The first element in these vectors is the x or north component, the second is the y or west component, and the third is the z or up component. When the quantities listed above are substituted into (1) we get the following useful expression:

$$A = \left\{ (1 + \cos\theta) \sin\left(\frac{3\pi}{4} \cos\theta\right) e^{j\phi} \right\} e^{j2\pi \frac{r}{\lambda}} \quad (2)$$

The bracketed term in (2) is the antenna pattern for the received electric field. The expression in (2) gives the complex amplitude of a received signal due to a source at range  $r$ , zenith angle  $\theta$ , azimuth  $\phi$ , transmitting circularly polarized radiation in the direction of the antenna.

A similar expression can be derived for signals reflected into the antenna from a perfectly reflecting mirror. We need to account for the extra delay and the change in direction due to reflection. Here again there is an amplitude factor (the same one that is in (1)) which is set to unity:

$$A_m = - \langle \vec{g}^* | \vec{D}^* R_m | \vec{p} \rangle \sin(\langle \vec{k} | R_m | \vec{g} \rangle) \exp(j \langle \vec{k} | (\vec{r} - 2\vec{m}) \rangle) \quad (3)$$

where  $|\vec{m}\rangle$  is a vector directed from the antenna phase center perpendicular to the plane of the reflector and having a length equal to the closest distance of the reflector plane to the antenna.  $R_m$  is the reflection operator, an identity transformation that projects objects and everything else into "mirror space":

$$R_m = I - 2|\hat{m}\rangle\langle\hat{m}|$$

The  $\vec{r} - 2\vec{m}$  factor in the complex exponential accounts for the excess propagation delay. We need to concern ourselves only with

multipath from reflectors placed less than a code chip away in light-time, because the cross-correlation properties of the pseudorandom codes automatically reject multipath from outside a chip delay. In most cases, in fact, we need to worry about delays of only a small fraction of a chip because the power attenuation on the skirts of the autocorrelation function of the code is relatively high. Also, Equation (3) neglects dielectric losses of nonideal reflectors, but considers instead only perfect reflection.

The total received signal is the sum of Equations (1) and (3):  $A_{tot} = A + A_m$ . For the general case of a randomly oriented and shaped reflecting surface it may be more convenient to resort to computational techniques to simplify  $A_{tot}$  into magnitude and phase. Two special cases are of interest: horizontal and vertical reflecting planes. Generally the horizontal case occurs because of the ground, which is mostly horizontal and so nearly similar at the two baseline ends that the effects should approximately cancel in the formation of the observable; thus the horizontal reflector case is fairly benign in most instances. The case of vertical reflectors is often more interesting and less benign because the vertical reflectors are not necessarily present at both antennas. In this case, for a reflector in the plane at distance  $m$  and azimuth  $\mu$ , the reflector orientation vector is

$$|\vec{m}\rangle = \begin{bmatrix} m \cos \mu \\ m \sin \mu \\ 0 \end{bmatrix}$$



and substitution into  $A_{tot}$  gives (after much simplification):

$$A_{tot} = (1 + \cos \theta) \left[ 1 - \tan^2 \frac{\theta}{2} \exp(j \{ 2(\mu - \phi) - \frac{4\pi m}{\lambda} \sin \theta \cos(\phi - \mu) \}) \right] \cdot \sin\left(\frac{3\pi}{4} \cos \theta\right) \exp(j(\frac{2\pi r}{\lambda} + \phi)). \quad (4)$$

The term in square brackets gives the deviation from the expected antenna pattern (cf. Equation (2)). This term can be resolved into polar form:

$$|[\cdot]| = \left\{ \left( 1 - \tan^2 \frac{\theta}{2} \cos(2(\mu - \phi) - \frac{4\pi m}{\lambda} \sin \theta \cos(\phi - \mu)) \right)^2 + \left( \tan^2 \frac{\theta}{2} \sin(2(\mu - \phi) - \frac{4\pi m}{\lambda} \sin \theta \cos(\phi - \mu)) \right)^2 \right\}^{1/2} \quad (5a)$$

$$\angle[\cdot] = \tan^{-1} \left( \frac{\tan^2 \frac{\theta}{2} \sin(2(\mu - \phi) - \frac{4\pi m}{\lambda} \sin \theta \cos(\phi - \mu))}{1 - \tan^2 \frac{\theta}{2} \cos(2(\mu - \phi) - \frac{4\pi m}{\lambda} \sin \theta \cos(\phi - \mu))} \right). \quad (5b)$$

The total phase angle of the total received signal is the phase that is observed and used in interferometry. This total phase angle is found by isolating the arguments of the complex exponential:

$$\angle A_{tot} = \frac{2\pi r}{\lambda} + \phi + \tan^{-1} \left( \frac{\tan^2 \frac{\theta}{2} \sin(2(\mu - \phi) - \frac{4\pi m}{\lambda} \sin \theta \cos(\phi - \mu))}{1 - \tan^2 \frac{\theta}{2} \cos(2(\mu - \phi) - \frac{4\pi m}{\lambda} \sin \theta \cos(\phi - \mu))} \right).$$

It is clear that the phase error is just the expression in (5b). This expression has been plotted in Figure 3 for  $\theta=30^\circ$  and  $\theta=60^\circ$ ,  $m=5$ , and  $10$ ,  $\mu=-90^\circ$ , with  $\phi$  varying from  $0^\circ$  to  $180^\circ$ . The behavior of the phase error is oscillatory for azimuths well away from opposition (satellite,

antenna, and center of mirror coplanar in vertical plane). One can see the dependence of the oscillation rate with respect to azimuth as  $\alpha$  is varied: the rate is higher for more distant reflectors. In the region away from opposition this error frequency may be high enough that the cumulative error should be zero mean over the course of an observation session. In the region of opposition, however, the phase error varies more slowly with respect to azimuth. It should be noted that in the course of an hour long observation a GPS satellite typically covers only about thirty or forty degrees in azimuth. It is possible that a satellite could be observed entirely within this central region and that the multipath-related error could contribute a non zero mean phase offset. In the next section we determine when this observation geometry may hold.

#### Geometry of Multipath

Equation (5b) gives the expression for phase error due to multipath given that a satellite located at  $(\theta, \phi)$  can be observed by the antenna in a vertical mirror located at azimuth  $\alpha$  and distance  $d$ . We now wish to determine conditions for observability of multipath for this specific reflecting structure: when can we see the satellite in the mirror? Some simple geometric constructions will show when this situation arises. First recall our definitions of  $\alpha$  and  $m$ :  $\alpha$  is the azimuth of the vector pointing from the antenna phase center and normal to the plane containing the reflector, and  $m$  is the distance from the antenna phase center to the plane of the reflector and measured along the direction of this normal vector. Our observation geometry is illustrated in Figure 4. It consists of a vertical mirror of height  $h$  and width  $w$  (height is measured with respect to the ground plane) located in the plane described by  $\alpha = (\alpha_{\text{min}}, \alpha_{\text{max}})$ . The rectangular mirror will reflect the signal from a satellite at elevation  $\theta$ , azimuth  $\phi$  if  $-\tan^{-1}(w/2m) < \phi - 180^\circ < \tan^{-1}(w/2m)$  and  $-\tan^{-1}(h/m) < \theta < \tan^{-1}(h/m)$ . The viewing geometry is identical to the problem of viewing the satellite from the image antenna (behind the mirror) through a window located where the mirror is located and cut out of an opaque plane.

A simple graphical technique for determining multipath visibility suggests itself. Using a polar plot of satellite trajectories in the local sky for the times at which observations are made, one can overlay the windowing function mapped into polar coordinates by drawing a curve,  $C$ , of  $\mu = \tan^{-1}(\hbar \cos(\phi - \gamma)/a)$  for the range  $\mu = 90^\circ < \mu < \mu = 270^\circ$ . Thus, if the mirror faces north ( $\gamma = 180^\circ$ ) the curve drawn will lie on the north half of the diagram. A satellite at position  $(\alpha_{sv}, \delta_{sv})$  for which elevation  $\delta_{sv}$  is lower than the curve  $C$  (position lies outside the curve  $C$ ) can be seen in a vertical reflector of height  $\hbar$  and distance  $a$  from the antenna. The azimuthal limits of visibility can be placed by drawing rays at  $\mu = (\mu = 180^\circ) - \tan^{-1}(\hbar/a)$  and  $\mu = (\mu = 180^\circ) + \tan^{-1}(\hbar/a)$ . A satellite at position  $(\alpha_w, \delta_w)$  which lies between these bounds in azimuth and outside the curve  $C$  can be seen in the plate centered in figure 4.

An example of the graphical technique just described is shown in figure 5, using actual satellite trajectories for periods of visibility used for ionospheric scatter data collection. In this example,  $\hbar = 1.1$ ,  $a = 1.3$ , and  $\gamma = 45^\circ$  (mirror faces northeast). The shaded portion  $\mathcal{V}$  ( $\mu = (180^\circ - \tan^{-1}(\hbar/a))$  to  $\mu = (180^\circ + \tan^{-1}(\hbar/a))$ ) is the region of the sky in which a satellite is visible in the reflector. In this example, SVF is the only satellite that may suffer phase error due to multipath reflections from the vertical plate.

#### Multipath Experiment

A baseline survey experiment was performed to investigate the effects of induced multipath on the phase observable. The survey was run twice, once without a reflecting plate and once with a 4 foot high, 2 foot wide aluminum plate placed 1.3 feet from the antenna, mounted vertically and facing approximately  $45^\circ$  west of north ( $\gamma = 135^\circ$ ). The graphical technique is used in figure 6 to show the region of visibility for this

This placement butted the mirror against the edge of the WTLB antenna groundplane, which is 3 feet on a side. This was considered to be a "worst-case" reflector placement.

situation. Of the satellites, only SV4 and SV9 are visible during some portion of the observation period. Because SV9 is at a lower elevation, we expect its maximum phase deviation to be higher than that of SV4, based on the plots in Figure 5. Both SV's pass through opposition with the mirror, where the phase error varies slowly with azimuth compared with elsewhere. We should look for this slow variation effect in the post-fit residuals. For further comparison, the theoretical phase error (Equation (57) applied for times of satellite visibility) is plotted for the trajectories of SV4 and SV9 in Figure 7. The large deviation of SV9 has a peak to trough value of approximately  $3''$  or about  $1 \text{ mm}$ .

Residuals after a least squares batch fit to phase measurements are presented in Figure 8 for all four satellites tracked (SV's 4, 6, 8, 9), without the plate on 16 Oct 61 and with the plate on 27 Oct 61. There is a pronounced deviation in the residuals of SV9 away from the session with the plate, as expected. The peak to trough deviation is  $11 \text{ mm}$ . Since the fit minimizes the squared error by adjusting the three baseline vector components and by adding a bias, it might be expected that the residuals would not precisely trace the theoretical curve. There is however an apparently strong correlation between the residuals of SV4 and the predicted errors. The size of the residuals of SV4 are much smaller and the correlation with the predicted error may be harder to make. The size of the residuals for SV4 and SV9 is of the same order as that of SV6 though these SV's cannot be seen in the plate. The residuals may be due to other reflect structures since a correlation can be seen from the 15th to the 17th.

The striking effect of the SV4 residuals is the most convincing argument for our model of multipath. The plot of residuals qualitatively resembles the predicted phase error fairly closely. There may be other error sources that are not cataloged but which might mask the true behavior of the error due to the plate. For this reason no more quantitative arguments will be pressed.

#### Conclusions

We have presented theoretical methods for predicting the observability and the magnitude of multipath interference with phase observables. A

general expression for the phase error was given in terms of the antenna pattern and the positions of the satellite and reflector. The special case of a vertical plate reflector was studied in some depth. For this special case, an observability criterion was developed using a geometric, graphical construction to determine when the transmitter is visible to the antenna in the reflector.

An experiment was conducted to investigate observability and size of multipath interference from a pathological, contoured reflector. The residual errors show a good correlation with theoretically predicted values.

The best method for reducing the effect of multipath is wise antenna placement when possible. We can site the antennas based on prior knowledge of satellite trajectories and computerized geometric modeling of the reflecting surfaces (often randomly oriented) to minimize the maximum error. Another method which bears investigation is to predict the multipath induced phase error and subtract it from the observable before the least squares parameter estimation. This method depends heavily on accurate computer models of the reflecting surfaces and correct computer implementation of the operator equations (1) and (2) to get the phase error out to a randomly oriented surface.



Arthur Y. Ng

### References

- (1) C.C. Counselman III and I.I. Shapiro, "Miniature Interferometer Terminals for Land Surveying," Proc. of the 2nd Int'l Geodetic Symposium on Satellite Doppler Positioning, vol. 2, pp. 105-107, 1976.
- (2) C.C. Counselman III and S.A. Gorevitch, "Simulation of Multipath in NITIS Experiments," Memo to I.I. GreenSPAN, 31 September 1980.
- (3) I.I. GreenSPAN, "Introduction to Program 90100-0100: Baseline Interferometry," Memo to I.I. GreenSPAN, 6 June 1981.

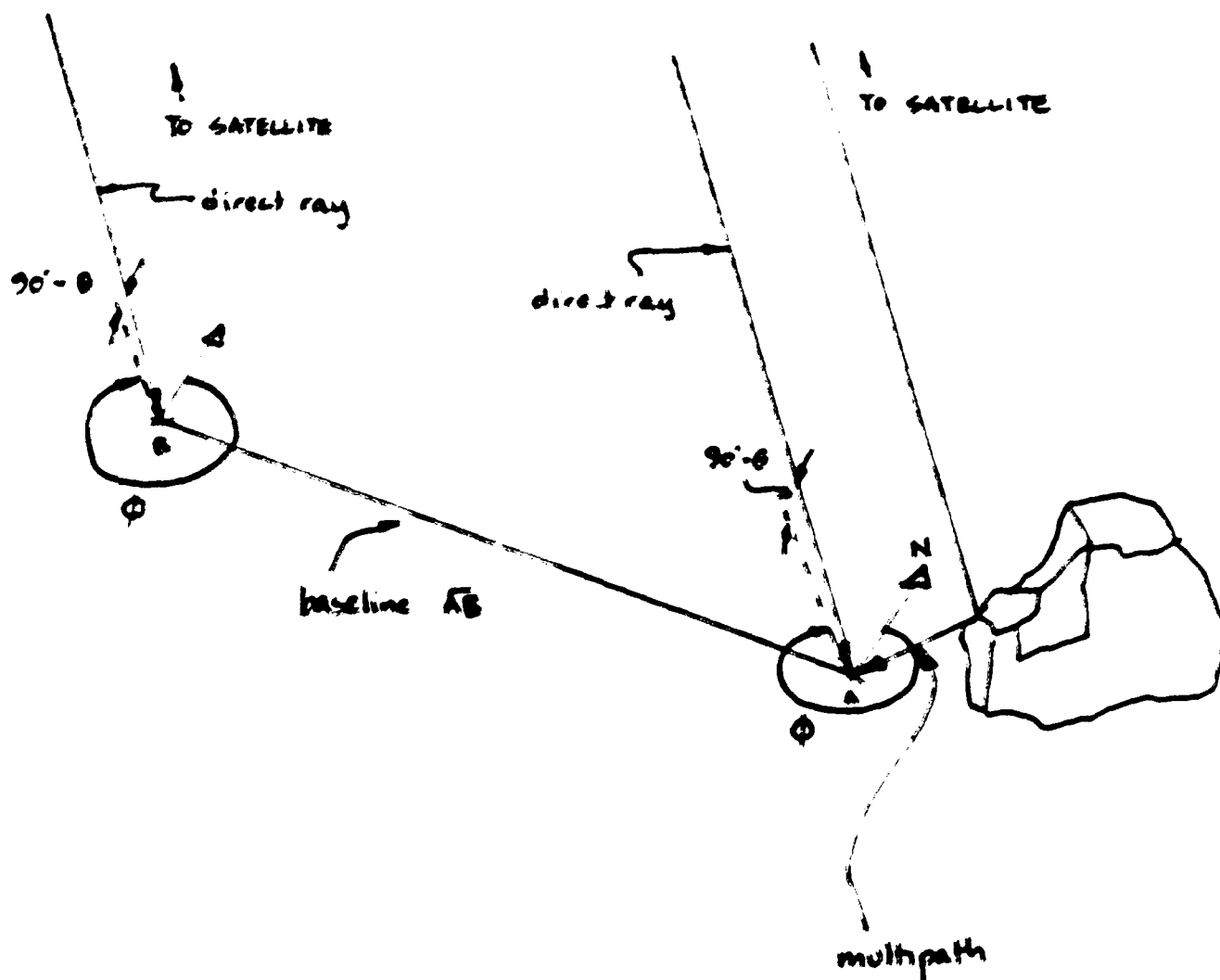


Figure 1. Baseline survey by satellite interferometry with a source of multipath.

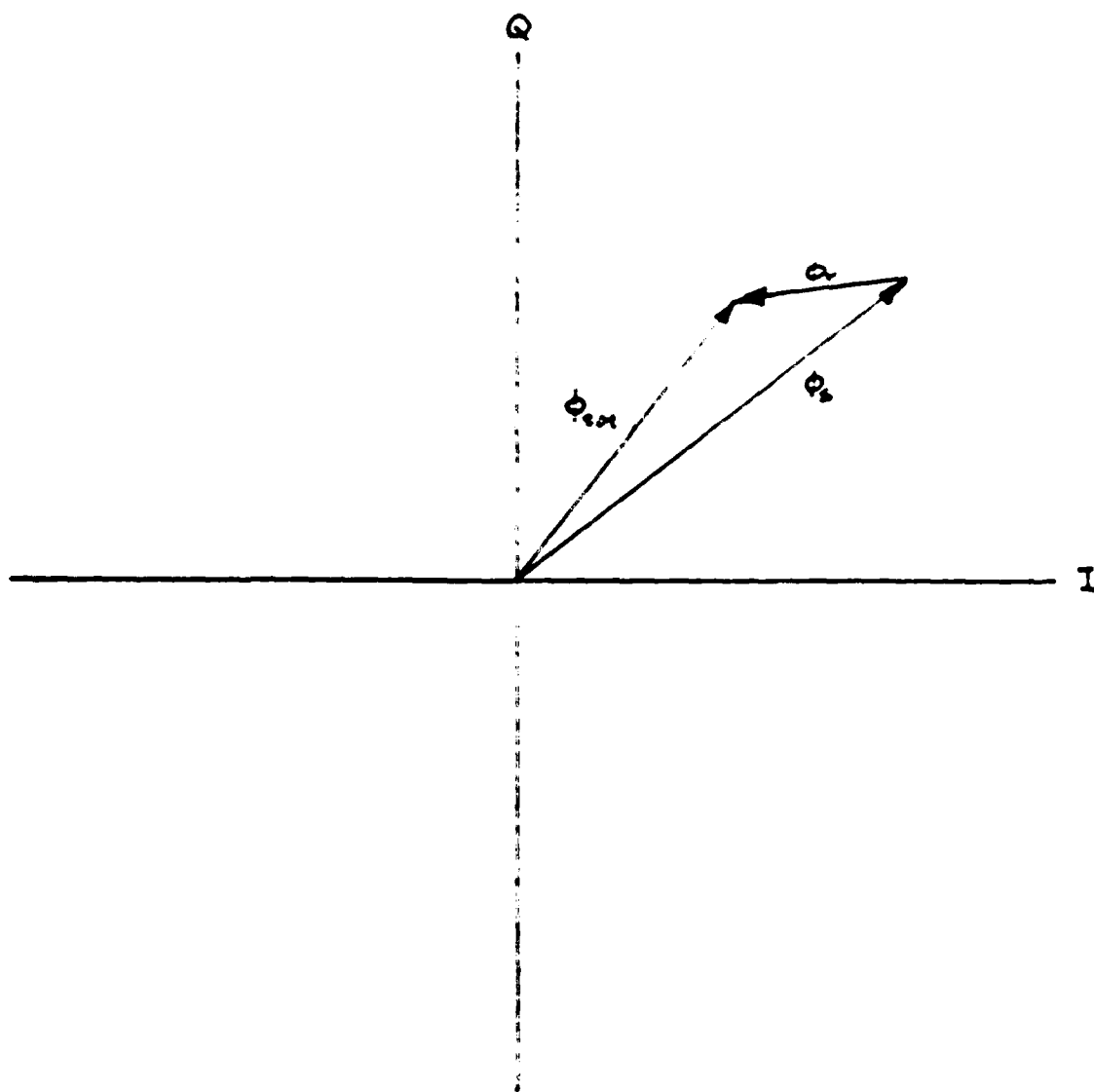


Figure 1. Effect of multipath on total phase measured, represented in a phasor diagram ( $\phi_{tot}$  = total phase,  $\phi_s$  = signal desired,  $a$  = reflection).



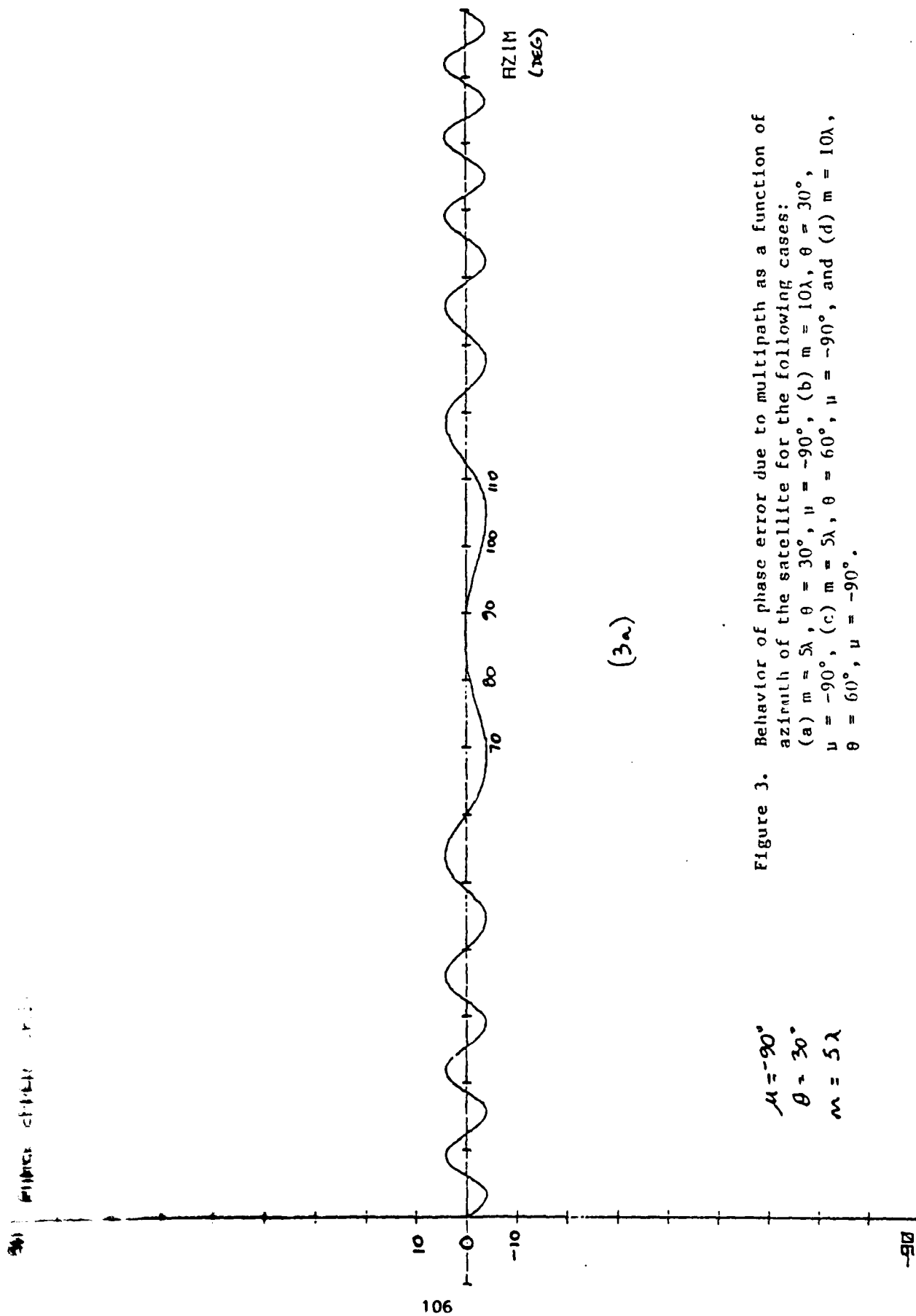


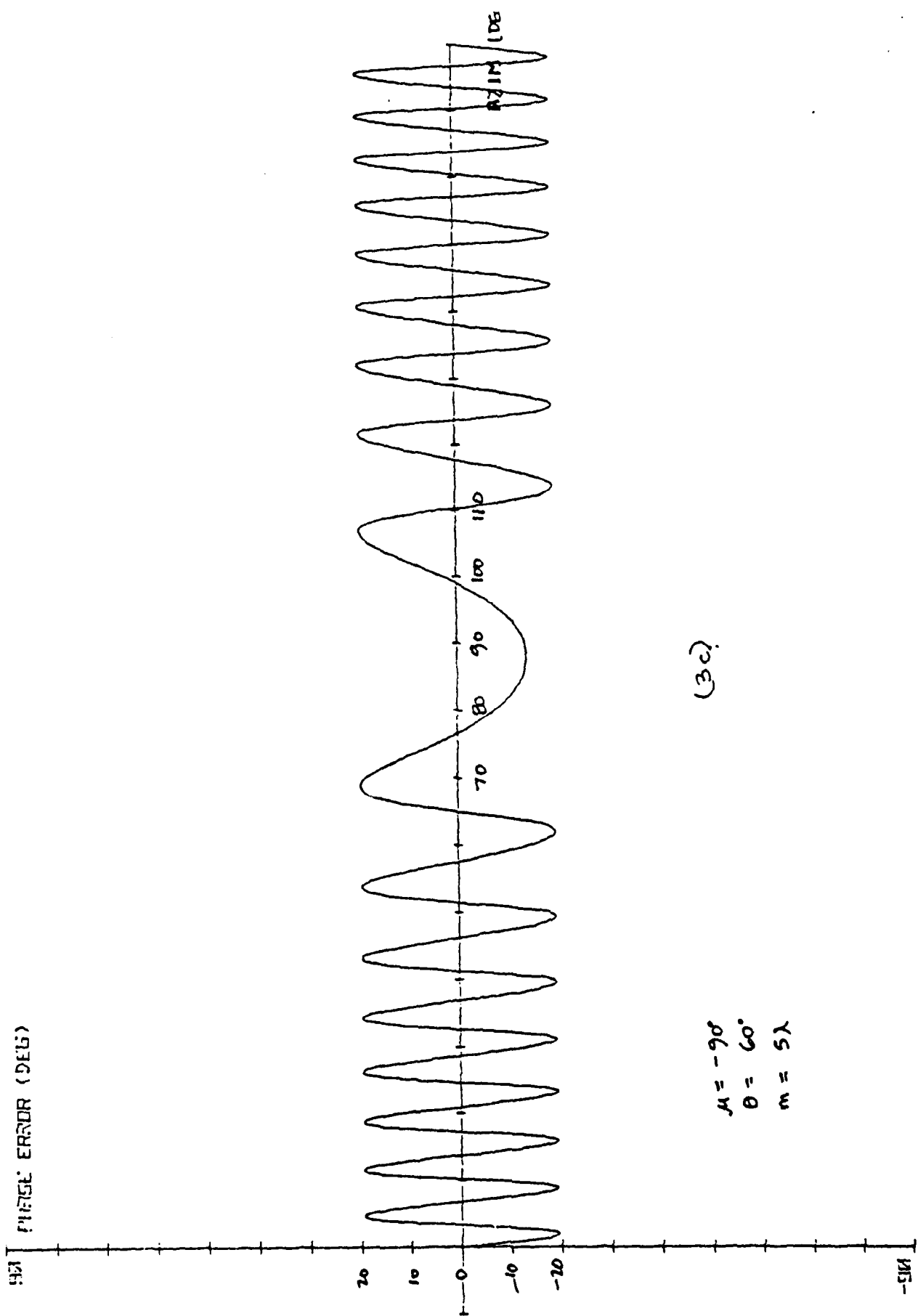
Figure 3. Behavior of phase error due to multipath as a function of azimuth of the satellite for the following cases:  
 (a)  $m = 5\lambda$ ,  $\theta = 30^\circ$ ,  $\mu = -90^\circ$ , (b)  $m = 10\lambda$ ,  $\theta = 30^\circ$ ,  $\mu = -90^\circ$ , (c)  $m = 5\lambda$ ,  $\theta = 60^\circ$ ,  $\mu = -90^\circ$ , and (d)  $m = 10\lambda$ ,  $\theta = 60^\circ$ ,  $\mu = -90^\circ$ .

1 mi

$$\mu = -90^\circ$$
 $\theta = 30^\circ$ 
$$x_0 = 3$$


(36)

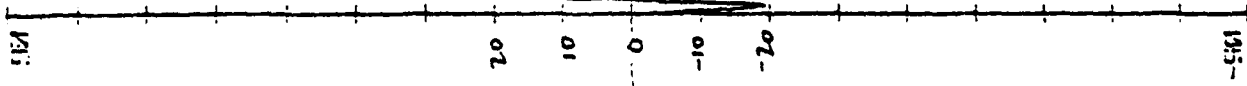
117.114  
(930)



(3c)

$$\begin{aligned} \mu &= -90^\circ \\ \theta &= 60^\circ \\ m &= 5\lambda \end{aligned}$$

PIECE ERROR (DEG)



$\mu = -90^\circ$   
 $\theta = 60^\circ$   
 $m = 101$

(34)

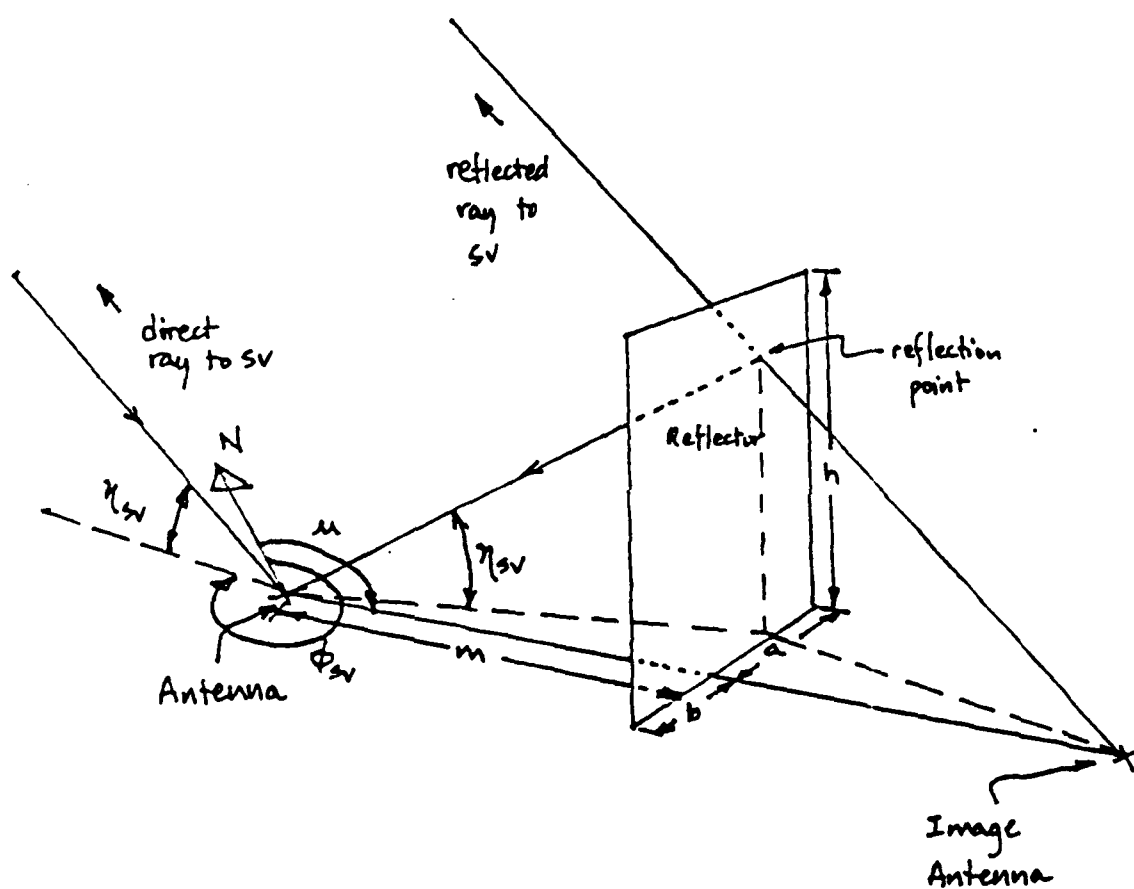
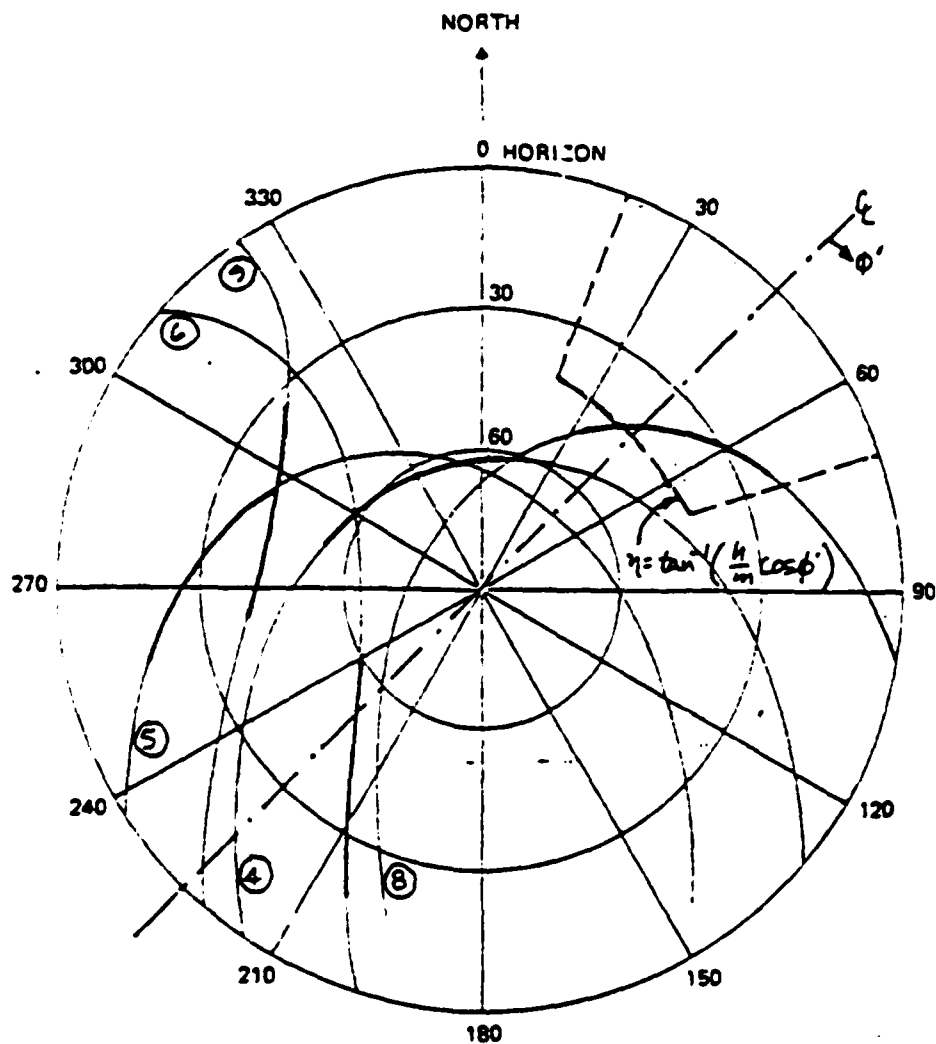
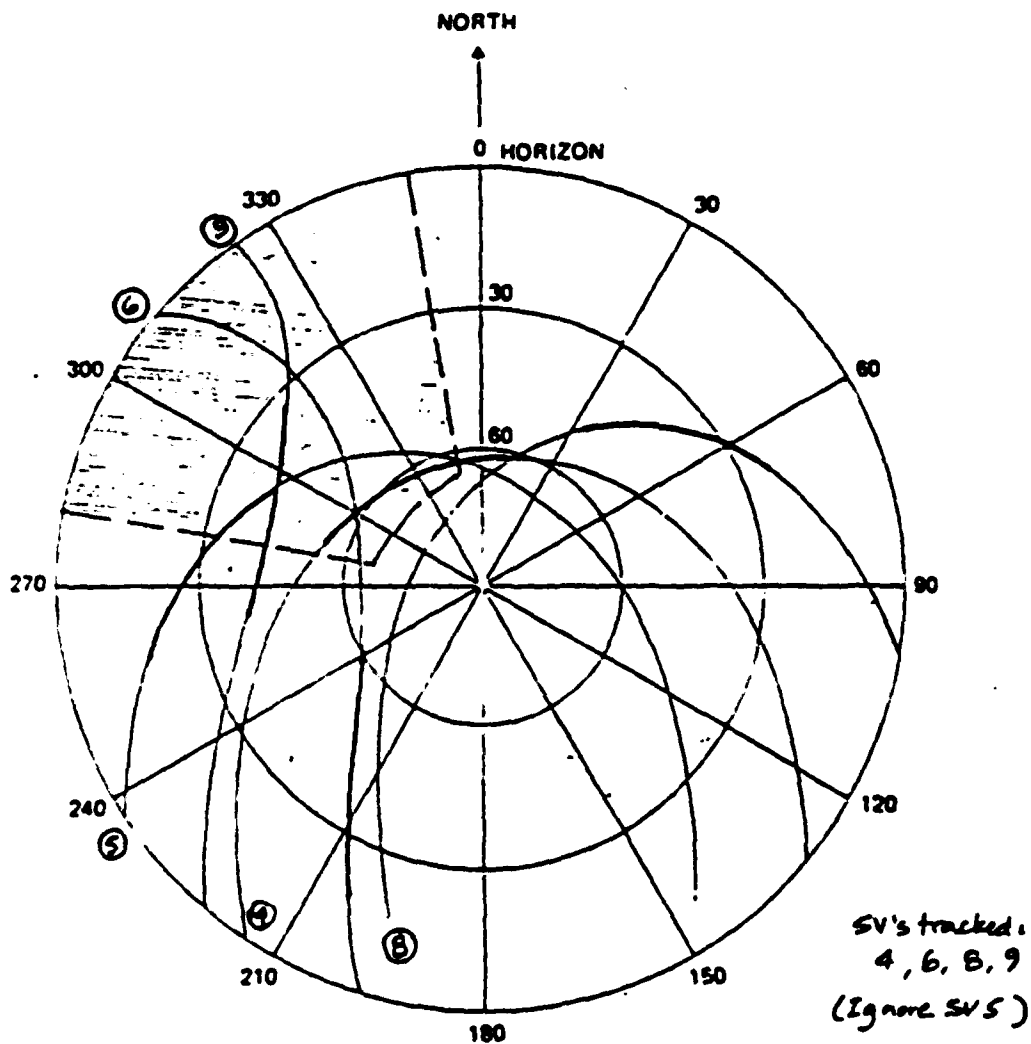


Figure 4. Antenna and reflector (vertical plane mirror) geometry. See text for discussion.



- CIRCLED NUMBERS ARE GPS NAVSTAR SATELLITE DESIGNATORS by PRN code number
- SATELLITE TRACKS ARE DARKENED TO INDICATE SIMULTANEOUS VISIBILITY ABOVE 20° ELEVATION

Figure 5. Field of view of vertical mirror on polar plot of satellite positions during an observation session. Analysis is for  $a = b = 0.5$ ,  $m = h = 1$ .



- CIRCLED NUMBERS ARE GPS NAVSTAR SATELLITE DESIGNATORS by PRN code number
- SATELLITE TRACKS ARE DARKENED TO INDICATE SIMULTANEOUS VISIBILITY ABOVE 20° ELEVATION

Figure 6. Field of view of multipath experiment with vertical mirror placed at  $\mu = 135^\circ$ , with  $m = 1.5$ ,  $h = 4$ ,  $a = b = 2$ .

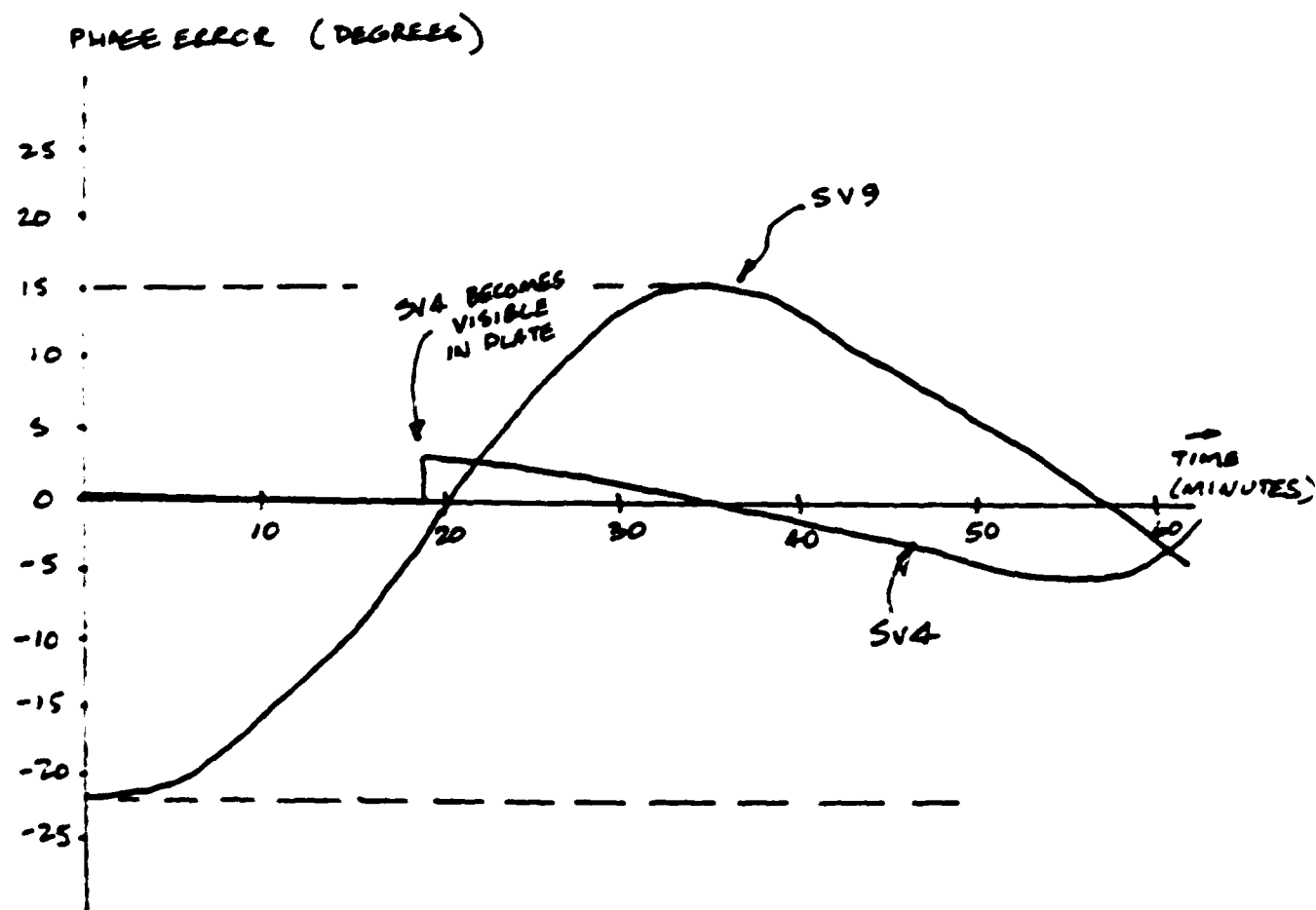
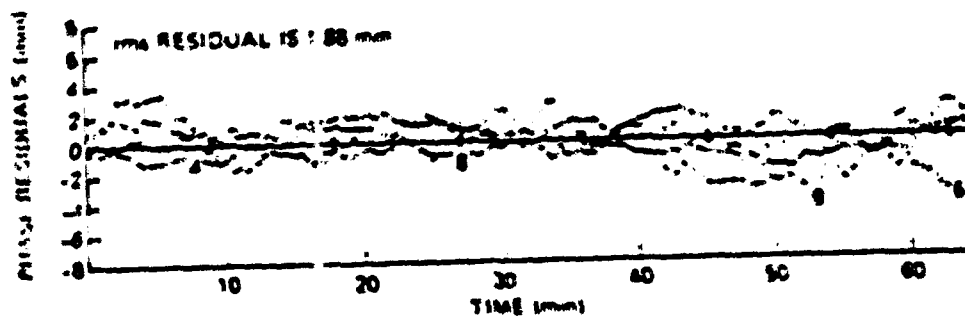
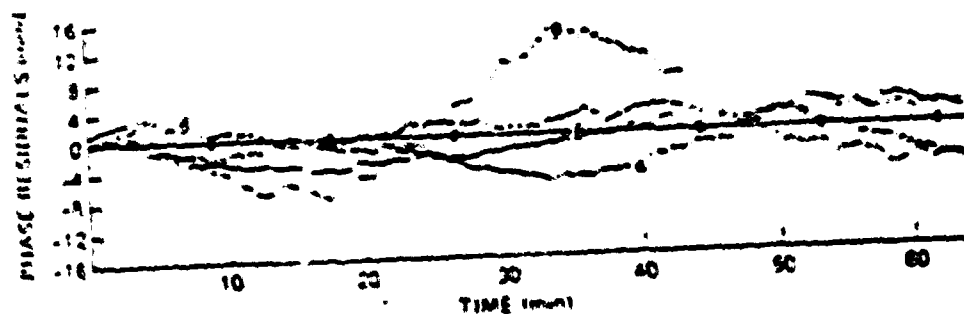


Figure 7. Predicted phase error due to satellites 4 and 9 for multipath experiment.





(a) PHASE RESIDUALS FOR BASELINE 54 OCTOBER 26, 1981



(b) PHASE RESIDUAL FOR BASELINE 54 WITH REFLECTING PLATE OCTOBER 27, 1981

SATELLITE IDENTIFIED: A (---)  
 B (---)  
 C (---)  
 D (---)

Figure 1. Residuals of least squares phase fit for multipath experiment baseline (a) without plate, (b) with plate. Compare residuals for SV4 and SV9 with predicted error shown in Figure 2.

**END**

**FILMED**

**3-85**

**DTIC**